10ᵗʰ South African Conference on Photonic Materials 2025

SACPM 2025

7 -11 April 2025
Amanzi Game Reserve
Free State
South Africa

Hosted by the Division for Physics of Condensed Matter and Applied Physics Division of the South African Institute of Physics.

events.saip.org.za/e/SACPM2050

Amanzi
PRIVATE GAME RESERVE

SOUTH AFRICAN INSTITUTE OF PHYSICS

Time	Monday 7-Apr	Tuesday 8-Apr	Wednesday 9-Apr	Thursday 10-Apr	Friday 11-Apr
07h30 - 09h00		Breakfast (Restaurant)	Breakfast (Restaurant)	Breakfast (Restaurant)	Breakfast (Restaurant)
09h00 - 09h15		Opening (Sable Hall)	Announcements	Announcements	Departure
		Chair H.C. Swart	Chair J.J. Terblans	Chair R.E. Kroon	
09h15 - 10h00		Plenary: Alexander Heidt	Plenary: Andrey Turshatov	Plenary: Bice Martincigh	
10h00 - 10h20		1. Boitumelo Tladi	7. Hope Ramolahloane	16. Ponaki Radebe	
10h20 - 10h40		2. Nadir Saeed	8. Murendeni Nemufulwi	17. Elizabeth Hagemann	
10h40 - 11h00		3. Japie Engelbrecht	9. Kashma Kashma	18. Vijay Kumar	
11h00 - 11h20		Tea / Coffee Break	Tea / Coffee Break	Tea / Coffee Break	
		Chair E. Coetsee	Chair M.M. Duvenhage	Chair E. van Dyk	
11h20 - 11h40		4. Edward Lee	10. Thandi Mazibuko	Invited: Ruediger Loeckenhoff (11h20-11h50)	
11h40 - 12h00		5. Abongile Bele	11. Konstantin Zloshchastiev		
12h00 - 12h20		6. Vinay Kumar	12. Thapelo Ephraim Seimela	19. Shivaramu Jayaramu	
12h20 - 13h30		Lunch (Sable Hall)	Lunch (Sable Hall)	Lunch (Sable Hall)	
		Chair W. Meyer	Chair J. Nel	Chair J.A.A. Engelbrecht	
13h30 - 14h00		Invited: Bryce S. Richards	Invited: Thomas Lippert	Invited: Per-Olof Holtz	
14h00 - 14h20	Arrival & Registration (Reception/Main Building)	Poster Session	13. Rethabile Makole	20. Richard Harris	
14h20 - 14h40			14. Chinedu Ahia	21 Sandile Thubane	
14h40 - 15h00			15. S.P. Khambule	22. Vishal Sharma	
15h00 - 16h00		Poster Session | Afternoon Tea (15h00 - 15h20) / Free Time / Game Drive1	Afternoon Tea (15h00 - 15h20) / Free Time / Game Drive2	Afternoon Tea (15h00 - 15h20) / Free Time / Game Drive 3	
16h00	Opening Function & Dinner (Restaurant)	Dinner (Restaurant)	Braai (Bush boma)	Gala Dinner & Awards (Mountain Lodge)	
17h00					
18h00					

10th South African Conference on Photonic Materials – Amanzi 2025

Conference Venue

Braai (Wednesday)

Gala Dinner (Thursday)

Breakfast (Everyday)
Dinner (Monday, Tuesday)

Amanzi
PRIVATE GAME RESERVE

NO ENTRANCE

ABLUTIONBLOCK

BUSH BOMA

SWIMMINGPOOL

SABLE HALL

CARAVANPARK

GUEST HOUSE

MAIN BUILDING

ⓘ RECEPTION

🍴 RESTAURANTT

MOUNTAIN CHALETS

3
1 2
4
5 6 7
9
10
8

MOUNTAIN LODGE

MAIN GATE

JOY PEACE LOVE PATIENCE FAITHFUL

FAMILY CHALETS

NO ENTRANCE

COTTAGES 1-6

ROOMS 1-6

GATE - CODE 93245#

8
9
DORMITORY
10
11

BOMA

TORTOISE SANCTUARY

SWIMMING POOL

RED REEDBUCK WALKING TRAIL

SUNSHINE CHALETS

MAP NOT TO SCALE

CROSS ROUTE

ANIMAL SANCTUARY
🐾 LEOPARD
🐾 MEERKAT
🐾 VELVET MONKEY
🐾 CARACAL

LEOPARS'S REST

Table of Contents

	African buffalo	Afrika Buffel	*Syncerus caffer*
	African civet	Afrika sivet	*Civettictis civetta*
	African leopard	Luiperd	*Panthera pardus*
	African wildcat	Vaalboskat	*Felis lybica*
	Antbears / anteater	Aardvark	*Orycteropus afer*
	Black impala	Swart rooibok	*Aepyceros melampus*
	Black springbuck	Swart springbok	*Antidorcas marsupialis*
	Black-backed jackal	Rooijakkals	*Lupulella mesomelas*
	Blue wildebeest	Blou wildebees	*Connochaetes taurinus*
	Bontebok	Bontebok	*Damaliscus pygargus pygargus*
	Cape eland	Kaapse eland	*Tragelaphus oryx*
	Caracal	Rooikat	*Caracal caracal*
	Common blesbuck	Gewone blesbok	*Damaliscus pygargus phillipsi*
	Common genet	Kleinkolmuskeljaatkat	*Genetta genetta*
	Common reedbuck	Rietbok	*Redunca arundinum*
	Common tsessebe	Basterhartbees	*Damaliscus lunatus lunatus*
	Common warthog	Vlakvark	*Phacochoerus africanus*
	Copper springbuck	Koper springbok	*Antidorcas marsupialis*
	European bush pig	Europese bosvark	*Sus scrofa*
	Fallow deer	Gewone takbok	*Dama dama*
	Gemsbok	Gemsbok	*Oryx gazella*
	Giraffe	Kameelperd	*Giraffa camelopardalis*
	Golden wildebeest	Goue wildebees	*Connochaetes taurinus*
	Greater kudu	Kaapse koedoe	*Tragelaphus strepsiceros*
	Grey rhebuck	Vaalribbok	*Pelea capreolus*
	Impala	Rooibok	*Aepyceros melampus*
	King springbuck	Koning springbok	*Antidorcas marsupialis*
	Kalahari springbuck	Kalahari springbok	*Antidorcas marsupialis*
	Lion	Leeu	*Panthera leo*
	Mountain reedbuck	Rooiribbok	*Redunca fulvorufula*
	Mountain zebra	Berg zebra	*Equus zebra*
	Nyala	Njala	*Tragelaphus angasii*
	Plains zebra	Vlakte sebra	*Equus quagga*
	Porcupine	Ystervark	*Hystrix africaeaustralis*
	Red hartebeest	Rooi hartebees	*Alcelaphus buselaphus caama*
	Red lechwe	Rooi lechwe	*Kobus leche*
	Roan antelope	Bastergemsbok	*Hippotragus equinus*
	Sable antelope	Swartwitpens	*Hippotragus niger*
	Saddleback blesbuck	Saalrug blesbok	*Damaliscus pygargus phillipsi*
	Serval	Tierboskat	*Leptailurus serval*
	Waterbuck	Waterbok	*Kobus ellipsiprymnus*
	White blesbuck	Wit blesbok	*Damaliscus pygargus phillipsi*
	White springbuck	Wit springbok	*Antidorcas marsupialis*
	Yellow blesbuck	Geel blesbok	*Damaliscus pygargus phillipsi*

Sponsors

CB van Wyk Family Trust

Organizing Committee

Prof Richard Harris	UFS	Chairperson
Prof Hendrik Swart	UFS	Plenary and Invited Speakers
Prof Koos Terblans	UFS	Logistics and Sponsors
Prof Ted Kroon	UFS	Website and sponsor adverts
Prof David Motaung	UFS	Abstracts
Prof Liza Coetsee	UFS	Book of Abstracts
Dr Mart-Mari Duvenhage	UFS	Program, graphic design
Dr. Lucas Erasmus	UFS	Sponsors
Prof Japie Engelbrecht	NMU	Plenary and Finance
Prof Andre Venter	NMU	KIC grant
Prof Ernest van Dyk	NMU	Sponsors
Prof Walter Meyer	UP	Sponsors
Dr Jackie Nel	UP	Sponsors
Mr. Johan van Rensburg	UP	Abstracts and Sponsors

UFS: University of the Free State; **NMU**: Nelson Mandela University; **UP:** University of Pretoria.

SAIP: The committee was assisted by the Office of the South African Institute of Physics, particularly **Brian Masara** and **Tebogo Mokhine**

Sponsors

CB van Wyk Family Trust	ufs.ac.za/natagri/departments-and-divisions/physics-home
NMU Dean of Faculty	science.mandela.ac.za/
UFS Dean of Faculty	ufs.ac.za/natagri/
Vacutec	vacutec.co.za
Busch Scientific	busch.co.za
AC Scientific	ac-scientific.com/en/
PV Insight	pvinsight.co.za
National Research Foundation: Knowledge, Interchange and Collaboration – KIC (Local Events support grant)	nrf.ac.za

CB van Wyk Family Trust

A Visionary Whose Legacy Lives On

In 1953, two professors from the University of the Free State envisioned organizing a Physics Conference in South Africa. Prof. C.B. van Wyk (Applied Mathematics) and Prof. J.H.N. Loubser (Physics) reached out to 27 scientists to gauge interest and feasibility. The response was overwhelmingly positive, leading them to contact Dr. Ernest Marais, head of the National Physical Laboratory.

On 17 August 1953, a meeting was held, and the provisional committee of the "South African Institute of Physics" decided to host a conference in Pretoria in July 1954. Prof. Van Wyk and Prof. Loubser continued inviting physicists to attend and discuss the establishment of the Institute for Physics.

Prof. Van Wyk's vision played a pivotal role in founding the **South African Institute of Physics**, which celebrates 70 years of growth and success this year. His enduring legacy lives on through the CB van Wyk *Gesinstrust*, which continues to sponsor plenary speakers and student prizes at this conference.

Message from the SAIP President

(South African Institute of Physics)

Message for SACPM 2025

A measure of the success of a specific research field is often found in the dedication and persistence with which practitioners in the field strive for excellence in their work. Using this measure, the members of the Division for Physics of Condensed Matter and Materials and the Applied Physics Division of the South African Institute of Physics (SAIP) can take great pride and satisfaction in the hosting of the 10th South African Conference on Photonic Materials 2025 (SACPM 2025) taking place from 7 – 11 April 2025 at Amanzi Private Game Reserve, Free State, South Africa.

The conference brings together South African and international scientists who are working on various topics in the field of photonic materials. I particularly welcome the invited speakers, many from highly regarded international institutions, and wish to thank you for your attendance and willingness to share knowledge and ideas. Any research field is heavily dependent on this type of cross-pollination and stimulation for continued excellence and international relevance in its outputs.

I would like to thank the organisers for the great deal of hard work that goes into hosting such a conference and I know that all the delegates will present excellent oral and poster contributions. These contributions will be published in *Physica Status Solidi A*, which is important to document progress and highlight novel findings.

I wish all delegates a productive and inspiring time at SACPM2025!

With best regards

Rudolph Erasmus

President: South African Institute of Physics (SAIP)

NELSON MANDELA
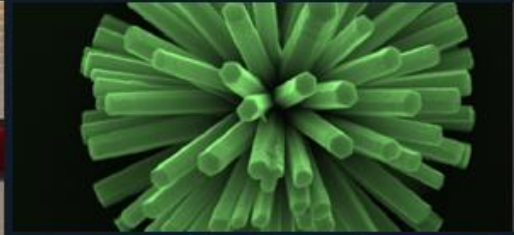
UNIVERSITY

Department of **Physics**

Electron Microscopy for Materials Research

The Centre for High Resolution Transmission Electron Microscopy (Centre for HRTEM) at Nelson Mandela University houses four state-of-the-art electron microscopes including the only aberration-corrected atomic resolution electron microscope in Africa. The wide range of research projects and MSc and PhD topics include:

- HRTEM and in situ HRTEM investigation of nanoparticle catalysts
- Irradiation damage and fission product transport in nuclear reactor materials
- Corrosion resistant nuclear reactor materials
- Refining of weldability limits of creep-aged power plant stainless steel
- Lifetime assessment of high value power plant components
- Characterisation of diamond, Pt, Ti and Al alloys, compound semiconductor structures and gold and platinum bearing ores

Prof Jaco Olivier
E jaco.olivier@mandela.ac.za

Semiconductor Materials Development

This research focuses on vapour phase and solution-based deposition of semiconductors for opto-electronic devices.

The Physics Department has unique equipment for the synthesis and characterization of semiconductor thin films and nano-structures, including a state-of-the-art reactor for compound semiconductor deposition.

We currently develop:

- Epitaxial InAsSb and related compounds for infrared detectors
- ZnO nanorods for high efficiency white LEDs and hybrid solar cells
- Nanostructured TiO_2 for solar water splitting

Our active collaborations with several local and overseas universities over many years, including groups in Sweden, Germany and the UK, have forged excellent academic links.

For information on these exciting research topics contact:

Prof Reinhardt Botha
E reinhardt.botha@mandela.ac.za

SACPM 2025

Message from the SACPM 2025 Chairman

Dear Esteemed Delegates,

It's a true pleasure to welcome you to the 10th South African Conference on Photonic Materials. This is a big moment for all of us in the scientific community, and I'm excited to share it with you. As we celebrate this milestone, it's a great time to reflect on how far we've come in the world of photonics, and how much it's impacting industries from telecommunications to healthcare to energy. This conference is a fantastic opportunity for us all to connect, share ideas, and collaborate in ways that will shape the future of photonic materials and technologies.

Looking back over the last decade, we've seen some truly groundbreaking developments—whether it's new nanomaterials or advancements in quantum optics, these innovations have made a real difference. It's amazing to see how diverse and interdisciplinary this field has become. The variety of topics and expertise here is a reminder of how much more we can achieve when we work together, and I'm excited to see what we'll discover over the course of this event.

As we gather in April 2025, I want to highlight something that brings us all here today: curiosity. It's our shared curiosity—our desire to explore, understand, and create—that drives us to solve big challenges and build a better world for everyone. It's what pushes us to make things that not only move science forward but also improve lives across the globe. So, I encourage you to embrace the many networking opportunities here, and to engage with your fellow delegates. These conversations and collaborations are what fuel progress and inspire us to do even greater things together.

Before I close, I want to take a moment to thank everyone who's made this event possible—our organizing committee, our sponsors, and all the hardworking individuals who've contributed to making this conference a reality. I'm truly looking forward to an inspiring week of conversations and ideas, and I have no doubt that the connections we make here will lead to exciting new discoveries and collaborations in photonics.

Warm regards,

Richard Harris

Chairman, South African Conference on Photonic Materials - 2025

NELSON MANDELA
UNIVERSITY

Department of **Physics**

Photovoltaics

Sustainable Energy for the Future

The Photovoltaics Research Group focusses on the characterisation of Photovoltaics (PV) materials, devices and systems. The facilities include:
- Photovoltaic Research Laboratory (PV Lab) for advance solar cell and PV module characterisation
- Outdoor Research Facility (ORF) for PV module and system monitoring and characterisation
- ISO17025 accredited Photovoltaic Test Laboratory (PVTL) – PVinsight (Pty) Ltd

The following Applied Physics skills are also acquired:
- Advance solar cell and PV module characterisation and evaluation
- Data acquisition an analysis, including curve fitting and parameter optimisation
- LabView programming and computer interfacing
- Data acquisition system design

For further information on student projects please contact the PVRG.

Prof Ernest van Dyk
E ernest.vandyk@mandela.ac.za

Optical Fibre Telecommunication Research

Escalating bandwidth demands fuelled by smartphones, tablet computers, social media and cloud computing makes Telecommunications an extremely challenging and rewarding field.

Nelson Mandela University has one of the best equipped Optical Fibre Research laboratories in Africa.

We offer an exciting range of MSc and PhD projects featuring:
- Dispersion measurement, compensation and emulation
- Fibre-to-the-home (FTTH) technologies
- Square Kilometer Array related optical fibre topics
- Polarization effects, wavelength division multiplexing, non-linear effects
- Modelling and simulation, OTDR, fusion splicing, bit error rate testing

The Optical Fibre Research Unit is part of the Telkom-sponsored Centre of Excellence.

Scholarship opportunities are available for good, motivated students.

Dr David Waswa
E david.waswa@mandela.ac.za

10th South African Conference on Photonic Materials – Amanzi 2025

PROUD SPONSOR OF THE
SACPM 2025 CONFERENCE

T: +27 51 401 2531 | E: VDBergE@ufs.ac.za | www.ufs.ac.za

Inspiring excellence, transforming lives through quality, impact, and care.

Plenary Speakers

Alexander M. Heidt

Institute of Applied Physics, University of Bern, Switzerland

"Silica optical fibers functionalized with nanoparticles and quantum materials" (page 21)

Alexander Heidt studied Physics at the University of Konstanz (Germany) before completing a bi-national PhD degree at the University of Stellenbosch (South Africa) and the University of Jena (Germany) in 2011. After working as Marie Curie Research Fellow at the Optoelectronics Research Centre in Southampton, UK, and founding a craft beer brewing company in Mexico, in 2019 he received a prestigious Eccellenza Professorship at the Institute of Applied Physics, University of Bern (Switzerland), where he was recently appointed Full Professor and head of the Laser Physics Group. His primary research interests revolve around shaping the temporal and spectral properties of light using nonlinear light-matter interactions, specialty optical fibers with novel functionalities, and dual-frequency comb technology with its applications in ultrafast imaging and spectroscopy.

Andrey Turshatov

Institute of Microstructure Technology, Karlsruhe Institute of Technology, Germany

"Bright Ideas: How Luminescent Tracers Improve Plastic Recycling, Energy Conversion, and Counterfeit Detection" (page 30)

Andrey Turshatov is a group leader at the Karlsruhe Institute of Technology (KIT) in Germany. He received his PhD in polymer chemistry from the Nizhny Novgorod State University in Russia. Following his doctorate, Dr Turshatov carried out postdoctoral research at the Technical University of Clausthal, where he used fluorescence methods to study polymer coatings, and at the Max Planck Institute for Polymer Research, where he focused on photon upconversion processes. At KIT, Dr Turshatov leads a research group working on a wide range of topics, including the chemistry and photophysics of both organic and inorganic luminescent materials and the development of innovative photocatalytic systems for water purification. His recent research interests have expanded to include the application of phosphor materials as luminescent tracers in next-generation plastics sorting technologies, a promising approach to improving recycling efficiency.

Bice S. Martincigh

School of Chemistry and Physics, University of KwaZulu-Natal, South Africa

"Carbon-based materials for third- generation solar cells" (page 42)

Bice Martincigh attended the University of Natal where she obtained her B.Sc.(Hons) and Ph.D. degrees. She taught at Natal Technikon before joining the University of Natal (now University of KwaZulu-Natal) where she currently holds the post of Professor in Physical Chemistry. She has held Visiting Professorships at West Virginia University, the University of Wales in Cardiff, Portland State University and the Gandhi Institute of Technology and Management (GITAM) in India. She served as President of the South African Chemical Institute (SACI) from 2015 to 2017. She is a recipient of the University's Distinguished Teacher Award and the SACI Merck medal. She has been elected as a Fellow of SACI, Royal Society of Chemistry (RSC), International Union of Pure and Applied Chemistry (IUPAC), and the Royal Society of South Africa, and as a member of the Academy of Science of South Africa (ASSAf). Her research encompasses the application of physical chemistry principles to solve problems related to health or the environment. In doing so she has investigated the photochemical behaviour of the absorbers used in sunscreen and cosmetic preparations to prevent reddening of the skin, and the application of nanomaterials for energy or wastewater remediation either through adsorption or photocatalysis. She is also involved in projects investigating environmental contamination caused by PAHs, PCBs and flame-retardant chemicals. She has successfully graduated 30 PhD and 29 MSc students. For many years she was involved with the organization of the annual FFS Expo for Young Scientists, where high school pupils exhibit projects they have undertaken, are judged and prizes are awarded. She is also one of the magicians in the annual SACI KZN Magic Show. Currently, she is one of the mentors for the South African team to the International Chemistry Olympiad (IChO). These initiatives aim to foster and develop an interest in science among our school learners.

Invited Speakers
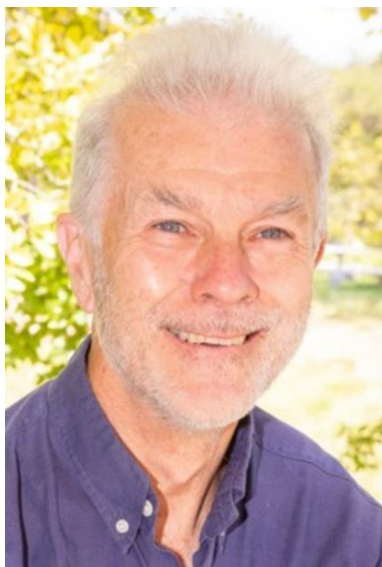
Per-Olof Holtz
Polar Light Technologies AB, Sweden

"Towards smaller, brighter and more efficient micro-LEDs" (page 48)

Prof. Holtz is currently employed at Polar Light Technologies AB, Linköping, Sweden and he is also an Emeritus professor at the Department of Physics, Chemistry and Biology (IFM), Linköping, Sweden. His fundamental research work focuses on optical characterization of different semiconductor-based quantum structures. He has experience in SiGe, ZnSe/Te/S, InGaAs/GaAs and InGaN/GaN/AlGaN material systems with his present focus being on the nitride system. His work was applied in InGaAs/GaAs quantum structure based infrared detectors and InGaN/GaN quantum structure based micro-LEDs. His research contributions include about 530 publications accepted at international conferences and published in scientific journals. He is the author of a book: "Impurities Confined in Quantum Wells, Springer Verlag, 2004". He was program director for the NANOPTO SSF program: "Quantum Wires/Dots for Optoelectronics", 2000-0 and for the NANO-N SSF consortium: "Nitride Based Quantum Wires and Dots for Optoelectronic Devices".

Bryce S. Richards
Institute of Microstructure Technology, Karlsruhe Institute of Technology, Germany

"Broadband spectral conversion and light management for next generation greenhouses" (page 28)

Bryce Richards studied physics at the Victoria University of Wellington (New Zealand) before completing a Masters and PhD in electrical engineering at University of New South Wales (Australia), in 1998 and 2002, respectively. He worked at both UNSW and the Australian National University. In 2006, he joined Heriot-Watt University (Edinburgh, U.K.) as a lecturer, being promoted to full professor in 2008. Since 2014 he is co-director of the Institute for Microstructure Technology (IMT) and Light Technology Institute (LTI) within the Karlsruhe Institute of Technology (Germany). His primary research areas lie in third generation photovoltaics (including perovskite solar cells), spectral conversion (up- and down-conversion), luminescent materials, light management, and solar-powered water treatment systems.

Ruediger F Loeckenhoff
AZUR SPACE Solar Power GmbH, Germany

"3 Junction and 5 Junction Solar Cells in Concentrating Photovoltaics (CPV) Systems: Considerations, Simulations and Field Studies" (page 46)

Ruediger F. Loeckenhoff studied physics at the University of Konstanz and received his first degree for the development of monolithically interconnected modules MIMs at Fraunhofer Institute for Solar Energy Systems ISE, Freiburg in 2003. His PhD thesis continued this work by addressing water cooled dense array solar cells and modules in a wider scope. Since 2007 he has been working at AZUR SPACE Solar Power on various kind of concentrating photovoltaics (CPV) system, projects, cells and systems including central receiver systems with dense array modules and point focus Fresnel modules. His expertise comprises III-V solar cell processing, CPV system design, measurement, simulation, and field monitoring, as well as more recently measurement hardware and robotics for automation.

Thomas Lippert
PSI Center for Neutron and Muon Sciences, Switzerland

"Pulsed Laser Deposition for Energy Materials" (page 37)

Thomas Lippert studied Chemistry at the University of Bayreuth, Germany, where he received his PhD in Physical Chemistry in 1993. He then stayed as Postdoctoral Fellow at NIMC in Tsukuba, Japan. After Japan he moved in 1995 to Los Alamos National Laboratory, USA, where he also became a Technical Staff Member. Since 2013 Thomas is also professor at the Laboratory of Inorganic Chemistry at ETH Zurich. Thomas Lippert is since 2002 head of the Thin Films and Interfaces group and since 2022 the head of the Laboratory for Multiscale Materials Experiments in the Research with Neutrons and Muons Division at the Paul Scherrer Institute. He has published more than 380 papers, delivered more than 180 invited talks, and organized more than10 international conferences. He is the Editor-in-Chief of Applied Physics A-Material Science & Processing and was the President of European Materials Research Society (E-MRS, from 2014-2015).

Scientific Program and Abstracts
Tuesday 8 April 2025

Time	Tuesday
	8 April
09h00 - 09h15	Opening (Sable Hall)
	Chair H.C. Swart
09h15 - 10h00	**Plenary: Alexander Heidt**
10h00 - 10h20	1. Boitumel Tladi
10h20 -10h40	2. Nadir Saeed
10h40 - 11h00	3. Japie Engelbrecht
11h00 - 11h20	Tea / Coffee Break
	Chair E. Coetsee
11h20 - 11h40	4. Edward Lee
11h40 - 12h00	5. Abongile Bele
12h00 - 12h20	6. Vinay Kumar
12h20 - 13h30	**Lunch (Sable Hall)**
	Chair W. Meyer
13h30 - 14h00	**Invited: Bryce S. Richards**
14h00 -16h00	**Poster Session**

Silica optical fibers functionalized with nanoparticles and quantum materials

Pascal Hänzi[1], Dariusz Pysz[2], Mariusz Mrózek[3], Robert Bogdanowicz[4], Ryszard Buczyński[2,5], Mariusz Klimczak[5], and <u>Alexander M. Heidt[1]</u>

[1] *Institute of Applied Physics, University of Bern, Sidlerstrasse 5, 3012 Bern, Switzerland*
[2] *Łukasiewicz Research Network, Institute of Microelectronics and Photonics, Al. Lotników 32/46, 02-668, Warsaw, Poland*
[3] *Institute of Physics, Jagiellonian University in Kraków, Łojasiewicza 11, Kraków, 30-348, Poland*
[4] *Gdańsk University of Technology, Faculty of Electronics, Telecommun. and Informatics, Gdańsk, Poland*
[5] *University of Warsaw, Faculty of Physics, Pasteura 5, 02-093 Warsaw, Poland*
Corresponding author e-mail address: alexander.heidt@unibe.ch

Silica optical fibers have revolutionized technology, enabling global high-speed communication and applications in sensing, medical surgery, and nonlinear optics. While telecommunications prioritize ultra-low loss, emerging technologies explore specialty fibers functionalized with dopants like rare-earth metals, semiconductors, and nanoparticles for enhanced optical and optoelectronic properties.

In this work, we present a novel laser-assisted preform manufacturing method for rapidly prototyping high-quality functionalized silica fibers [1]. The laser vitrification process generates an ultra-thin heat blade, allowing precise heat localization and the integration of heat-sensitive dopants. Using this technique, we demonstrate the first direct doping of silica fibers with nitrogen-vacancy fluorescent nanodiamonds (Fig. 1), enabling single-photon quantum emitter integration into existing optical networks.
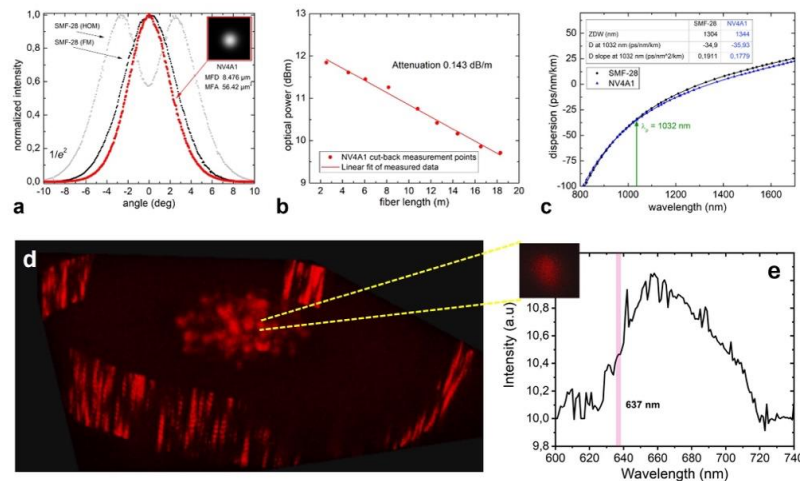
Fig. 1. Linear characteristics of the developed fiber and its preform: a) Mode field diameter and mode field area, b) attenuation, c) chromatic dispersion of the nanodiamond-silica fiber labelled NV4A1 compared with the SMF-28 fiber dispersion, d) vitrified preform disk-slice image (5×2 mm), e) NV color center fluorescence of the nanodiamonds embedded in the silica glass.

Additionally, we show that nanoparticle doping offers a new approach to controlling the nonlinear Kerr effect in silica fibers, where the refractive index depends on light intensity, impacting applications in ultrafast photonics and biophotonic imaging [2]. Nanodiamonds are particularly promising as they can exhibit a negative nonlinear refractive index (n_2), which could potentially reduce or even neutralize the positive Kerr nonlinearity of silica glass. However, their low dissociation temperature (~600 °C) has historically limited their use in silica fibers.

The laser-assisted vitrification approach overcomes this barrier, enabling the first fabrication of optical-quality silica fibers with embedded nanodiamonds. The ND-doped fibers exhibit a reduced n_2 value while maintaining sufficiently low attenuation for nonlinear characterization. This breakthrough advances fiber-based nonlinear optics and quantum photonics, paving the way for novel ultrafast and quantum optical devices.

References

[1] P. Hänzi, D. Pysz, M. Mrózek, R. Bogdanowicz, R. Buczynski, M. Klimczak, T. Feurer, V. Romano, and A. M. Heidt, "Laser-assisted rapid prototyping of silica optical fibers functionalized with nanodiamonds and multiple active rare earth dopants," Opt. Mat. Express (in press).

[2] G. Stępniewski, P. Hänzi, A. Filipkowski, M. Janik, M. Mrózek, Y. Stepanenko, R. Bogdanowicz, V. Romano, A. Heidt, R. Buczyński, M. Klimczak, "Nonlinearity shaping in nanostructured glass-diamond hybrid materials for optical fiber preforms," Carbon 215, 118465 (2023).

Band gap engineering from noble metals decoration on Co_3O_4/rGO for ultrasensitive LPG gas sensing at low temperatures

B.C. Tladi, Z.P. Tshabalala, R.E. Kroon H.C. Swart, D.E. Motaung

Department of Physics, University of the Free State, Bloemfontein 9300, South Africa
Corresponding author email address: Boitumelotladi@gmail.com

1. Introduction

Liquefied petroleum gas (LPG) production is imperative in the global energy mix. Despite being a clean energy source, it possesses flammable and explosive properties [1]. Hence, its efficient and reliable detection is crucial for ensuring safety in both industrial and domestic environments. For decades semiconducting metal oxides (SMOs) have been investigated in gas-sensing devices to detect toxic and explosive gases [2]. Many strategies have been explored to improve their sensing performance, especially lowering their operating temperature for better energy efficiency. Among these, noble metals-decoration on the sensing material can reveal the effective gas sensing capability at low temperatures [3]. The primary cause of this is the combination of the noble metals' catalytic nature and efficient electron transfer between the sensing surface and the target gas [3]. Thus, herein, we investigate the gas-sensing properties of Co_3O_4/rGO decorated with different noble metal (Ag, Ru, and Pd) nanoparticles at 1 wt% towards LPG gas-sensing applications.

2. Results

The successful decoration of various noble metal nanoparticles was confirmed by transmission electron microscopy (TEM), elemental mapping, and X-ray photoelectron spectroscopy (XPS). Using Tauc's relation, the band gap energy (E_g) was estimated from absorbance measurements (Fig.1(a)). The band gap value of pure Co_3O_4/rGO was ~1.63 eV whereas the band gap of the Ag, Ru, and Pd decorated heterostructures were found to be 1.94, 1.71, and 2.16 eV, respectively. This was indicative that the introduction of metal nanoparticles created new hybridized states that tuned the E_g [4] These new states facilitated charge transfer, i.e. removal of electrons and the creation of holes, resulting in a wider E_g. The conductivity of p-type SMOs, such as Co_3O_4, is governed by holes in the valence band, thus the wider E_g due to metal nanoparticles enhanced the conductivity of the prepared sensors. The 1 wt% Pd-Co_3O_4/rGO-based sensor revealed enhanced sensitivity and selectivity towards LPG at lower temperatures, which is observed in Fig. 1(b). Pd exhibited better sensing performance followed by Ag and lastly Ru. This may be due to the superior catalytic activity of Pd. The excellent gas sensing properties were influenced by the chemical state, the amount of dispersion, and new electron pathways of Pd nanoparticles decorated onto the Co_3O_4/rGO surface.
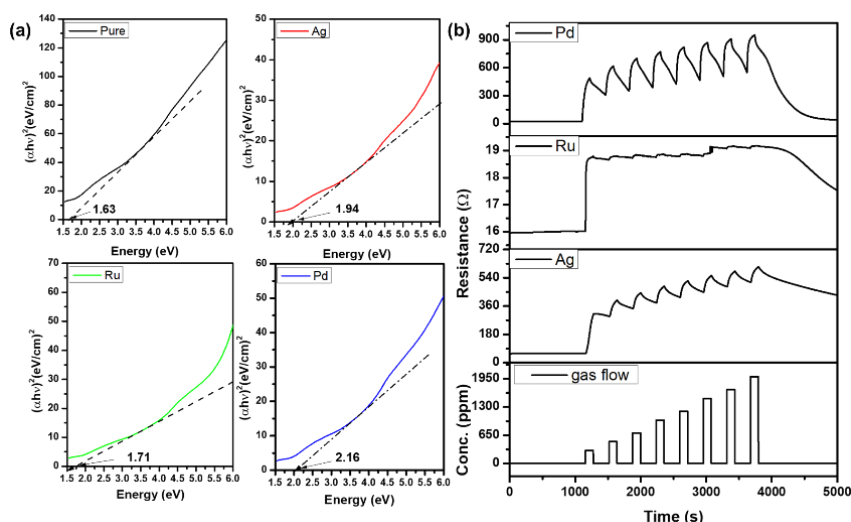
Fig. 1(a): UV-Vis absorbance spectra, and (b) Dynamic resistance curves of decorated sensors towards LPG at 70 °C

3. References

[1] U. Kumar, B.C. Yadav, K. Kumar, T. Haldar, V.V. Ravi Kanth, et al. *Sens. Actuators A* **379** (2024) 115851
[2] A. Dey. Semiconductor metal oxide gas sensors. *Mater. Sci. Eng B* **229** (2018) 206-217.
[3] Z. Wang, L. Zhu, J Wang, R. Zhuang, Pe. Mu, J. Wang, W. Yan. *RSC Adv.* **12** (2022) 24614-24632.
[4] Y. Pan, J. Zhang. *Vacuum* **187** (2021) 110112.

Pulsed laser deposition of NiO thin films as a hole transport layer.

N.A.M. Saeed, R.A Harris, H.C. Swart and E. Coetsee

Department of Physics, University of the Free State, PO Box 339, Bloemfontein, ZA9300, South Africa
Corresponding author e-mail address: Nadirazhari989@gmail.com

1. Introduction

The challenges of introducing a cheap and proper hole transport layer (HTL) for thin film solar cells drew a lot of attention in recent years [1,2]. The importance of these layers includes the hole extraction facilitation as well as the blocking of the electron flux [2]. As an example, the available commercial Spiro-OMeTAD is quite expensive for cost-effective thin-film solar cells. An alternative is to introduce p-type metal oxide materials such as NiO thin films. NiO has a cubic structure (space group Fm3m (225)) [3] with a wide band gap (3.6 – 4 eV) [4]. Whereas, the stoichiometric NiO is considered an insulator ($>10^{13}$ Ω.cm) [4], its resistivity can be lowered by introducing monovalent atoms such as lithium, nickel vacancies, and/or interstitial oxygen [4]. It is considered an excellent candidate as an HTL due to the transparency in the visible region as well as having a large work function [5].

2. Results

The pulsed laser deposition method (266 nm Nd-YAG laser) was utilized to prepare different NiO thin films at a laser energy of ~37 mJ. The deposition was kept neutral without heating the substrate or post-deposition heat treatment, with a Ni metal target for deposition under different oxygen pressures. The structural information confirmed the formation of cubic NiO films through X-ray powder diffraction. Additionally, the compositional analysis was examined with X-ray photoelectron microscopy (XPS) (fig. 1) with a clear assignment of Ni 2p peaks [6]. The lowest recorded sheet's resistance was for the film deposited at 25 mTorr (Fig. 2).
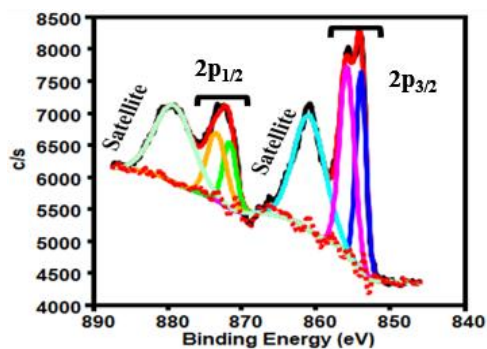
Fig. 1: XPS fit for the sample deposited at 30 mTorr.
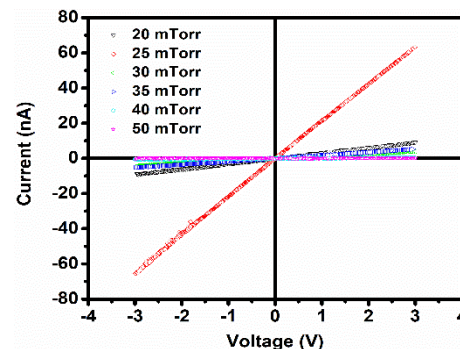
Fig. 2: I-V curves of different NiO thin films.

3. References

[1] M. Dada, P. Popoola, Recent advances in solar photovoltaic materials and systems for energy storage applications: a review, Beni-Suef Univ. J. Basic Appl. Sci. 12 (2023) 1–15. https://doi.org/10.1186/s43088-023-00405-5.

[2] C. Anrango-Camacho, K. Pavón-Ipiales, B. A. Frontana-Uribe, A. Palma-Cando, Recent Advances in Hole-Transporting Layers for Organic Solar Cells, Nanomaterials. 12 (2022) 1–54. https://doi.org/10.3390/nano12030443.

[3] M. Wang, Y. Thimont, L. Presmanes, X. Diao, A. Barnabé, The effect of the oxygen ratio control of DC reactive magnetron sputtering on as-deposited nonstoichiometric NiO thin films, Appl. Surf. Sci. 419 (2017) 795–801. https://doi.org/10.1016/j.apsusc.2017.05.095.

[4] H. Sato, T. Minami, S. Takata, T. Yamada, Transparent conducting p-type NiO thin films prepared by magnetron sputtering, Thin Solid Films. 236 (1993) 27–31. https://doi.org/10.1016/0040-6090(93)90636-4.

[5] M. Napari, T.N. Huq, R.L.Z. Hoye, J.L. MacManus-Driscoll, Nickel oxide thin films grown by chemical deposition techniques: Potential and challenges in next-generation rigid and flexible device applications, InfoMat. 3 (2021) 536–576. https://doi.org/10.1002/inf2.12146.

[6] G. Pagot, M. Benedet, C. Maccato, D. Barreca, V. Di Noto, XPS study of NiO thin films obtained by chemical vapor deposition, Surf. Sci. Spectra. 30 (2023) 1–8. https://doi.org/10.1116/6.0003008.

Observations on the refractive index of $Al_xGa_{1-x}As$ in the infrared region

Japie Engelbrecht[1,2]**, Ettienne Minnaar**[1]**, Reinhardt Botha**[1]**, Mike Lee**[1,2] **and William Goosen**[2]

[1]*Physics Department, Nelson Mandela University, South Africa*
[2]*Centre for HRTEM, Nelson Mandela University, South Africa*
Corresponding author e-mail address: Japie.Engelbrecht@mandela.ac.za

1. Introduction

The ternary semiconductor alloy $Al_xAl_{1-x}As$ is used in high electron mobility transistors (HEMT) [1], high-speed, high-frequency microwave devices [2], quantum well-infrared photo detectors [3], and other electro-optic devices. The refractive index of the utilized alloy of $Al_xGa_{1-x}As$ must thus be known to design the specific devices with given optical properties.

The use of infrared reflectance and the parallel-plate interference formula is well-established as a means of determining the thickness of an epilayer on a substrate [4]. The formula requires the refractive index n at the relevant wavelength λ. In the case of ternary semiconductor alloys, the refractive index is a function not only of the wavelength λ, but also the mole fraction x of the alloy [5]. A relationship has been shown to exist between the refractive index and the band gap E_g of a semiconductor [6], as well as between the band gap and the mole fraction x [7]. Determination of the band gap E_g has been shown to be obtained from the point of inflection of an infrared reflectance spectrum [8], and thus the mole fraction x of the sample being investigated.

In the case of $Al_xAs_{1-x}As$, two formulas for the calculation of the refractive index n were previously proposed by Afromowitz [9] and Adachi [10]. The present investigation reports on the use of the two theoretical equations for which the refractive index of $Al_xAl_{1-x}As$ samples (having various values for x) were determined in the infrared range. The as-determined values of n were used for the subsequent calculation of the epilayer thicknesses.

2. Results
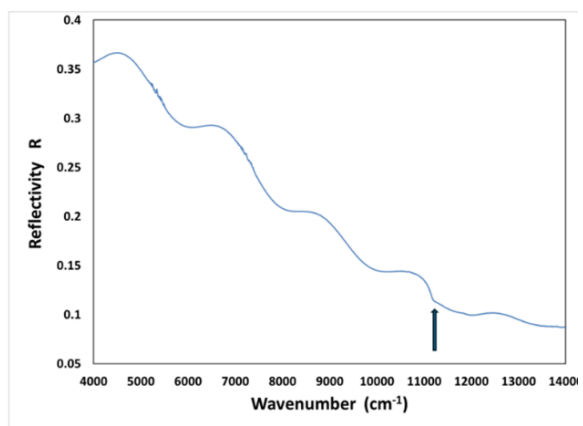
Fig. 1: Infrared reflectance spectrum, indicating the position of the band gap, as well as interference fringes.
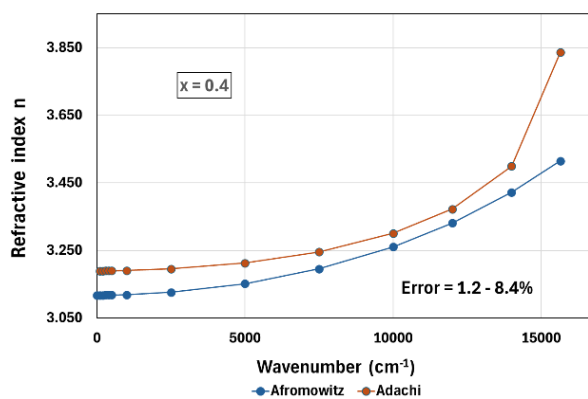
Fig. 2: Refractive index as function of wavenumber and Al mole fraction x = 0.4 from Afromowitz and Adachi formulas.

3. References

[1] T. R. Lenka and A. K. Panda, *International Journal of Recent Trends in Engineering* **1** (2009) 186.
[2] S. Adachi, *Physical properties of III-V semiconductor compounds* (John Wiley and Sons, NY 1992) Chap. 4.
[3] A. Billaha and M.K. Das, *Opto-Electronic Review* **24** (2017) 25.
[4] F. Reizman, *J. Appl. Phys.* **36** (1965) 3804.
[5] B. Jensen and A. Torabi, *J. Appl. Phys.* **54** (1983) 5945.
[6] P. Hervé and L.K.J. Vandamme, *Infrared Phys.Technol.* **35** (1994) 609.
[7] R.E. Nahory, M.A. Pollack, W.D. Johnston Jr and R.L. Barns, *Appl. Phys Lett*. **33** (1978) 659.
[8] M. Holtz, T. Prokofyeva, M. Seon, K. Copeland, J. Vanbuskirk, S. Willliams, S.A. Nikishin, V.Tretyakov and H. Temkin, *J. Appl. Phys.* **89** (2001)7977.
[9] M. Afromowitz, *Solid State Comm*. **15** (1974) 59.
[10] S. Adachi, *J. Appl. Phys.* **85** (1985) R1.

Strontium vanadate thin films prepared by using spin coating

Edward Lee[1,2], **Richard A. Harris**[1], **Jacobus J. Terblans**[1,2] **and Hendrik C. Swart**[1]

[1] *Department of Physics, University of the Free State, Nelson Mandela Drive, Bloemfontein, South Africa*
[2]*Centre for Microscopy, University of the Free State, Nelson Mandela Drive, Bloemfontein, South Africa*
Corresponding author e-mail address: LeeE@ufs.ac.za

1. Introduction

Transparent conductive oxide (TCO) thin films are of significant interest due to their importance in commercial applications. These materials have been used in devices, such as displays, electronics, and energy devices for their visible transparency, while still being electrically conductive [1]. Indium tin oxide (ITO) films are currently the most widely used TCO, making up close to 90 %. ITO has been adopted in electronic applications due to its wide transparency in the visible region of more than 85 %, while having a high electrical conductivity, and charge carrier concentration. However, indium resources are of great concern due to their increasing scarcity, resulting in a limited supply and high cost. Therefore, it is desirable to develop cost-effective alternatives to ITO. Early reports showed that $SrVO_3$ thin films with a thickness of 12 nm displayed a resistivity comparable to that of ITO with a transparency of 80 % in the visible region [2]. More importantly, the cost of the raw materials is significantly lower than that of ITO.

In this study, $SrVO_3$ thin films were prepared using spin coating. The strontium-vanadium solution used for spin coating was prepared by combining equal quantities of 0.2 M strontium solution and 0.2 M vanadium solution. The 0.2 M strontium solution was obtained by dissolving strontium acetate in distilled water, and the 0.2 M vanadium solution was prepared by dissolving vanadium acetylacetonate in distilled water containing 10 % ethanol. Additionally, two different treatment techniques were carried out on the glass substrates to improve the wettability. The first method was through hydrolysis, where the glass substrate was placed in a 200 mL hydrothermal reactor containing 70 mL of distilled water and heated for 24 h at varying temperatures. The second method was through immersion of the substrate in 40 mL of 5 mM $KMnO_4$ solution containing 0.4 mL of methanol. The coating parameters were constant for all substrates: rotation speed (2000 RPM), ramping rate (500 RPM/s), spin duration (30 s), solution volume (100 μL), substrate size (25 mm x 25 mm), and drying (70 °C, 1 min).

2. Results

For the best possible adhesion, the surface tension of the liquid should ideally be less than that of the surface free energy of the substrate, which can be observed by a decrease in the contact angle of the liquid on the substrate. Fig. 1 shows the effect of wettability on untreated and treated glass substrates. Compared to the untreated substrate, the treated substrates showed a significant decrease in the contact angle of the 50 μL water droplet, indicating an improvement in the substrate's wettability. Fig. 2 shows the high-resolution transmission electron microscope (HR-TEM) bright field image along with an energy X-ray dispersive spectroscopy (EDS) map of the thin film layer. From the micrograph, the thin film thickness was found to be 14 nm, and the EDS map showed that the elements of interest, vanadium, and strontium were uniformly distributed across the film.
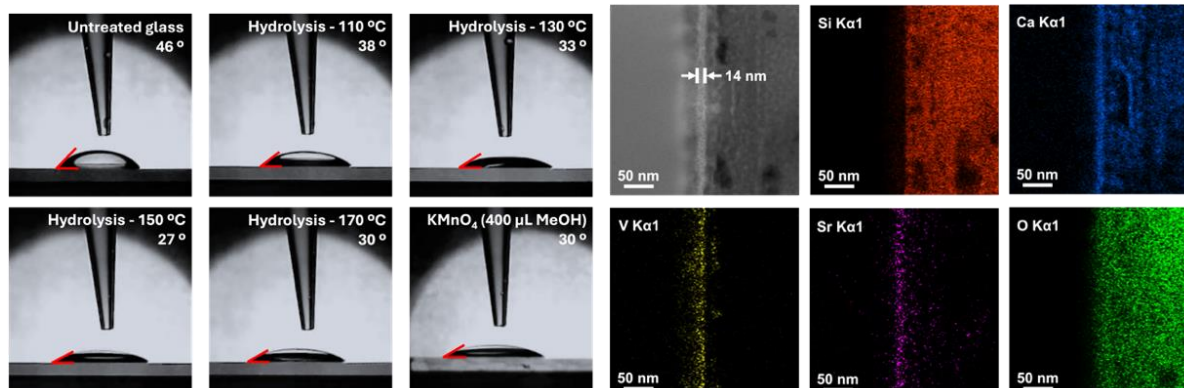
Fig. 1: Contact angle of 50 μL of water on untreated and treated glass substrates.

Fig. 2: HR-TEM bright field micrograph with EDS mappings of the thin film cross-section on a hydrolysed substrate.

3. References

[1] Jayathilake, D.S.Y. and Mirmal, P.T.A., J. Mater. Chem. Eng., **1** (2018) 1-7
[2] Frank, G. and Höstlin, H., Appl. Phys. A Soldis Surfaces, **27** (2082) 197-206

Analysis of Er^{3+} concentration on the structural, and optical properties of $CaAl_2O_4$: 0.1 % Y^{3+}, x % Er^{3+} (0 < x ≤ 2.0) synthesized using citrate sol-gel method

E. Nkuna[1][**], M.R. Mhlongo[1], C. Dlamini[1,2], L.T. Melato[2], R.E. Kroon[3], V.M. Maphiri[1][*], A. Bele[1][***]

[1]*Department of Physics, Sefako Makgatho Health Sciences University, P. O. Box 94, Medunsa, 0204, South Africa*
[2]*Department of Applied Physical Sciences, Vaal University of Technology, Andries Potgieter Blvd, Vanderbijlpark, 1900, South Africa*
[3]*Department of Physics, University of the Free State, P. O. Box 339, Bloemfontein 9300, South Africa*
Corresponding author:abongile.bele@gmail.com, vusanimuswamaphiri@gmai.com and erencele@gmail.com

1. Introduction

Rare earth ions (RE^{3+}) doped nanophosphors have emerged as materials with great potential in light-emitting diode (LED) manufacturing [1]. This work presents a study on $CaAl_2O_4$ doped with Y^{3+} and Er^{3+}, respectively. The concentration of 0.1 mol% Y^{3+} has been chosen based on prior knowledge, experimental considerations, and the desire to explore a specific range of dopant concentrations for the purpose of understanding and optimizing the structural and optical properties of the synthesized material. Hence in this study, we are presenting for the first time the visible luminescence of $CaAl_2O_4$ phosphor co-activated by Er^{3+} synthesized using the citrate sol-gel route. Therefore, this present study aims to thoroughly examine the effect of Er^{3+} co-doping on $CaAl_2O_4$:0.1 mol% Y^{3+}, x mol% Er^{3+} (0 < x ≤ 2.4) to gain a comprehensive understanding of the material properties of $CaAl_2O_4$. The primary objective is to develop more promising oxides for various applications. Our results suggest that this phosphor has the potential for application in lighting where blue-emitting phosphors are desired.

2. Results

The citrate sol-gel was successfully adopted to synthesize $CaAl_2O_4$: 0.1 % Y^{3+}, x % Er^{3+} (0 < x ≤ 2.0) samples. The X-ray diffraction (XRD) peaks appear well-defined and sharp, indicating a high level of crystallinity. Furthermore, the patterns verified that each sample exclusively comprised the monoclinic $CaAl_2O_4$ structure, indicating the presence of a single phase in all samples. The Rietveld analysis confirmed that all the samples consist of a single phase, and the unit cell dimensions of the host are a = 8.748 Å, b = 8.093 Å, c = 15.15 Å, and $α$ = $γ$ = 90 º, $β$ = 90.029º. The EDS confirmed the expected elemental composition. SEM revealed that the introduction of dopants causes a change in the morphology of the synthesized nanophosphor. UV–vis results showed that the optical bandgap (E_g) can be tuned between 4.93 – 5.44 eV by increasing the concentration of Er^{3+}. The PL shows the presence of the host and Er^{3+} which are at 417, 440, 467, 522, 546, 557, and 568 nm corresponding to the oxygen vacancies and the Er^{3+} transitions. The Commission Internationale de l'Eclairage (CIE) shows that the emission colour can be tuned from greenish blue to yellowish green by varying the concentration of Er^{3+}.
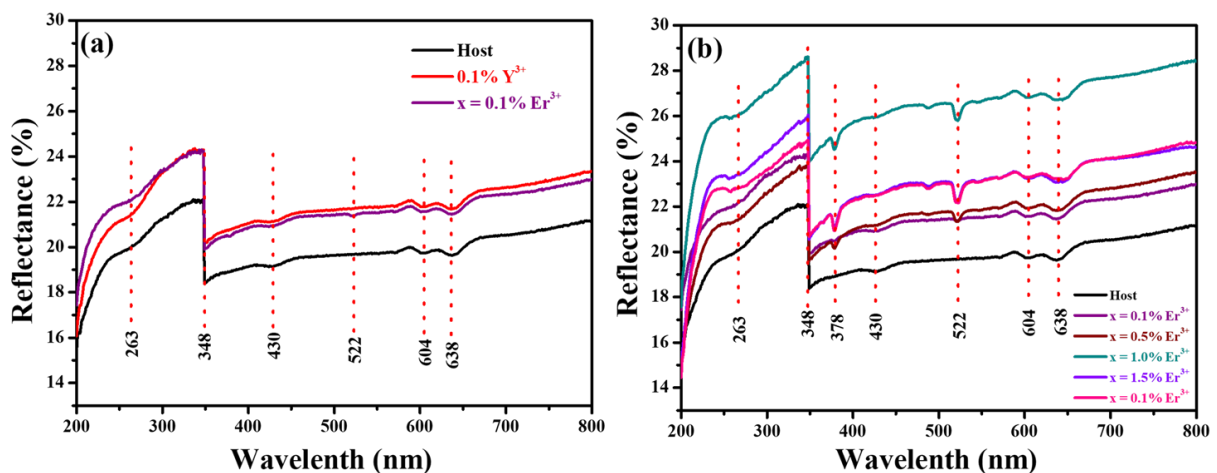
Fig. 2: The diffuse reflectance spectra of (a) host, singly doped with 0.1 mol% Y^{3+} (b) host and co-doped $CaAl_2O_4$:0.1 mol% Y^{3+}, x mol% Er^{3+} at varying concentration of Er^{3+}

3. References

[1] Y. Takebuchi, H. Fukushima, T. Kato, D. Nakauchi, N. Kawaguchi, T. Yanagida. *Jap. J. of App. Phys.* **59** (2020) 052007.

10th South African Conference on Photonic Materials – Amanzi 2025

$(VO_4)_2$ phosphors for light emitting diodes

A. K. Bedyal[1], H. C. Swart[2] and Vinay Kumar[2, 3]

[1]*Department of Physics, School of Sciences, Cluster University of Jammu, Canal Road, J & K 180001, India*
[2]*Department of Physics, University of the Free State, P.O. Box 339, Bloemfontein, ZA9300, South Africa*
[3]*Department of Physics and Astronomical Sciences, Central University of Jammu, Raya-Suchani, Samba, J & K, India*
Corresponding author: *vinaykdhiman@yahoo.com, ankushkumar@clujammu.ac.in*

1. Introduction

Currently, the increasing demands for low-cost, energy-saving, high-efficiency, and durable lighting devices have attracted the attention of researchers to develop new phosphor-converted LEDs that can effectively be excited in the blue, near-ultraviolet and ultraviolet range [1-2]. In particular, white light-emitting diodes (w-LEDs) are now rapidly replacing the traditional incandescent, fluorescent, and discharge lamps because of their highly desirable characteristics [3]. A lot of attention has been given to Zinc-based vanadates doped with the trivalent rare-earth (RE) ions due to their unique luminescence properties under UV and near-UV excitation for different potential applications in lighting devices. In this study, we have chosen $Zn_3(VO_4)_2$ as the host matrix due to its self-emitting property in the yellow region. This study reports the luminescence and surface properties of the $Zn_3(VO_4)_2$ doped with varying concentrations of Eu^{3+} synthesized by combustion method. These properties of this phosphor are considered to explore their importance in solid-state lighting and LED displays based on near-UV (300–400 nm) LED chips.

2. Results:

Fig. 1 shows the emission spectra of the Eu^{3+} doped $Zn_3(VO_4)_2$ phosphors excited at 397 nm. The spectra consist of a broad band from 400 to 800 nm and four sharp peaks at 593 nm, 613 nm, 655 nm, and 699 nm. The broadband arises due to the charge transfer of an electron from the oxygen 2p orbital to the vacant 3d orbital in the tetrahedral VO_4 with T_d symmetry in the host matrix, whereas the sharp peaks at 593 nm, 613 nm, 655 nm, and 699 nm correspond to $^5D_0 \rightarrow ^7F_1$, $^5D_0 \rightarrow ^7F_2$, $^5D_0 \rightarrow ^7F_3$ and $^5D_0 \rightarrow ^7F_4$ transitions of Eu^{3+} ions, respectively. The spectra also depict that the intensity of the sharp peaks corresponds to the Eu^{3+} ions increases with the increase in Eu^{3+} ions concentration. Luminescence is very much related to the surface of the material; hence surface properties of the synthesized materials have been investigated. The X-ray photoelectron spectroscopy (XPS) survey scan spectrum of the phosphors is presented in Fig. 2. The spectrum confirms the presence of all the elements (Zn, V, O, Eu) of the phosphor on the surface of the material. The corresponding XPS peaks are indexed along with the Auger peaks corresponding to their binding energies.
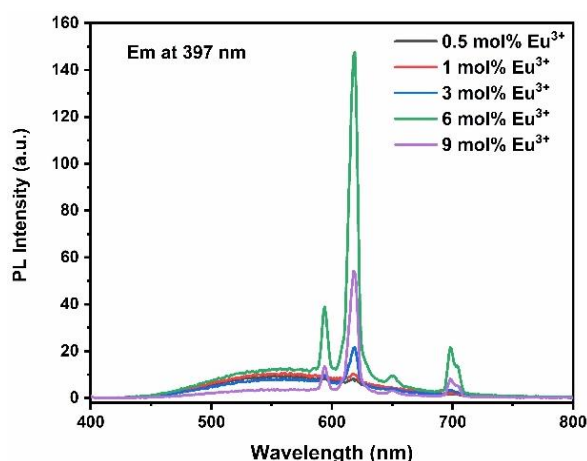
Fig.1 Photoluminescence spectra of Eu^{3+} doped $Zn_3(VO_4)_2$ phosphor at various Eu^{3+} concentration.
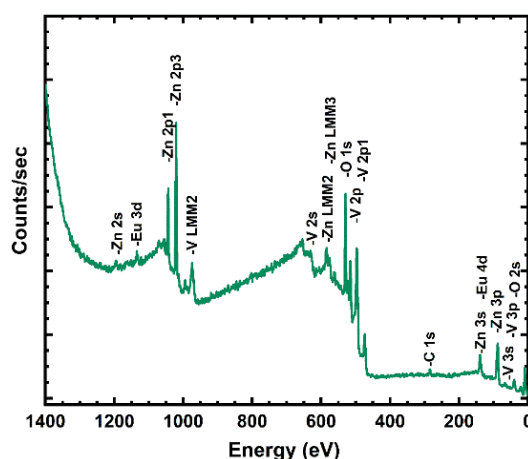
Fig.2 Survey scan spectra of the Eu^{3+} doped $Zn_3(VO_4)_2$ phosphor synthesized.

3. References:

1. A. K. Bedyal, Vinay Kumar, R Prakash, OM Ntweaborwa, Swart H C *Appl. Surf. Sci*. **329** (2015) 40.
2. J. Huang, Q Li, D Chen, *Mater Sci Eng B* **172** (2010) 108.
3. S Ye, F Xiao, YX Pan, YY Ma, QY Zhang, *Mater Sci Eng R Rep*. **71**(1) (2010) 1

Broadband spectral conversion and light management for next generation greenhouses

Bryce S. Richards[1,2]**, Ewan Gage**[3]**, Boris Breiner**[4]**, Monica Saavedra**[4]**, Norbert Janowicz**[5]**, Dominic S. Wright**[5]**, A. Yousif**[1,6]**, Yu Tian**[1]**, J.N. Fru**[1]**, Andrey Turshatov**[1]**, D. Busko**[1]**, Gan Huang**[1]

[1] *Institute of Microstructure Technology, Karlsruhe Institute of Technology, 76344 Eggenstein-Leopoldshafen, Germany*
[2] *Light Technology Institute, Karlsruhe Institute of Technology, 76133 Karlsruhe, Germany*
[3] *Centre for Soil, Agrifood and Biosciences, Cranfield University, Bedford, U.K.*
[4] *Lambda Energy Ltd., Cambridge, U.K.*
[5] *The Yusef Hamied Department of Chemistry, University of Cambridge, Cambridge CB2 1EW, U.K.*
[6] *Department of Physics, Box 321, University of Khartoum, Omdurman, 11115, Sudan*
Corresponding author e-mail address: bryce.richards@kit.edu

Summary

In today's agriculture, greenhouses play a key role in realising the security of the global food supply. Year-round crop production is enabled – even in extreme climates – via their controlled environment. Greenhouses feature strongly in the food-energy-water nexus, seeking to utilise advanced technologies that optimise resource use. One example of this is the drastically reduced water consumption, which in some cases can be up to 90% less than open-field farming. With the global population projected to be more than 9.7 billion by 2050, greenhouses are important for feeding these hungry mouths and realising sustainable agriculture. Currently, it is estimated that greenhouses occupy about 1.2 million acres of agricultural land in 130 countries around the world – convincing evidence of the level of adoption of the technology and its role in modern food systems.

Traditional greenhouses are made of either i) metal frames with glass walls and ceiling; or ii) simpler plastic materials formed into what is known as a polytunnel. More advanced greenhouses now implement climate-control systems, which are very energy-intensive, indeed their environmental footprint is strongly impacted by this. More recent advances in greenhouse technology have aimed to further improve their performance. For example, the use of *agri-photovoltaic* systems can enable electricity generation and, at the same time, crop cultivation – ideally while land-use efficiency is optimised. In addition, spectral-conversion (luminescent) materials are able to boost the rate of photosynthesis – and thus plant growth – by converting the underutilised wavelengths in the solar spectrum – predominantly in the ultraviolet and green – into wavelengths that are more useful plants, i.e. matching better the photosynthetically active radiation (PAR) spectrum. Recent advances in passive daytime radiative cooling allow for improved thermal management to passively dissipate heat, minimising the reliance on electrical cooling/ventilation systems. Finally, novel water harvesting systems that rely on advanced materials and designs can enable moisture to be captured directly from the atmosphere, assisting with meeting water scarcity challenges. Altogether, these advances demonstrate significant potential for the next-generation of greenhouse technologies that can assist in overcoming traditional limitations, whilst enabling food production in a more sustainable and resource-efficient manner.

Plant growth is affected by four key factors: i) light – spectrum, intensity, and the level of diffusivity; ii) water availability, including moisture in the air and soil); iii) the temperature – again, both in the air and in the soil; and iv) the levels of carbon dioxide (CO_2) concentration inside the greenhouse. These factors are all strongly interlinked and combine to impact plant growth and productivity. A key goal for next-generation greenhouses is to achieve net-zero energy (NZE) consumption. This currently poses a major challenge due to the energy consumption needed for the regulation of the greenhouse microclimate. Additionally, one also needs to avoid competing for the same resource, e.g. photosynthesis and photovoltaics both require space and access to sunlight. Here, compromises must be avoided, and synergies need to be found. To achieve this, a transdisciplinary effort is required to pave the way toward developing next-generation NZE greenhouses. This paper will discuss the opportunities and challenges for next-generation greenhouses.

Wednesday 9 April 2025

Time	Wednesday
	9 April
09h00 - 09h15	Announcements
	Chair J.J. Terblans
09h15 - 10h00	**Plenary: Andrey Turshatov**
10h00 - 10h20	7. Hope Ramolahloane
10h20 -10h40	8. Murendeni Nemufulwi
10h40 - 11h00	9. Kashma Kashma
11h00 - 11h20	Tea / Coffee Break
	Chair M.M. Duvenhage
11h20 - 11h40	10. Thandi Mazibuko
11h40 - 12h00	11. Konstantin Zloshchastiev
12h00 - 12h20	12. Thapelo Ephraim Seimela
12h20 - 13h30	**Lunch (Sable Hall)**
	Chair J. Nel
13h30 - 14h00	**Invited: Thomas Lippert**
14h00 - 14h20	13. Rethabile Makhole
14h20 - 14h40	14. Chinedu Ahia
14h40 - 15h00	15. S.P. Khambule
15h00 – 15h20	Afternoon Tea (15h00 - 15h20)

Bright Ideas: How Luminescent Tracers Improve Plastic Recycling, Energy Conversion, and Counterfeit Detection

Turshatov Andrey

Institute of Microstructure Technology, Karlsruhe Institute of Technology, Hermann-von-Helmholtz-Platz 1, 76344 Eggenstein-Leopoldshafen, Germany
Corresponding author e-mail address: andrey.turshatov@kit.edu

Over the past few decades, lanthanide-activated materials have attracted considerable attention from researchers worldwide. Extensive studies have explored their synthesis protocols, as well as their structural, morphological, and luminescence properties. This growing interest stems from their broad range of industrial applications, including phosphors for light-emitting diodes, lasers, scintillation materials, and luminescent tracers in medicine. In this work, I present a critical analysis of unconventional (UC) and short-wave infrared (SWIR) light applications of lanthanide-based materials, focusing on their emerging roles as markers for plastics recycling[1,2] and spectral conversion materials in photovoltaics[3,4]. These novel applications highlight the expanding potential of lanthanide-based materials in advanced sustainable technologies.

References

[1] I. A. Howard, D. Busko, G. Gao, P. Wendler, E. Madirov, A. Turshatov, J. Moesslein, B. S Richards *Resources, Conservation and Recycling* **205** (2024) 107557.
[2] N. M. Bhiri, H. Duim, E. Madirov, J. Nyarige, B. S. Richards, A. Turshatov *Journal of Materials Chemistry C* (2025) https://doi.org/10.1039/D4TC04096A
[3] B. S Richards, D. Hudry, D. Busko, A. Turshatov, I. A. Howard *Chemical Reviews* **121** (2021) 9165-9195.
[4] R. Singh, E. Madirov, D. Busko, I. M. Hossain, V. A. Konyushkin. A. N. Nakladov, S. V. Kuznetsov, A. Farooq, S. Gharibzadeh, U. W. Paetzold, B. S. Richards, A. Turshatov *ACS Applied Materials & Interfaces* **13** (2021) 54874-54883

Ca$_5$M$_4$(VO$_4$)$_6$) (M = Mg, Zn) and its applications in latent fingerprint imaging

Hope Ramolahloane, Govind Nair, Hendrik Swart

Department of Physics, University of the Free State, P. O. Box 339, Bloemfontein, 9300, South Africa,
Corresponding author e-mail address: SwartHC@ufs.ac.za

1. Introduction

Calcium magnesium vanadate (Ca$_5$Mg$_4$(VO$_4$)$_6$) (CMV) is a self-activated phosphor, has a broad emission in the 400-700 nm region of the electromagnetic spectrum and benefits from a simple solid-state synthesis technique at relatively low temperatures [1]. Calcium zinc vanadate (CZV) and CMV have received very little research attention. To the best of our knowledge, the earliest study of the photoluminescent properties of CMV or CZV was published in 2012, and since then, very little attention has been given to the materials [2] As of January 2025, the number of search results for "Ca$_5$Mg$_4$(VO$_4$)$_6$" and "Ca$_5$Zn$_4$(VO$_4$)$_6$" on Google Scholar, were 35 and 3, respectively. The number of search results for the less common variations of CMV and CZV, namely, "Ca$_5$Mg$_4$V$_6$O$_{24}$" and "Ca$_5$Zn$_4$V$_6$O$_{24}$" were 14 and 0, respectively. Among these total 52 search results, only 13 were studies focused on either CMV or CZV. The little research attention received by CMV and CZV provides the opportunity to produce new information about the luminescent properties of the materials. The large Stoke's shift of these materials makes them ideal for fingerprint imaging, since this property is expected to result in low interference from the exciting light source and high contrast of the latent fingerprint images. CMV and CZV demonstrate excellent thermal stability and high stability in wet air atmospheres, making them ideal for the long-term storage of latent fingerprints [3]. For this study, CMV and CZV will be fabricated using a solid-state reaction and investigated for latent fingerprint detection.

2. Results

The XRPD patterns of CMV and CZV showed a cubic garnet structure with space group Ia-3d. CMV and CZV were fabricated via solid-state synthesis at different temperatures. CMV was fabricated with reaction temperatures up to 1100 °C. Temperatures above 900 °C were too high for the fabrication of CZV. Both CMV and CZV showed a PL emission in the range of 400-800 nm, with a peak at 550 nm. The reaction temperature of 800 °C produced the most intense peak for both CMV and CZV.
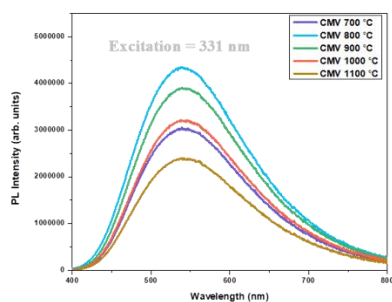
Fig. 3: PL spectra of Ca$_5$Mg$_4$(VO$_4$)$_6$ crystals synthesized with reaction temperatures of 700-1100 °C
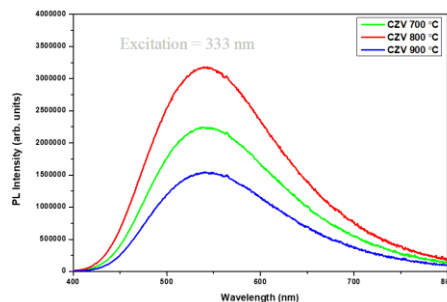
Fig. 2: PL spectra of Ca$_5$Zn$_4$(VO$_4$)$_6$ crystals synthesized with reaction temperatures of 700-900 °C.

3. References

[1] K. Li, J. Liu, D. Mara, and R. Van Deun, "Synthesis and up-conversion luminescence properties of a novel Yb^{3+}, Er^{3+} co-doped Ca$_5$Mg$_4$(VO$_4$)$_6$ phosphor," J Alloys Compd, vol. 737, pp. 767–773, Mar. 2018, doi: 10.1016/j.jallcom.2017.12.171.
[2] Y. Huang, Y. M. Yu, T. Tsuboi, and H. J. Seo, "Novel yellow-emitting phosphors of Ca$_5$M$_4$(VO$_4$)$_6$ (M=Mg, Zn) with isolated VO$_4$ tetrahedra," Opt Express, vol. 20, no. 4, p. 4360, Feb. 2012, doi: 10.1364/OE.20.004360.
[3] A. S. Tolkacheva, S. N. Shkerin, K. G. Zemlyanoi, O. G. Reznitskikh, S. V. Pershina, and P. D. Khavlyuk, "Thermal and electrical properties of Ca$_5$Mg$_{4-x}$Zn$_x$(VO$_4$)$_6$ (0 ≤ x ≤ 4)," J Therm Anal Calorim, vol. 136, no. 3, pp. 1003–1009, May 2019, doi: 10.1007/s10973-018-7780-z.

Induced Structural Defects by Anion Doping of ZnO for Gas Sensing Application

Murendeni I. Nemufulwi[1,], Mosima B. Kgomo[1], Gugu H. Mhlongo[1,2], Mokhotjwa S. Dhlamini[1,2]

[1] *Department of Physics, University of the Free State, Bloemfontein ZA9300, South Africa*
[2] *Centre for Nanostructures and Advanced Materials (CeNAM), DSI-CSIR Nanotechnology Innovation Centre, Council for Scientific and Industrial Research, Pretoria 0001, South Africa*
[3] *Department of Physics, University of the Free State, Bloemfontein ZA9300, South Africa*
Corresponding author e-mail address: murenn@unisa.ac.za

1. Introduction

ZnO is well well-known semiconducting metal oxide gas sensing material suitable for applications in several fields. The good chemical stability, low cost, and ease of fabrication make it suitable for agricultural applications. However, high operating temperatures, poor sensitivity, and selectivity still hinder its wide exploitation. This work aims to improve the sensing properties of ZnO by inducing structural defects through anion doping. A hydrothermal method was used to synthesize pure and suphur-doped- ZnO rods. The microstructure and morphology were analysed using XRD and HRTEM. Optical properties and structural defects of the products were studied using PL and EPR, while XPS was used for surface composition analysis.

2. Results

Fig. 1 shows the PL spectrum of the produced products after excitation at 325nm, which showed a substantial emission in the range of 470-600nm. A structural disorder occurs with the incorporation of S dopant resulting in an increase of defects at 0.5mol% of S [1]. The SEM images displayed in Fig. 2 (insert) show that the 0.5mol% S-doped ZnO is composed of one-dimensional rod-like structures, which are tangled together. The gas sensing results (Fig. 2) showed that the sensor based on 0.5% S-doped ZnO had an enhanced response of 14.2-90 ppm ammonia at an operating temperature of 280°C. The improved sensing properties can be attributed to structural defects induced by sulfur dopant which facilitate electron exchange during methanol oxidation [2].
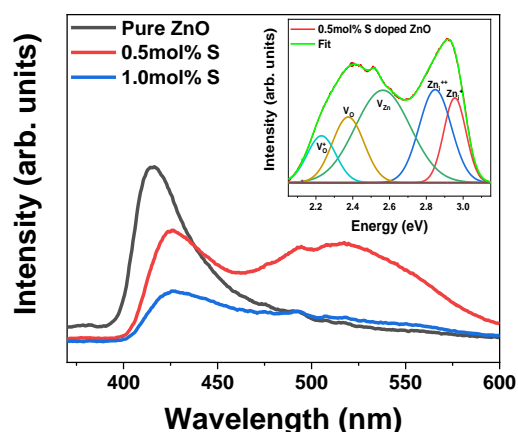
Fig. 4: PL emission spectra pure and S-doped ZnO products with insert of Gaussian fitting on the 0.5mol% S-doped ZnO product.
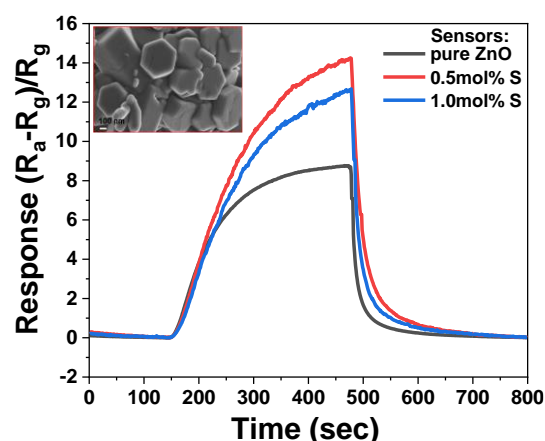
Fig. 2: Transient response curves of the S doped ZnO based sensors towards 90 ppm methanol at 280 °C and the corresponding SEM micrograph of 0.5mol% S doped ZnO.

3. References

[1] H. Von Wenckstern, H. Schmidt, M. Brandt, A. Lajn, R. Pickenhain, M. Lorenz, M. Grundmann, D.M. Hofmann, A. Polity, B.K. Meyer, H. Saal, M. Binnewies, A. Börger, K. Becker, V.A. Tikhomirov, K. Jug, Progress in Solid State Chemistry. 37 (2009) 153.
[2] Y. Li, B. Zhang, J. Li, Z. Duan, Y. Yang, Z. Yuan, Y. Jiang, H. Tai, Chemosensors. 12 (2024) 43.

Luminescence properties of $Ba_2La_8(SiO_4)_6O_2$: Sm^{3+} oxyapatite phosphors for near-UV-based solid-state lighting

Nisar Hussain[1], Seemin Rubab[1], Vishal Sharma[2], Hendrik C. Swart[3], Vijay Kumar[1,3], <u>Kashma Sharma[4*]</u>

[1]*Department of Physics, National Institute of Technology Srinagar, Jammu and Kashmir, 190006, India*
[2]*Institute of Forensic Science & Criminology, Panjab University, Chandigarh-160014, India*
[3]*Department of Physics, University of the Free State, P.O. Box 339, Bloemfontein, ZA9300, South Africa*
[4]*Department of Chemistry, DAV College, Sector-10, Chandigarh 160011, India*
Corresponding author e-mail address: shama2788@gmail.com (K. Sharma)

1. Abstract

In this study, a series of samarium (Sm^{3+}) doped silicate-based oxyapatite phosphors $Ba_2La_8(SiO_4)_6O_2$:xSm^{3+} (x = 0.01-0.05 mol%) was synthesized through the conventional high-temperature solid-state method. Phase confirmation was assessed using an X-ray powder diffraction (XRPD) analysis. Also, the photoluminescence excitation (PLE) and emission (PL) spectra of the synthesized phosphors were studied in detail. The PLE and PL spectra possess broadband peaks, with the most intense at 407 nm and 600 nm, respectively. The non-radiative energy transfer process occurred via multipolar interactions. Besides studying the concentration quenching mechanism, the decay dynamics of the synthesized phosphor were also investigated. The lifetime of the phosphors was found to decrease with increasing the concentration of dopants due to the increased likelihood of energy transfer between Sm^{3+}. Furthermore, the CIE coordinates of the synthesized phosphor were found to lie in the orange-reddish region of the color gamut with increasing color purity (70.2–95.9%) towards the reddish region with the ideal correlated color temperature (2090K). The obtained results suggest that the synthesized phosphor $Ba_2La_8(SiO_4)_6O_2$:xSm^{3+} can be effectively used for different applications of light-emitting diodes (LEDs) in various fields, especially for display and lighting purposes.

2. Results

Fig. 1 (a-b) shows the PLE and PL spectra of all synthesized $Ba_2La_8(SiO_4)_6O_2$:xSm^{3+} (x = 1-5 mol%) oxyapatite phosphors recorded at emission and excitation wavelengths of 600 and 407 nm, respectively. As shown in Fig. 1 (a), the multiple strong peaks in PLE spectra correspond to $4f^5$-$4f^5$ intra-configurational transitions from the Sm^{3+} ground state (6H5/2) to distinct excited states such as $^6H_{5/2} \rightarrow {}^4G_{9/2}$ (344 nm), $^6H_{5/2} \rightarrow {}^4D_{3/2}$ (369 nm), $^6H_{5/2} \rightarrow {}^4P_{7/2}$ (375 nm), $^6H_{5/2} \rightarrow {}^4P_{3/2}$ (406), $^6H_{5/2} \rightarrow {}^4P_{5/2}$ (419 nm), $^6H_{5/2} \rightarrow {}^4M_{17/2}$ (442 nm), and $^6H_{5/2} \rightarrow {}^4I_{11/2}$ (471 nm) [1]. PL spectra depicted in Fig. 1(b) show the emission profile from 525 to 750 nm. All the levels that get populated during the excitation process, including the main excitation level $^6P_{3/2}$ relax to the emitting level $^4G_{5/2}$ without giving off specific radiation. Multiphoton relaxation in-between the emitting level $^4G_{5/2}$ and the higher energy level of the ground state ($^6F_{11/2}$) does not take place due to the energy difference of 7200 cm^{-1} [2]. Therefore, the luminescence process occurs via non-radiative energy transfer and is highly affected by the cross-relaxation phenomenon occurring in between the Sm^{3+}-ions [3].
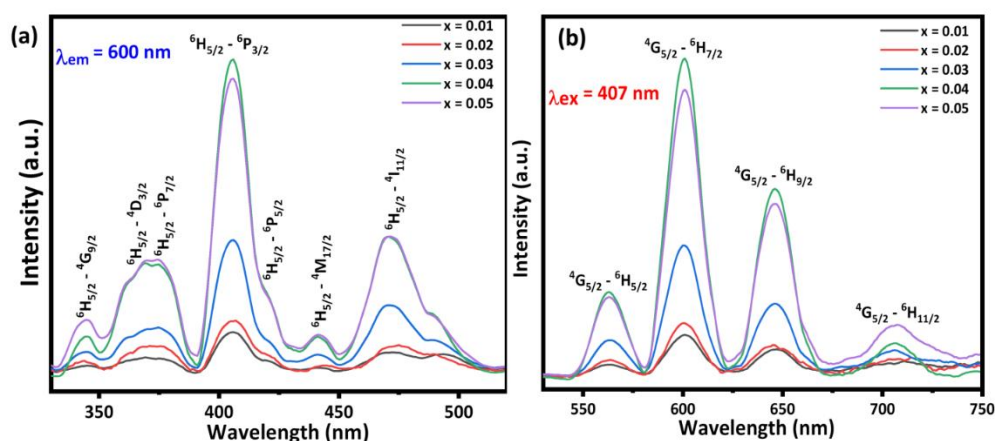
Fig. 5: (a) PLE (λ_{em} = 600 nm) and (b) PL (λ_{ex} = 407 nm) spectra of the synthesized $Ba_8La_2(SiO_4)_6O_2$:xSm^{3+} (x = 0.01, 0.02, 0.03, 0.04, 0.05 mol%) oxyapatite phosphor.

3. References

[1]   P. Kaur, S. Kaur, G.P. Singh, D.P. Singh. *Solid State Communication* **171** (2013) 22–25.
[2]   S. Kaur, A.S. Rao, M. Jayasimhadri. *Ceramic International* **43** (2017) 7401–7407.
[3]   V. Singh, G. Lakshminarayana, D.E. Lee, J. Yoon, T. Park. *Solid State Science* **98** (2019) 106042.

High colour purity red-emitting $Ca_2Y_{1-x}Zr_2(AlO_4)_3:xEu^{3+}$ phosphors for white LED applications.

Thandi Mazibuko, David Motaung, Hendrik Swart

Department of Physics, University of the Free State, 205 Nelson Mandela Dr, Bloemfontein, 9301
Corresponding author e-mail address: swarthc@ufs.ac.za

1. Introduction

White light-emitting diodes (wLEDs) have emerged as superior alternatives to traditional light sources due to their numerous advantages, including lower power consumption, extended lifetimes, and environmental friendliness [1-4]. The most successful approach to fabricating wLEDs involves combining a blue LED chip with a yellow-emitting phosphor (YAG:Ce^{3+}) [1-4]. However, due to the lack of a red component, the white light produced by YAG:Ce-based wLEDs exhibits a low color rendering index and highly correlated color temperature, which do not meet the requirements for warm white light emission [3,4]. Therefore, it is crucial to develop red-emitting phosphors as color converters [2,3]. Here, we report on red-emitting Eu^{3+}-activated $Ca_2Y_{1-x}Zr_2(AlO_4)_3$ (CYZA) garnet-type phosphors with high color purity. The crystal structure and spectroscopic properties of these phosphors were investigated in depth. Our work demonstrates that the prepared CYZA:Eu^{3+} red phosphor is a promising candidate for the red component in warm wLEDs based on n-UV LED chips (380–410 nm).

2. Results

Fig. 1 displays the room-temperature spectral properties of CYZA:xEu^{3+} ($0.01 \leq x \leq 0.05$). Five intense red emission peaks at 587, 588, 609, 654, and 705 nm, corresponding to the $^5D_0 \rightarrow {}^7F_J$ ($J = 0-4$) transitions of Eu^{3+} ions, are observed under 393 nm excitation. Fig. 2 presents the normalized integrated emission intensity of CYZA:xEu^{3+} phosphors as a function of Eu^{3+} doping concentration. The highest emission intensity was achieved at x = 4 mol% due to the concentration quenching effect. The calculated critical distance (R_c) value of 22.51 Å exceeds 5 Å, indicating that the Eu^{3+} non-radiative energy transfer process arises from electric multipole interactions [1-3]. The detailed energy transfer mechanism between Eu^{3+} ions in CYZA:xEu^{3+} phosphors was investigated using the following mathematical expression:

$$\log(I/x) = A - (\theta/3)\log(x) \tag{1}$$

Here, I refers to the emission intensity, x represents the doping concentration, and A denotes a constant [1-3]. The θ value for CYZA:xEu^{3+} phosphors was calculated to be 3.013, which is close to 3, suggesting that nearest-neighbour interactions caused the observed concentration quenching effect [5].

The optimal CYZA:$0.04Eu^{3+}$ sample exhibited CIE chromaticity coordinates of (0.635, 0.365) with a color purity of 92.9%, surpassing that of $Ca_2LaHf_2Al_3O_{12}:50\%Eu^{3+}$ (color purity = 92.7%) [3]. The decay lifetimes of the CYZA:xEu^{3+} samples were determined to be 2.26, 2.25, 2.20, 2.17, and 2.05 ms for x = 0.01, 0.02, 0.03, 0.04, and 0.05, respectively. The increasing Eu^{3+} concentration leads to a decrease in decay lifetimes, as the higher Eu^{3+} content increases the probability of non-radiative energy transfer. This is crucial evidence for energy transfer occurrence and the resulting concentration quenching of Eu^{3+} [1].
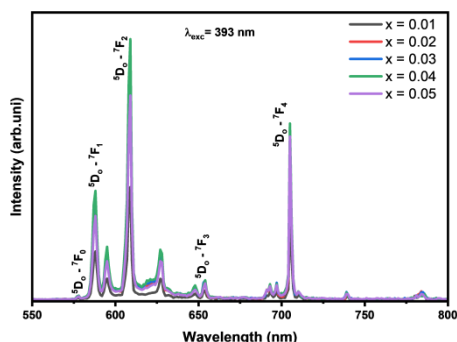
Fig. 6: Photoluminescence emission spectra of the CYZA:xEu^{3+} ($0.01 \leq x \leq 0.05$) phosphor.
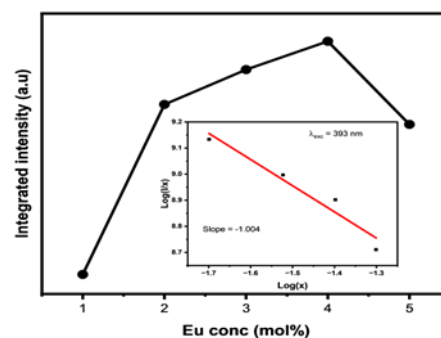
Fig. 2: The relative emission intensity of the CYZA:xEu^{3+} ($0.01 \leq x \leq 0.05$) samples (the inset represents the curve of log(x) and log(1/x).

3. References

[1] Y. Li, Q. Wei, H. Chen, and Y. Wang. *J. Alloys. Compd.* **864** (2021) 158840.
[2] M. Qu, Z. Pang, T. Li, Q. Liu, Y. Yang, and X. Zhang. *Ceram. Int.* **49** (2022) 792.
[3] N. Ma, W. Li, B. Devakumar, and X. Huang, X. *Inorg. Chem.* **61** (2022) 6898.
[4] H. Zhang, Y. Chen, X. Zhu, K. Liu, H. Zhou, X. Sun, N. Li, and Y. Feng. *J. Lumin.* **236** (2021) 118131.
[5] H. Deng, Z. Gao, N. Xue, J.H. Jeong, and R. Yu. *J. Lumin.* **192** (2017), 684.

Modern Statistical Approach to Open Quantum-Optical Systems

Konstantin G. Zloshchastiev[1]

[1] Institute of Systems Science, Durban University of Technology, Durban 4000, South Africa
Corresponding author e-mail address: kostiantynz@dut.ac.za

1. Introduction

In the conventional quantum mechanics of conserved systems, Hamiltonian is assumed to be a Hermitian operator. However, when it comes to open quantum systems, a strict Hermiticity requirement is no longer necessary. In fact, it can be substantially relaxed: the non-Hermitian part in a Hamiltonian is allowed, to account for the effects of the dissipative environment, whereas its Hermitian part would be describing the subsystem's energy. Within the framework of the quantum-statistical approach based on reduced density operators, utilizing both non-Hermitian Hamiltonian and Lindblad's jump operators, we derive various generalizations of the von Neumann equation for the reduced density operator, also known as the NH-Lindblad (a.k.a. NH-GKSL) hybrid master equation framework. This approach is arguably the most general quantum-statistical method based on reduced density matrices to date, an extensive bibliography can be found in [1].

2. Results

In a special case, if one is restricted to the evolution of pure states only then one can derive quantum-mechanical equations of the Schrodinger type [2]. In general, these equations are nonlinear with respect to wavefunction and nonlocal, which increases their capacity of describing complex quantum-optical phenomena in the presence of dissipation and noise. Among other features, they can describe not only systems, which remain in the stationary eigenstates of the Hamiltonian as time passes but also those, which evolve from those eigenstates.

As an example, we apply the method to a three-level atom interacting with two optical and one microwave fields in the adiabatic approximation resulting in a simplified description in terms of a two-level system. We assume this two-level system to be affected by two types of environments, described by some ad hoc non-Hermitian Hamiltonian and GKSL's models. We compare the three types of dissipative evolution, which can occur: driven by equations for a normalized density matrix, a non-normalized density matrix, and a normalized state vector. Using the latter type, we derive an effective Hamiltonian, which encodes information about not only the Hamiltonian part of an original master equation but also its non-Hamiltonian (Liouvillian) part. The Hamiltonian turns out to be dependent on the wavefunction itself: the effects of the above-mentioned environments induce, respectively, cubic and quintic nonlinear terms with respect to the wavefunction's magnitude [3].

3. References

[1] K. G. Zloshchastiev et al. *Project: Density Operator Approach for non-Hermitian Hamiltonians*. (ResearchGate, 2016-2025).
[2] K. G. Zloshchastiev. *Universe* **10** (2024) 36.
[3] K. G. Zloshchastiev. *J. Mod. Opt.* **71** (2025) 781.

Enhancing light absorption in photoactive layer of organic solar cells using plasmonic copper nanorods

Thapelo Ephraim Seimela[1], **Mohammed Hamed**[1], **Mmantsae Diale**[1]

[1]*Department of Physics, University of Pretoria, Private Bag X20, Hatfield 0028, South Africa*
Corresponding author e-mail address: mmantsae.diale@up.ac.za

1. Introduction

Bulk-heterojunction organic solar cells have brought much interest in renewable energy due to low cost and large-scale fabrication. Their power conversion efficiency (PCE) suffers from charge recombination limiting commercialisation. In this study, the plasmonic resonance of colloidal copper nanorods (CuNRs) have been employed to enhance light absorption inside phenyl-C_{60}-butyric acid methyl ester: poly(3-hexylthiophene) (P3HT:PCBM). The CuNRs with a diameter of 20.60 ± 0.54 nm and length of 57.81 ± 1.5 nm induced transverse and longitudinal absorption peaks at 450 and 680 nm respectively inside P3HT:PCBM (Fig. 2). The peaks intensify with an increase in the concentration of CuNRs. The lifetime of P3HT:PCBM in Fig. 1 is improved with the incorporation of CuNRs. The CuNRs have improved the ITO/PEDOT:PSS/P3HT:PCBM: CuNRs/Ag device by a PCE of 3.78%. Incorporating Cu NRs in P3HT:PCBM has the potential to improve the power conversion efficiency of ITO/PEDOT: PSS/P3HT:PCBM: CuNRs/Ag organic solar cell by inducing plasmonic resonance.

2. Results
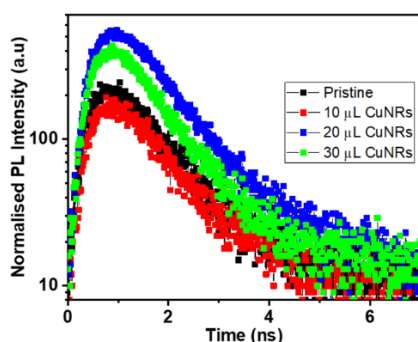
Fig. 7: TRPL spectra of P3HT:PCBM with different volumes of CuNRs using 473 nm excitation laser
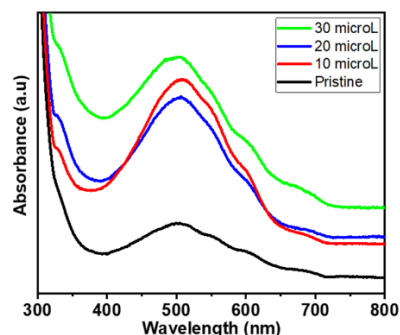
Fig. 2: UV-Vis spectra of CuNRs incorporated in P3HT:PCBM at different volumes

3. References

[1] P. Shen, Y. Liu, Y. Long, L. Shen, and B. Kang, "High-Performance Polymer Solar Cells Enabled by Copper Nanoparticles-Induced Plasmon Resonance Enhancement," The Journal of Physical Chemistry C, vol. 120, no. 16, pp. 8900-8906, 2016/04/28 2016.
[2] J. Rivera-Taco et al., "The role of silver nanoparticles in the hole transport layer in organic solar cells based on PBDB-T: ITIC," Journal of Electronic Materials, vol. 50, no. 7, pp. 4118-4127, 2021.

Pulsed Laser Deposition for Energy Materials

T. Lippert[1,2,3]

1- PSI Center for Neutron and Muon Sciences, 5232 Villigen PSI, Switzerland
2- International Institute for Carbon-Neutral Energy Research (WPI-I2CNER), Kyushu University, Fukuoka 819-0395, Japan
3- Laboratory of Inorganic Chemistry, Department of Chemistry and Applied Biosciences, ETH Zürich, 8093 Zürich, Switzerland

Corresponding author e-mail address: thomas.lippert@psi.ch

1. Introduction

A fundamental understanding of material properties and reactions in energy materials can often be achieved through advanced large-facility techniques, such as those available at synchrotrons or neutron sources. These techniques provide unique insights but often require well-defined samples with controlled properties, including crystallinity, surface roughness, and interface quality. Such requirements are frequently met by using thin films. To this end, we employ Pulsed Laser Deposition (PLD) (1) to fabricate thin films, enabling the application of complementary methods ranging from neutron reflectometry (NR) to grazing incidence X-ray absorption spectroscopy (GIXAS).

2. Results

One material system we study involves Li-containing materials for Li-ion batteries, with the ultimate goal of developing a thin-film battery entirely fabricated by PLD. A major challenge in this approach is identifying a suitable solid electrolyte that retains its properties in thin-film form. Many oxide electrolytes, such as LLZO ($Li_7La_3Zr_2O12$) or LLTO ($Li_{3x}La_{(2/3-x)}TiO_3$), do not meet these criteria. Additionally, it is essential to identify oxide-based electrode materials (anode and cathode) that are compatible with the solid electrolyte, particularly in terms of deposition conditions and interfacial properties.

Another key area of our work focuses on oxynitrides, which are used as photoanodes for photo-electrochemical (PEC) water splitting. Despite their promise, this material class suffers from rapid activity decay during the initial electrochemical cycles and a gradual long-term decline. The long-term decay is likely linked to material degradation, such as nitrogen loss. However, the fast decay remains poorly understood, hindering the development of strategies to address it.

By utilizing thin films as model systems, we studied the mechanisms behind the fast decay. Using neutron reflectometry (NR), we observed a surface modification within a 3 nm region, manifested as a density change. Concurrently, X-ray absorption spectroscopy (XAS) revealed alterations in the oxidation states of constituent elements. Specifically, the A cation exhibited changes in oxidation state, while the B cation (e.g., in LaTiOxNy) (2,3) traditionally considered the active site, underwent localized disordering. This surface modification compromises water-splitting activity. However, we identified a co-catalyst capable of suppressing these modifications.

Our investigations uncovered critical steps in the PEC water-splitting mechanism. During surface modification, the formation of NO_x competes with the desired oxygen evolution reaction (OER). Without highly defined, high-quality PLD-fabricated thin films, it would not have been possible to leverage large-facility techniques to uncover and mitigate the origins of activity decay in oxynitrides for water splitting.

Additionally, a new PLD chamber has been setup that allows the deposition of halide perovskites, and the first results of single-oriented films will be shown.

3. References

[1] N. A. Shepelin, Z. P. Tehrani, N. Ohannessian, C. W. Schneider, D. Pergolesi and T. Lippert; *A practical guide to pulsed laser deposition,* Chem. Soc. Rev. **52**, 2294–2321 (2023)
[2] D. Pergolesi; C. Lawley; and T. Lippert, *Thin-Film Oxynitride Photocatalysts for Solar Hydrogen Generation: Separating Surface and Bulk Effects Using Synchrotron X-Ray and Neutron-Based Techniques,* Sol. RRL, 2200286 (2022)
[3] C. Lawley; Z. Pourmand Tehrani; A. H. Clark. O. V. Safonova; M. Döbeli; V. N. Strocov; T. J. Schmidt; T. Lippert; M. Nachtegaal; and D. Pergolesi; *Protagonists and spectators during photocatalytic solar water splitting with SrTaO_xN_y oxynitride,*J. Mater. Chem. A, **10**, 2374–2387 (2022)

Temperature-dependent PL emission and catalytic oxidation of xylene isomers by Co_3O_4 nanostructures

Rethabile Makole, Hendrik C. Swart, David E. Motaung

Department of Physics, University of the Free State, Bloemfontein, Park West, 9301

Rethabilemakole09@gmail.com

1. Introduction

Catalytic oxidation of volatile organic compounds such as carbon monoxide, ethanol, toluene, propane, and xylene by Co_3O_4 is a chemical process that is largely influenced by the presence of Co^{3+}, Co^{2+} cations, and oxygen vacancies [1,2]. In particular, the Co^{3+}/Co^{2+} ratio has been proven to be beneficial towards improved catalytic performance of Co_3O_4. It follows that the amount of Co cations in Co_3O_4 is reliant on the dominating crystal plane on the surface and surface morphology [1,2]. Other material properties that have been reported to play a vital role during catalytic reactions are the configuration of the particles and their sizes, surface area, and crystal defects [3]. These properties can be modified and are ultimately determined by the synthesis method and parameters. A simple approach to correlating these properties to the catalytic performance of Co_3O_4 is by studying how they influence each other.

The photoluminescence (PL) is one of the techniques used to study crystal defects relating to oxygen vacancies. Paired with UV-Vis absorbance/reflectance measurements, more information regarding crystal defects and their origin within the material can be understood. Herein, we investigate the effects of crystal defects on the selective catalytic oxidation of p-xylene by Co_3O_4 nanostructures hydrothermally synthesized at different temperatures.

2. Results

In a series of tests done to determine the catalytic performance of Co_3O_4 nanostructures to xylene isomers (m-xylene, o-xylene, p-xylene), the highest sensitivity was shown by Co_3O_4 nanostructures synthesized at 160 °C, named Co-160. As shown in Fig. 1, high sensitivity is also observed for m-xylene and o-xylene at 150 °C operating temperature. The temperature-dependent PL emission spectrum of Co-160 shows that as the temperature is increased, the emission is quenched. This indicates that at high temperatures, the effect of crystal defects may be minimized and therefore result in improved sensitivity of Co-160 to xylene isomers.
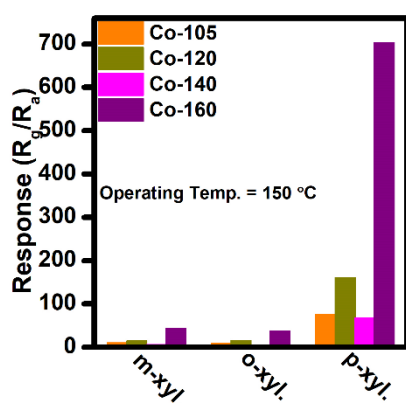
Fig. 1: Response of Co_3O_4 nanostructures to xylene isomers at 150 °C working temperature.
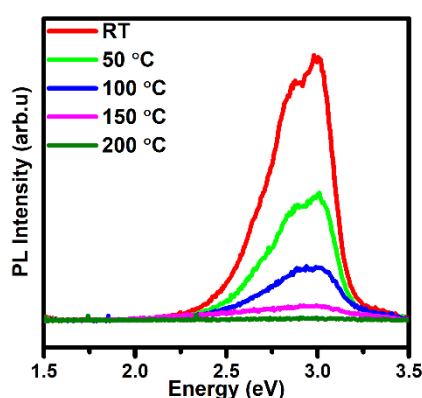
Fig. 2: Temperature-dependent PL emission spectrum of Co-160.

3. References

1. Dey, S. and Dhal G.C. *Mater. Today Chem.* **19**, 100198 (2019).
2. Zhu, W. *et al. Chin. J. Cata.l* **41**, *679–690* (2020).
3. Kozlovskiy, A.L. and Zdorovets, M.V. *Compos. B Eng.* **191,** 107968 (2020)

Numerical Simulation and Performance Optimization of Antimony-based Halide Perovskite Solar Cell Using Kesterite as Hole Transport Material

Chinedu Christian Ahia[1], **Nicholas Rono**[1], **Edson Leroy Meyer**[1]

[1] Fort Hare Institute of Technology, University of Fort Hare, Private Bag X1314, Alice 5700, South Africa
Corresponding author e-mail address: chinedu@aims.ac.za

1. Introduction

Numerous studies and advancements in solar energy technologies have been reported due to the consistent increase in energy demand and the transition to a solar-dominated energy mix. All-inorganic cesium antimony iodide ($Cs_3Sb_2I_9$) are halide perovskites which have attracted remarkable attention from researchers due to their unique properties and prospective applications in optoelectronics and photovoltaics. They have a bandgap of 2.05 eV [1] and have been investigated as a light-absorbing layer during the development of lead-free perovskite solar cells (PSCs) [2]. Likewise, kesterites are quaternary chalcogenide semiconductors that have been explored as potential hole transport materials in PSCs because of their tunable bandgap, p-type conductivity, non-toxicity, and good stability under ambient conditions. This study is aimed at addressing challenges linked with device performance optimization and exploring sustainable alternative materials for reducing recombination and facilitating hole transport in Pb-free PSCs.

2. Results

Numerical simulation of the device with general architecture $FTO/WS_2/Cs_3Sb_2I_9/CZTSe/Au$ was executed using SCAPS-1D software with CZTSe as the hole transport layer (HTL), while $Cs_3Sb_2I_9$ was used as the absorber material. The influence of various parameters on the device such as the effect of changing the doping density of the HTL, the density of defect of the absorber layer, and the device operational temperature were investigated in the present study for optimal performance of the device. In this study, an optimal power conversion efficiency (PCE) of up to 21.02% with a fill factor (FF) of 81.94% was achieved for the proposed device configuration. Furthermore, an open-circuit voltage (V_{oc}) of 0.817 V and a short-circuit current density (J_{sc}) of 31.4 mAcm^{-2} were achieved for the structure. Detailed discussion on the interface engineering, charge dynamics, and the device physics of the proposed architecture will be discussed.
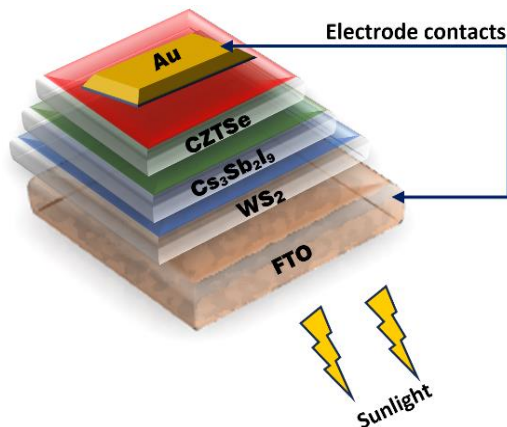
Fig. 8: Schematic cross-sectional representation of device structure
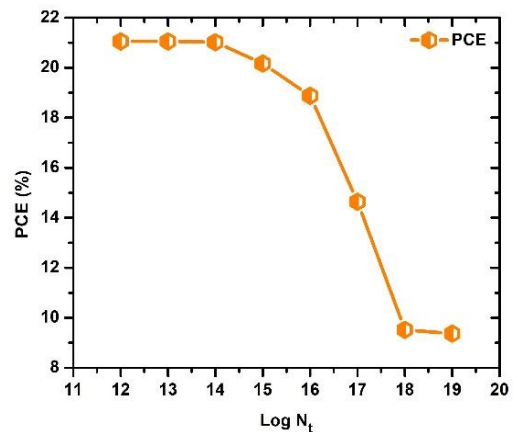
Fig. 2: Effect of defect density on the PCE of the proposed device.

3. References

[1] B. Saparov, F. Hong, Jon-Paul Sun et al. *Chem. Mater.* **27** (2015) 5622−5632.
[2] K. Ahmad, M. Q. Khan, H. Kim. *Optical Materials* **128** (2022) 112374.

Impact of annealing time on the properties of $ZnAl_2O_4$-CuO nanomaterials: A comparative study of NaOH and NH_4 as precipitating agents

S. P. Khambule[1]*, L. F. Koao[2], M. A. Malimabe[1]

[1]*Department of Chemistry, University of the Free State (Qwa Qwa Campus), Private Bag X13, Phuthaditjhaba, 9866, South Africa*
[2]*Department of Physics, University of the Free State (Qwa Qwa Campus), Private Bag X13, Phuthaditjhaba, 9866, South Africa*
Corresponding author email address (*): spkhambule31@gmail.com

1. Introduction

An increased interest in metal oxides is due to their ability to modify their properties for various applications[1]. Morphology and size can influence nanoparticle properties; therefore, synthesis conditions are altered to control these factors, including reaction time, temperature, pH, etc [2,3]. Nanomaterials containing other semiconductors and metal nanoparticles are incredibly efficient. Precipitating agents, solvents, and surfactants influence the nanoparticle's properties. Annealing is advantageous for nanomaterials as it enhances their durability, reduces their stiffness, and improves their machinability, thereby increasing their overall workability. Therefore, this study seeks to investigate the influence of synthesis conditions and heat treatment on $ZnAl_2O_4$-CuO, which will be used in an ongoing study of modifying road materials.

2. Results

Thermogravimetric analysis revealed that the material exhibits good thermal stability in the temperature range of 500 to 800 °C. The X-ray diffraction analysis confirmed the monoclinic CuO and cubic $ZnAl_2O_4$ phases. The phases showed better crystal formation. Scanning electron microscopy analysis revealed that the annealing time changed the morphology of the nanopowdered samples. The band gap becomes smaller with a longer annealing time for the precipitating agents.
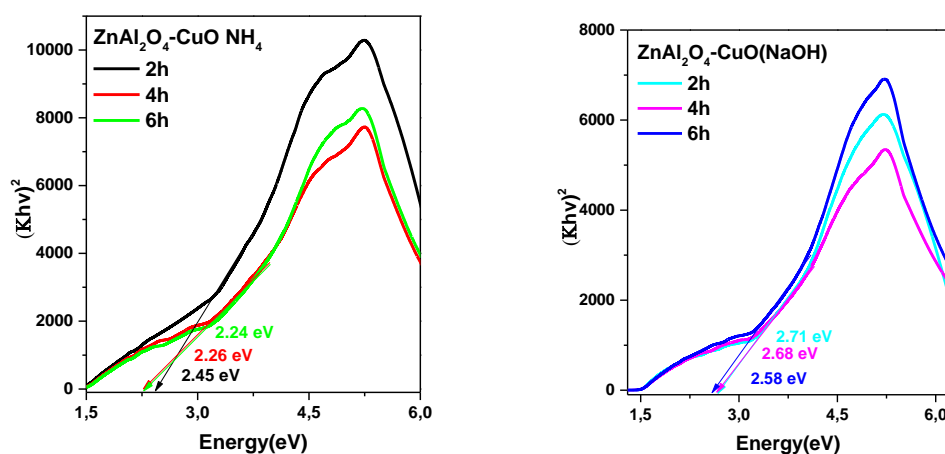
Fig. 9: Plot to determine the bandgap of the (a) $ZnAl_2O_4$-CuO (NH4) and (b) $ZnAl_2O_4$-CuO (NaOH).

3. References

1. D. M. Fernandes, R. Silva, A. A. W. Hechenleitner, E. Radovanovic, M. A. C. Melo, and E. A. G. Pineda, Mater Chem Phys **115**, 110 (2009).
2. R. Ridolfo, S. Tavakoli, V. Junnuthula, D. S. Williams, A. Urtti, and J. C. M. Van Hest, **22**, 133 (2020).
3. D. V. Kladko, A. S. Falchevskaya, N. S. Serov, and A. Y. Prilepskii, Int J Mol Sci **22**, (2021).

Thursday 10 April 2025

Time	Thursday
	10 April
09h00 - 09h15	Announcements
	Chair R.E. Kroon
09h15 - 10h00	**Plenary: Bice Martincigh**
10h00 - 10h20	16. Ponaki Radebe
10h20 -10h40	17. Elizabeth Hagemann
10h40 - 11h00	18. Vijay Kumar
11h00 - 11h20	Tea / Coffee Break
	Chair E. van Dyk
11h20 - 11h50	**Invited: Ruediger Loeckenhoff**
12h00 - 12h20	19. Shivaramu Jayaramu
12h20 - 13h30	**Lunch (Sable Hall)**
	Chair J.A.A. Engelbrecht
13h30 - 14h00	**Invited: Per-Olof Holtz**
14h00 - 14h20	20. Richard Harris
14h20 - 14h40	21. Sandile Thubane
14h40 - 15h00	22. Vishal Sharma
15h00 - 15h20	Afternoon Tea (15h00 - 15h20)

Carbon-based materials for third-generation solar cells

Bice S. Martincigh

School of Chemistry and Physics, University of KwaZulu-Natal, Westville Campus, Private Bag X54001, Durban, 4000, South Africa
Corresponding author e-mail address: martinci@ukzn.ac.za

Recent technological advancements have resulted in a pronounced increase in the global energy demand to an extent where conventional energy sources, particularly fossil fuels, are depleting and in a predicament due to their non-renewability. In addition, fossil fuels emit greenhouse gases, which contribute to undesirable global warming and climate change. Thus, renewable and sustainable energy sources, particularly solar energy, which is abundant, clean, and cost-effective, can conceivably overcome the drawbacks of traditional energy sources. Currently, the most commonly used photovoltaic devices for converting solar energy into electricity are first-generation (crystalline silicon) solar cells, which have been commercialized due to their sustainability and relatively high power conversion efficiencies (PCEs) of more than 26%. Nonetheless, silicon solar cells are rigid, expensive, and require complex fabrication procedures, which limit their large-scale production. Hence, second-generation (thin-film) solar cells have been developed with inexpensive amorphous silicon and several semiconducting materials. Regardless of having cost-effective and ease of fabrication protocols, second-generation solar cells exhibit lower PCEs than their first-generation counterparts. Recently, third-generation solar cells, such as perovskite solar cells, dye-sensitized solar cells, and organic solar cells, have attracted significant research interests owing primarily to their simple fabrication procedures, low cost, lightweight, flexibility, easy scalability, low environmental impact, and ever-increasing PCE. However, the commercialization of third-generation solar cells has been set back by their instability and relatively lower PCEs when compared with commercially available silicon solar cells. Therefore, with the recent emergence of novel materials, particularly carbon-based materials, future research is envisaged to assist in bridging the gap between third-generation solar cells and silicon solar cells. Carbon-based materials, such as carbon nanotubes, graphene, and its derivatives, and graphitic carbon nitride, due to their outstanding optoelectronic properties, excellent stability, nontoxicity, and low cost, have prompted much research effort. Their incorporation into third-generation solar cell components, as additives or replacements for traditional solar cell materials, is envisaged to significantly increase the PCE, sustainability, environmental friendliness, and cost-effectiveness of devices. This presentation will discuss the basics of photovoltaics, carbon-based materials, and third-generation solar cells, as well as current advances in this area. Merits, limitations, and recommendations for the fabrication of highly efficient, sustainable, and cost-effective third-generation solar cells will be highlighted to pave the way for commercialization.
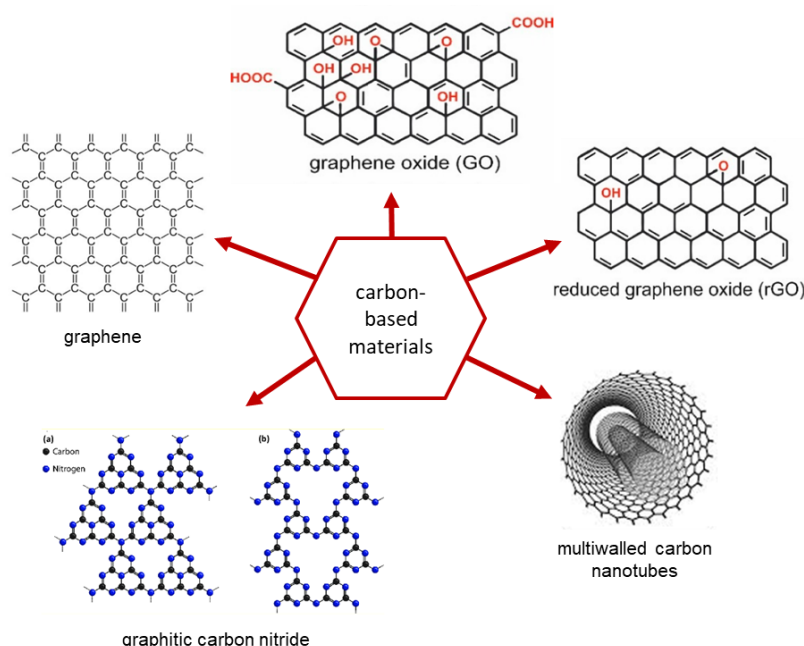
Comparative upconversion of Tm, Yb doped Y$_2$O$_3$, YOF, and YF$_3$ hosts

<u>Ponaki Radebe</u>[*], R.E. Kroon[*]

Department of Physics, University of the Free State, Bloemfontein, 9300, South Africa
Corresponding authors e-mail addresses: ponakiradebe5@gmail.com; KroonRE@ufs.ac.za

1. Introduction

Upconversion involves the conversion of multiple low-energy photons into a single higher-energy photon [1]. Upconverting phosphors have applications in security printing, forensics, biomedical research, and temperature sensing. Achieving efficient upconversion luminescence requires a suitable host material with low phonon energy and stability [2]. One such host material is YF$_3$. During annealing in air, oxygen can enter the YF$_3$ lattice and form Y$_2$O$_3$ and the process is via intermediate phases of YOF. This study aims to determine which host material between YF$_3$, YOF, and Y$_2$O$_3$ gives the highest blue upconversion emission from Tm^{3+} ions after exciting the Yb^{3+} ions with an infrared diode laser at 980 nm.

A co-precipitation method was used to make starting material that was subsequently annealed at different temperatures to create YF$_3$, YOF, and Y$_2$O$_3$, each doped with 0.5 mol% Tm^{3+} and 10 mol% Yb^{3+}. X-ray photoelectron spectroscopy (XPS) was used to monitor the chemical composition of the different stages of host formation using the same starting material for different annealing temperatures. The XPS peaks associated with yttrium and fluorine were detected in YF$_3$, whereas an oxygen peak appeared, which increased during the formation of YOF and Y$_2$O$_3$. Under 980 nm laser excitation, the upconversion luminescence emission bands corresponding to Tm^{3+} were obtained in the visible and near-infrared spectral regions.

2. Results

The XPS survey, as shown in Fig. 1, revealed the presence of all principal elements and indicated the loss of F and the gain of O in the host as the annealing temperature was increased. The upconversion emission spectra shown in Fig. 2 depicts an intense band in the near-infrared region, with weaker band emission in the visible region. The upconversion emission at 451 nm and 475 nm of the blue region, shown in the zoomed-in inset, was attributed to $^1D_2 \rightarrow {}^3F_4$ and $^1G_4 \rightarrow {}^3F_4$ Tm^{3+} transitions, respectively. The lowest emission from YF$_3$ at 451 nm suggests the $^1D_2$ level was not populated directly through the energy transfer between Yb^{3+} levels and the higher Tm^{3+} energy levels, leading to weaker emission for the shorter wavelength. The Tm^{3+} ions in Y$_2$O$_3$ exhibited intense Stark splitting for the lowest emission in the blue region, with the complex splitting being attributed to the different sites of Y$_2$O$_3$ [3]. The highest blue upconversion intensity was registered from the sample S$_1$-YOF (annealed at 950 °C). The phases of YOF showed higher emission within the blue region as compared to YF$_3$ and Y$_2$O$_3$ which suggested that the mixed oxygen and fluorine environment in the crystal lattice plays a favourable role in enhancing upconversion emission intensity, particularly in the blue region [4].
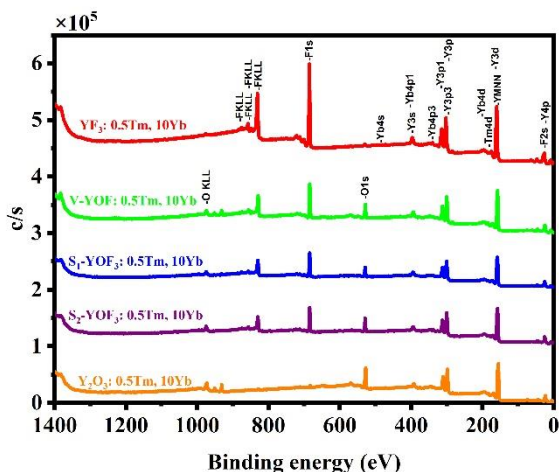
Fig. 10: XPS survey spectra of the prepared samples.
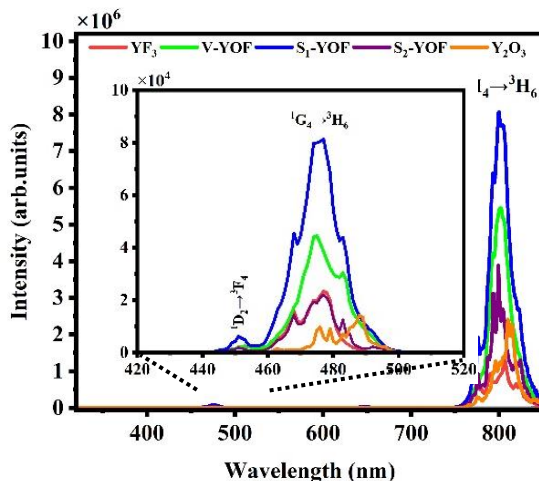
Fig. 2: Upconversion emission spectra.

3. References

[1] L. D. Sun, H. Dong, P. Z. Zhang, and C. H. Yan. *Annu. Rev. Phys. Chem.* **66** (2015) 619.
[2] J. M. F. Van Dijk and M. F. H. Schuurmans. *J. Chem. Phys.* **78** (1983) 5317.
[3] D. Avram, B. Cojocaru, M. Florea, and C. Tiseanu. *Opt. Mater. Express* **6** (2016) 1635.
[4] K. K. Markose, R. Anjana, A. Antony, and M. K. Jayaraj. *J. Lumin.* **204** (2018) 448.

Addressing the Specific Operational Requirements of Multi-junction Solar Cells Under Diverse Spectral Conditions

Elizabeth M Hagemann[1], **Frederik J Vorster**[1], **E Ernest van Dyk**[1], **Ruediger F Loeckenhoff**[2]

[1]Department of Physics, Nelson Mandela University, Port Elizabeth, South Africa
[2]AZUR SPACE Solar Power GmbH, Theresienstr. 2 74072 Heilbronn, Germany
Corresponding author e-mail address: s221440003@mandela.ac.za

1. Introduction

Concentrated photovoltaic (CPV) modules utilize multi-junction solar cells (MJSCs) to convert solar energy to electricity. However, the performance of MJSCs is influenced by the variations in the solar spectral composition and the intensity experienced under operational conditions.

MJSCs are typically monolithically stacked, series connected p-n junctions with each subcell manufactured from III-V semiconductors on a Germanium subcell such that it can absorb a broad range of the solar spectrum. However, series connections between subcells introduce a potential for current mismatch, whereby the worst-performing subcell limits the current of the MJSC [1], [2]. Furthermore, voltage losses in MJSCs can occur as the result of internal current flow caused by variations in the distribution of spectrum across the individual subcells. To analyze MJSCs under operational conditions, an experimental module was designed and deployed on a dual-axis solar tracker at Nelson Mandela University, Port Elizabeth. The module contains numerous MJSC configurations. Power measurements were performed for 3- and 5-junction cells, respectively created from GaInP/GaInAs/Ge and AlInGaP/InGaP/AlInGaAS/InGaAs/Ge, to assess the cell performance under varying operational conditions [3].

This paper investigates the influence of real operating conditions with changing spectra on the performance of MJSCs. The findings provide insight for the design optimizations of CPV cells and modules.

2. Results

Fig. 1 shows the solar spectral compositions at 1-sun, with an irradiance of 900 W/m^2, for two different dates: 18 February 2024 at 08:38 and 3 August 2024 at 08:48. It shows the variation in the spectral composition under operational conditions compared with the standard spectral composition from the IEC Concentrator Standard Operating Conditions utilised during testing [4]. Table 1 summarises the differences in key cell parameters for a 3-junction and three different 5-junction cells under these solar spectral compositions.
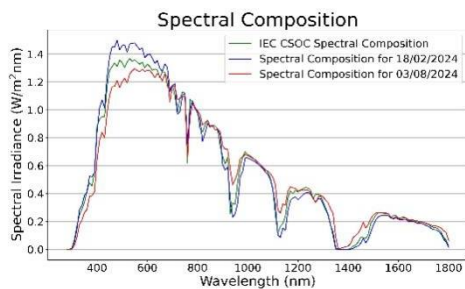
Fig. 11: Solar spectral composition on 18/02/2024 and 03/08/2024.

Table 1: 3- and 5-junction cell parameters on 03/08/2024 (red-rich spectrum) compared to 18/02/2024 (similar to standard spectrum).

	D Isc [%]	D Voc [%]	D FF [%]	D Pmp [%]
3-J	-1.89	-0.12	1.56	-0.45
5-J version h	-3.54	0.52	3.49	0.47
5-J version f	-3.74	0.19	2.79	-0.76
5-J version g	-4.46	-0.15	3.43	-1.18

The short circuit current (Isc) is the most affected parameter for all cell configurations, illustrating the dependency of the MJSC performance on the bandgap sensitivities of the III-V semiconductor materials. Yet an increase of fill factor (FF) under the red-rich spectrum partially compensates for the loss in Isc. Additionally, the performance variation within the 5-junction cells, where versions h, f, and g have different subcell current balances, indicates a further dependency on cell parameters beyond cell materials. A further comparison of additional MJSCs, a positional shift of the MJSC with respect to the module and operational temperature variations, may give a further understanding of the current and voltage variations. These results emphasise the importance of considering a range of spectral compositions during the design of MJSCs.

3. References

[1] R Núñez, C Jin, M Victoria, C Domínguez, S Askins, R Herrero, I Antón and G Sala 2016 Prog. Photovolt.: Res. Appl. **24** 1214–28.
[2] K Araki and M Yamaguchi 2003 Sol. Energy Mater. Sol. Cells **75** 707-14.
[3] P Schroth, R Löckenhoff, D Fuhrmann, M Meusel, A Frey, M Steiner, G Siefer 2022 AIP Conf Proc **2550.**
[4] IEC 2017 62670-1.

10th South African Conference on Photonic Materials – Amanzi 2025

Investigations into the structural, optical, and photoluminescence properties of Dy^{3+}-activated calcium vanadium oxide

Irfan Ayoub[1], Umer Mushtaq[1], M.Y.A. Yagoub[2], Vishal Sharma[3], Hendrik C. Swart[2], <u>Vijay Kumar</u>[1,2*]

[1] Department of Physics, National Institute of Technology Srinagar, Jammu and Kashmir, 190006, India
[2] Department of Physics, University of the Free State, P.O. Box 339, Bloemfontein, ZA9300, South Africa
[3] Institute of Forensic Science & Criminology, Panjab University, Chandigarh-160014, India

Corresponding author e-mail address: vijaykumar@nitsri.ac.in, vj.physics@gmail.com (V. Kumar).

1. Abstract

A series of Ca$_2$V$_2$O$_7$:xDy^{3+} (x =1-8 mol%) phosphors were prepared via a high-temperature solid-state reaction method. Phase confirmation and crystal structure information of the synthesized phosphor series were acquired through the X-ray powder diffraction technique. From the reflectance spectra, it was found that the bandgap value of the synthesized phosphor was found to be 2.86 eV. The impact of doping on the surface morphology was assessed through field emission scanning electron microscopy. It was found that incorporating the dopant tends to change the morphology slightly. The elemental composition was verified with the help of energy-dispersive X-ray spectroscopy. Further elemental composition and oxidation state were assessed using X-ray photoelectron spectroscopy. Photoluminescence excitation and emission spectra were recorded, and it was found that absorption and emission peaks are the characteristic peaks of Dy^{3+}. 6 mol% was found to be the optimum value of doing. Concentration quenching was found to occur via an exchange mechanism. Lifetime analysis was also done, and it was found that the lifetimes vary from 0.13-0.08 ms. From the photometric analysis, it was found that the CIE coordinates for the synthesized phosphor lie in the white region of the color gamut. All the results suggest that the synthesized phosphor can be effectively used for white light-emitting diode application purposes.

2. Results

The photoluminescence excitation and emission spectra for Ca$_2$V$_2$O$_7$:xDy^{3+} (x =1-8 mol%) were recorded with excitation and emission wavelengths of 573 and 290 nm, respectively. Besides, the different absorption peaks from Dy^{3+} a strong, wide absorption band with a peak at 300 nm, that corresponds to the $^1A_1 \rightarrow {}^1T_1$ transitions of the VO_4^{3-} group was observed[1]. The emission spectra were found to consist of characteristic emission peaks attributed to Dy^{3+}. While looking into the recorded spectra, it was found that 6 mol% is the optimum value of doping.
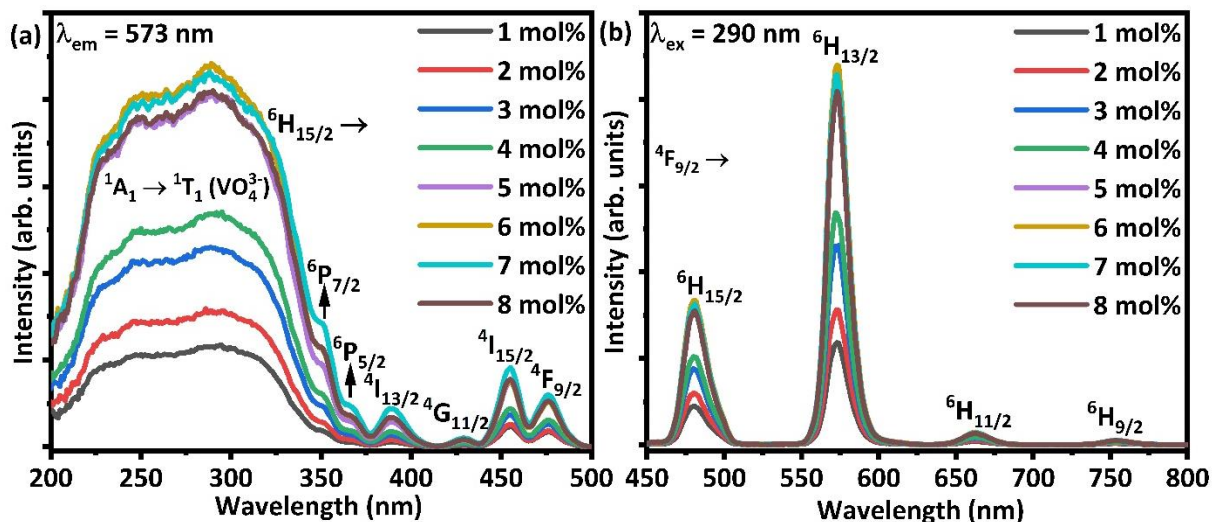
Fig. 12: (a, b) Photoluminescence excitation and emission spectra corresponding to the Dy^{3+} activated Ca$_2$V$_2$O$_7$ phosphor material.

3. References

[1]   L. Li, X. Liu, H. M. Noh, S. H. Park, J. H. Jeong, K. H. Kim, *J. Lumin.* **161** (2015) 318.

3 Junction and 5 Junction Solar Cells in Concentrating Photovoltaics (CPV) Systems: Considerations, Simulations and Field Studies

Ruediger F Loeckenhoff[1], Philipp Schroth[2], Elizabeth M Hagemann[2], Frederik J Vorster[2],
Juan F. Martínez[3], Marc Steiner[3]

[1]*AZUR SPACE Solar Power GmbH, Theresienstr. 2, 74072 Heilbronn, Germany*
Corresponding author e-mail address: Ruediger.Loeckenhoff@azurspace.com
[2]*Department of Physics, Nelson Mandela University, Port Elizabeth, South Africa*
[3] *Fraunhofer Institute for Solar Energy Systems, Freiburg, Germany*

1. Introduction

Multi Junction III/V on Germanium solar cells excel in Space due to their radiation hardness, in CPV due to their high-intensity tolerance, and in both applications because of their efficient spectrum utilization and performance. While the spectrum in Space is mostly constant it changes during a terrestrial day which induces a shift of the current generation to the lower (red-rich) or the upper (blue-rich) sub-cells. Moreover, refractive concentrators like Fresnel lenses will usually generate spectrally inhomogeneous light spots resulting in non-matching local current densities in the stacked sub-cells while reflective systems like heliostats don't show this behaviour. Consequently, CPV solar cells need to be adapted to a range of operating conditions rather than to a single homogeneous standard spectrum. This careful "current balancing" is particularly necessary for our 5C46 5 junction (5J) solar cell where any of the four upper cells may become current limiting as the spectrum changes. In our own C3PV modules, the 5C46 solar cell outperforms the 3C44 cell by 18% (best modules compared, to standard operating conditions) [1].

2. Scope

Within the project QuintuMod the 5C46, the module structure and the optics have been jointly optimized to create an economical and highly efficient CPV module. For this task we developed a simulation method, which combines ray tracing simulations [2] with Quantum Efficiency measurements and electronic network simulations [3] to calculate IV curves of 5J solar cells within the C3PV module (Fig.1). To add representative operating conditions, Fraunhofer ISE condensed thousands of spectra from typical PV sites into just six clustered spectra. These theoretical results are compared to direct spectra and IV curves of 60 individual cell receivers measured by a special analysis module. The CPV-receivers in the module vary in optical adjustment and cell design such as our 3C44 3-junction cells and different versions of 5-junction cells. Presently this module is installed and monitored at Nelson Mandela University, Port Elizabeth [4]. In combination, the simulations and real results confirm that the 5C46 cell performs well in a variety of application conditions.
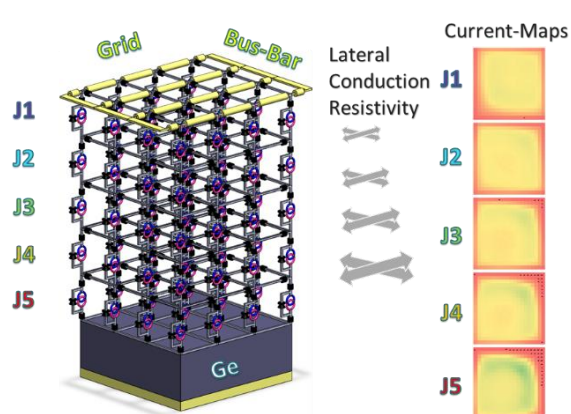
Fig. 13: Electronic Network Simulation of a 5J solar cell.   Fig. 14: Analysis module on a solar Tracker at NMU.

3. References

[1] P.Schroth et al., "AZUR's New 5C46 CPV Cell: Final Design for Optimized Outdoor Performance", 2022 AIP Conf Proc **2550.**
[2] R. Branke et al., "Raytrace3D-power tower - a novel optical model for central receiver systems," in: Proc. of 16th SolarPACES Conf., Sept 21-24, 2010, Perpignan, France (2010).
[3] R. Loeckenhoff et al,"Electronic network simulation of 5-junction solar cells and impacts on the ideal current matching", AIP Conf. Proc. **2841**, 020002 (2023).
[4] E. Hagemann et al. "Addressing the Specific Operational Requirements of Multi-junction Solar Cells Under Diverse Spectral Conditions", this conference.

Long-persistent red-light emission in Pr^{3+}-doped $LiYGeO_4$ phosphor for latent fingerprint detection and anticounterfeiting

Shivaramu Nagarasanakote Jayaramu,* Elizabeth Coetsee,** Hendrik C. Swart

Department of Physics, University of the Free State, Bloemfontein, ZA-9300, South Africa
Corresponding author e-mail address: nj.shivaram@gmail.com, coetseee@ufs.ac.za***

1. Introduction

Lanthanide-doped lithium yttrium germanate ($LiYGeO_4$) has attracted considerable interest in recent years owing to its advantageous optical and luminous characteristics. $LiYGeO_4$ is a synthetic crystal classified among garnet-like materials, recognized for its exceptional chemical stability, superior thermal conductivity, and distinctive optical properties. Pr^{3+} doped $LiYGeO_4$ has broad 4f-5d transitions that provide unique emission peaks in the visible spectrum [1]. In this study, Pr^{3+}-doped $LiYGeO_4$, with varying concentrations, was synthesized via the solid-state reaction. Different Pr^{3+} doping concentrations on the crystal structure, morphology, elemental distribution, bandgap, oxidation states, and defects were analyzed using X-ray powder diffraction (XRPD), field emission scanning electron microscopy (FE-SEM), energy dispersive X-ray spectroscopy (EDS), UV-vis diffuse reflectance, X-ray photoelectron spectroscopy (XPS), and electron paramagnetic resonance (EPR). Persistent luminescence (PersL) was studied and correlated with photoluminescence (PL) and thermoluminescence (TL). The optimized phosphor was evaluated for fingerprint detection and anticounterfeiting applications.

2. Results

The synthesized $LiY_{(1-x)}GeO_4:xPr^{3+}$ (x= 0-1) phosphors have an orthorhombic crystal structure [1]. The XPS and PL results revealed the presence of Pr^{3+}. The UV-vis-near infra-red (NIR) diffuse reflection spectra showed an absorption band at 200 nm for all the samples. This absorption band corresponds to the band edge of the host [1]. Another broad band located in the range of 210–280 nm corresponded to the $4f^2 \rightarrow 4f5d$ transition of Pr^{3+}. All the other bands corresponded well with the Pr^{3+} transitions [1]. PL showed two excitation peaks at 236 and 250 nm that corresponded to the $4f \rightarrow 4f5d$ transition under 650 nm emission. All the phosphors showed a wide excitation band from 414 to 500 nm, as well as peaks at 529 and 565 nm, attributable to f-f transitions. $LiY_{(1-x)}GeO_4:xPr^{3+}$ (x = 0-1) exhibits blue, red, and deep red emissions that correspond to the f-f transitions of the Pr^{3+} ions. Upon excitation with a blue laser (473 nm), the phosphor displayed emission ranging from blue-green to red and extended into the NIR to mid-IR regions. A series of PersL and TL experiments were performed to examine the characteristics of PersL. The Pr^{3+} doped material exhibits trap distributions ranging from 0.8 to 1.6 eV. The findings demonstrated that the inclusion of Pr^{3+} ions created additional shallow traps within the material, thus boosting the PersL performance at room temperature. This phosphor can act as an efficient multimodal luminescence material, which simultaneously exhibits long-lasting (>14 h) blue-green and red dual-band persistent luminescence after irradiation by 254 nm (Fig.1(a)). Moreover, the material exhibits exceptional color purity, positioning it as a viable choice for red PersL applications [2]. Latent fingerprint detection using the $LiYGeO_4:0.25 \% Pr^{3+}$ phosphor proved to be an excellent marking agent for applications in forensic science and anticounterfeiting (Fig.1(b)).
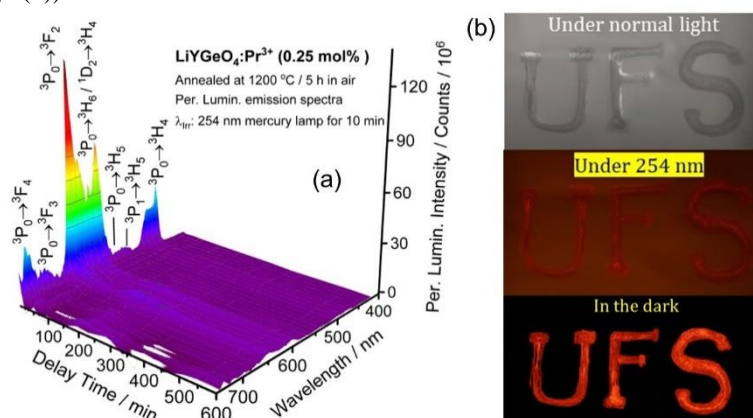
Fig.1: (a) PerL emission spectra of the $LiYGeO_4:Pr^{3+}$ (0.25 mol%) phosphor and (b) a picture of the "UFS" pattern drawn with handmade ink ($LiYGeO_4:Pr^{3+}$ (0.25 mol%) + PVA) under ambient light, under the excitation of 254 nm and the afterglow (in the dark) at RT.

3. References

[1]   T. Zhang, H. Guo, Q. Shi, J. Qiao, C. Cui, P. Huang and L. Wang, *J. Lumin*. **267** (2024) 120382.
[2]   S. Nagarasanakote Jayaramu, D. Janardhana, L.J.B. Erasmus, E. Coetsee, D.E. Motaung and H.C. Swart, *Dalt. Trans*. **53** (2024) 16557.

Towards smaller, brighter and more efficient micro-LEDs

I. Martinovic [1,2], S. P. Le [1,2], C. W. Hsu [1,2], L. Rullik [2] and P. O. Holtz [1,2]

[1] *Dept of Physics, Chemistry and Biology (IFM), Linköping University, Sweden*
[2] *Polar Light Technologies AB, Teknikringen 7, Linköping, Sweden*

Corresponding author e-mail address: per-olof.holtz@polar-light-technologies.com

1. Introduction

A novel bottom-up approach enabling fabrication of smaller, brighter, and more energy-efficient micro-LEDs than conventional top-down techniques will allow, has been displayed. By this approach, pyramidal micro-LEDs can be manufactured without destructive etching damages as the LED dimensions are decreasing to the mm or even sub-mm regime. Pyramidal micro-LEDs with bright and efficient blue and green emissions have earlier been demonstrated, and recently also red-emitting pyramidal micro-LEDs were demonstrated.

In the prevailing miniaturization race for achieving high performance micro-LEDs, the commonly employed top-down approach is reaching its limit due to the etching procedure. As the dimensions of the etched areas of the 2D quantum well structures are reaching decreasing mm sizes, the surface damages caused by this etching will become increasingly problematic as these damages are devastating for the optical performance of an LED structure.

2. Pyramidal LED concept

In this work, an alternative bottom-up approach is presented in order to realize new 3D mLED-structures, with sizes down to mm or even sub-mm dimensions. This concept is based on InGaN/GaN pyramidal quantum structures with a deterministic design, essentially defined by the hexagonal lattice structure, i.e. pyramids with six symmetric facets (See Fig. 1). The pyramidal GaN structures are fabricated by a re-growth process on lithographically patterned SiN-masked GaN templates. InGaN quantum wells on the facets of the mm-sized GaN pyramids with almost perfect surfaces act as the active light emitters. Based on this concept, pyramidal mLEDs have been demonstrated with bright emission at 470 and 520 nm, respectively. The breakthrough of the pyramidal mLEDs took place recently with the demonstration of a red emission at 630 nm (See Fig. 2). This means that R/G/B (red/green/blue) emitters from the same material system have been realized.

3. Pyramidal micro-LED applications

The high quality of homogeneous pyramidal microLED structures combined with a flexible design paves a promising route for microLED applications such as AR-based microLED projectors and displays. The combination of smaller dimensions down to mm or even sub-mm dimensions, with maintained high emission rate (i.e. brightness) and a recombination process occurring at a high efficiency are key features for the microLEDs performance in display and projector applications.

July 2023   October 2023   December 2024
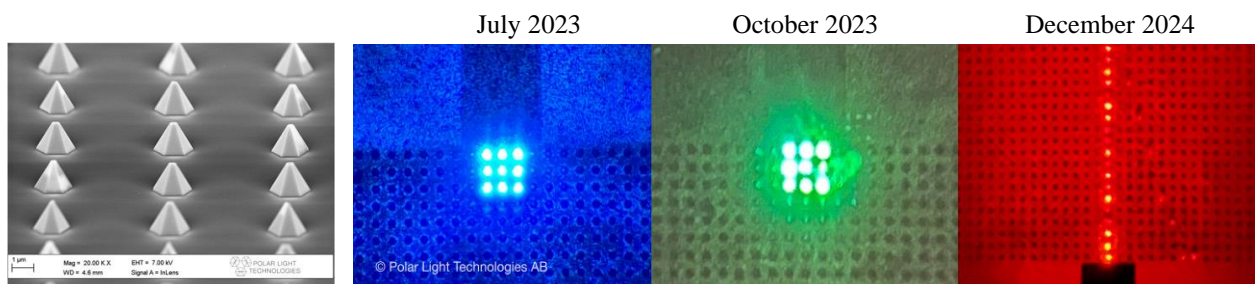
Fig 1. Images of mm-sized pyramidal GaN structures.

Fig. 2 Configurations of pyramidal InGaN/GaN mLED-structures lighting up at 470, 520 and 630 nm, respectively.

4. References

- C.W. Hsu, A.Lundskog, K F. Karlsson, U. Forsberg, E. Janzén and P.O. Holtz, Nano Lett. (2011), 11, 2415–2418
- A. Lundskog, C.W. Hsu, K F. Karlsson, S. Amloy, D. Nilsson, U. Forsberg, P.O. Holtz, and E. Janzén, Light: Science & Applications (2014) 3, e139; doi:10.1038/lsa.2014.20
- S.P. Le, C.W. Hsu, I. Martinovic, I.G. Ivanov and P.O. Holtz, Appl Phys A, (2022), 128:801
- S.P. Le, C.W. Hsu, I. Martinovic, and P.O. Holtz, Appl Phys Lett 118, 142102 (2021)

Towards light-controlled multi-value logic neuromorphic devices.

Richard A. Harris, Edward Lee

Department of Physics, University of the Free State, Bloemfontein, 9301, Republic of South Africa

Corresponding author e-mail address: harrisra@ufs.ac.za; raharrisphd@gmail.com

1. Introduction

Neuromorphic computing is a rapidly developing approach that seeks to create computing systems inspired by the functioning of the human brain. The goal is to achieve brain-like efficiency in cognitive tasks [1] Recently, significant advancements in neuromorphic hardware have been showcased, such as IBM's '*TrueNorth*' [2] and Intel Labs' '*Loihi*' [3] systems. These are built using complementary metal-oxide-semiconductor (CMOS) technology. CMOS-based designs require a large number of transistors to replicate neuronal and synaptic functions, resulting in higher energy consumption and increased spatial requirements. Therefore, the downscaling of each computing unit (i.e. neuron) to the nanoscale, or even smaller, is critical.

Apart from the traditional logic-gate-computations, a neuromorphic device should also fulfill the following criteria: (a) each neuronic unit should be able to have a memory as well as the ability to compute, (b) be able to forget stored information after some time, (c) have a reset function. Additionally, it would be useful (but not a requirement), to (d) process differing sets of input data at once, and in parallel (perform parallel computations) and to operate with (e) multi-value logic (MVL). A typical example of MVL is ternary logic, which uses three distinct states: VDD (supply voltage), GND, and an indeterminate third logic value. This differs from the more familiar binary logic (Boolean logic), which only uses two states—VDD and GND.

Here, we show that photoactive materials may be used to design and fabricate such a device that fulfill these criteria. This is done by precise design and control of the architecture of a nano-scaled photoactive ZnO, Al_2O_3, Au, and Si-based device.

2. Results

Fig. 1 shows the UV-Vis absorption of three of the materials (ZnO, Au, and Al_2O_3) used to fabricate the device. Whereas ZnO alone absorbs mainly in the UV band, the combination ($ZnO/Au/Al_2O_3$) allows us to engineer a system that also absorbs visible light photons. Thus, different data sets on a combined light beam (containing both UV and visible light) may be absorbed by the system to input multiple data sets at once. Fig. 2 shows an example of the 'memory effect' in the device. UV light is switched on and off at different intervals. The system remembers its previous 'on' state (in terms of output current) when the UV light is turned off and remains in that state for some time. Each 'on' state is therefore built on top of the previous and is visible in the stepwise increase in current.
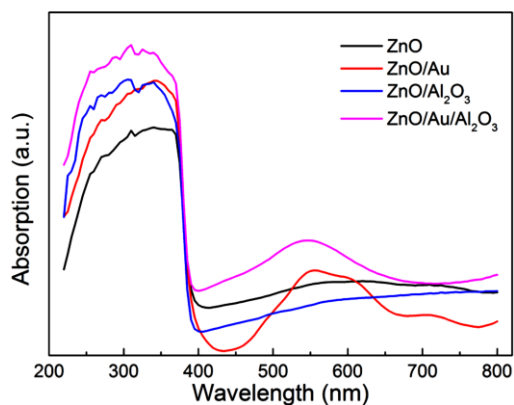
Fig. 15: UV-Vis of ZnO, ZnO/Au, ZnO/Al_2O_3 and $ZnO/Au/Al_2O_3$
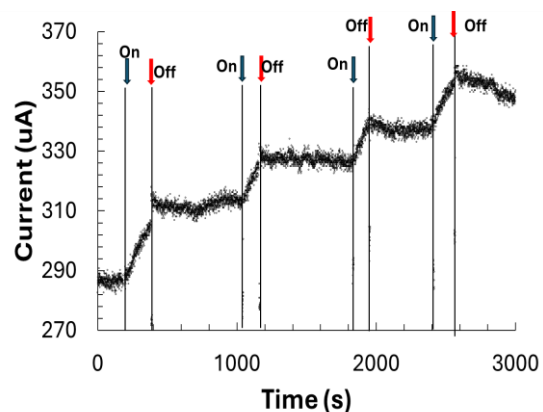
Fig. 2: Change in current with UV light ON and OFF. The memory effect is observed where the device remembers its previous ON state.

3. References

[1] E.Baek, N. R. Das, C.V. Cannistraci, T. Rim, et al. *Nature Electronics*, **3** (2020) 398-408.
[2] P.A. Merolla, J.V. Arthur, R. Alvarez-Icaze, A.S. Cassidy et al. *Science*, **345**,6197 (2014) 669-673.
[3] M. Davies, N. Srinivasa, T.-H. Lin, G. Chinya, Y. Cao, S.H. Choday et al. *IEEE Micro*, **38**,1 (2018) 82-99.

The defect passivation in CsPbBr$_3$ perovskite using phenethylammonium bromide

Sandile Thubane[1], Nolwazi Nombona[2], Mmantsae Diale[1*]

[1]*Department of Physics, University of Pretoria, Private Bag X20, Hatfield 0028, South Africa*
[2]*Department of Chemistry, University of Pretoria, Private Bag X20, Hatfield 0028, South Africa*
Corresponding author e-mail address: mmantsae.diale@up.ac.za

1. Introduction

Perovskite materials possess attractive properties such as bandgap tunability, low exciton binding energy, stimulated emission at ambient temperature, high electron mobility, strong optical absorption, and long electron-hole diffusion lengths. However, the stability of conventional organic-inorganic perovskites is impaired in at ambient environment due to highly volatile organic components within the material and weak chemical bonding between metal cations (Pb$^+$) and halide anions (I$^-$, Br$^-$, or Cl$^-$). The ionic nature of perovskites also induces ion migration in iodide-rich materials [1]. Conversely, CsPbBr$_3$ perovskites have high stability in ambient environments and elevated temperatures due to the stable [PbBr$_6$] octahedral framework and non-volatile Cs$^+$ cation [2].

The concentration difference between Cs$^+$ and Pb^{2+} in the same solvent during a one-step spin-coating method led to the introduction of a two-step deposition method [3]. However, the perovskite materials synthesised using the two-step deposition method are populated by large pinholes which ultimately act as recombination centres for electrons and facilitate the degradation of the material. In this work, phenethylammonium (PEA$^+$) was used as a passivation layer to reduce pinholes and improve the luminescence in CsPbBr$_3$ perovskite.

2. Results

X-ray diffraction (XRD) patterns revealed cubic structure with the *Pm3m* space group where PEA$^+$ did not affect the intrinsic crystal structure of CsPbBr$_3$ perovskite. Field emission scanning electron microscopy (FESEM) images of CsPbBr$_3$ revealed pinholes within the perovskite film. Spin-coating PEABr on CsPbBr$_3$ improved morphology and surface coverage resulting in pinhole-free films. Fig. 16 shows the absorption spectra and emission of CsPbBr$_3$ thin film showing a broad absorption with an onset at 530 nm and an excitonic peak at 515 nm. Furthermore, CsPbBr$_3$/PEABr preserves the optical properties of CsPbBr$_3$. However, the two excitonic peaks that appear at 405 and 436 nm were attributed to a 2D perovskite with n=1 and n=2 phase of a quasi-2D [PEA$_2$Cs$_{n-1}$Pb$_n$Br$_{3n+1}$] perovskite, see Fig. 2.
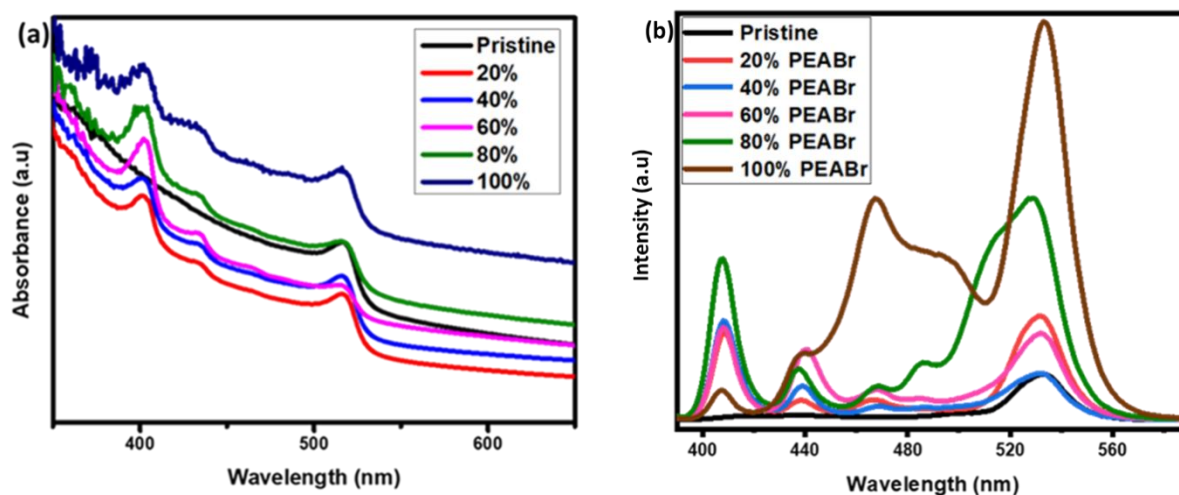
Fig. 16. (a) Absorbance and (b) emission in CsPbBr$_3$ thin film with and without PEABr.

3. References

1. Zhu, W., et al., *Ion migration in organic–inorganic hybrid perovskite solar cells: current understanding and perspectives.* Small, 2022. **18**(15): p. 2105783.
2. Calisi, N. and S. Caporali, *Investigation of open air stability of CsPbBr3 thin-film growth on different substrates.* Applied Sciences, 2020. **10**(21): p. 7775.
3. Cao, X., et al., *Water, a green solvent for fabrication of high-quality CsPbBr3 films for efficient solar cells.* ACS applied materials & interfaces, 2019. **12**(5): p. 5925-5931.

Role of monovalent charge compensators (Li⁺, K⁺) in Sm³⁺-activated Ca₂Ga₂GeO₇ phosphor for enhancing emission intensity

Umer Mushtaq¹, Irfan Ayoub¹, Hendrik C. Swart², Vijay Kumar¹,², <u>Vishal Sharma³*</u>

¹ Department of Physics, National Institute of Technology Srinagar, Jammu and Kashmir, 190006, India
²Department of Physics, University of the Free State, P.O. Box 339, Bloemfontein, ZA9300, South Africa
³Institute of Forensic Science & Criminology, Panjab University, Chandigarh-160014, India
Corresponding author e-mail address: vishalsharma.pu@gmail.com (V. Sharma)

1. Abstract

This study presents the enhancement of emission intensity in Sm^{3+}-doped $Ca_2Ga_2GeO_7$ phosphors through the incorporation of monovalent co-dopants, such as K^+ and Li^+, acting as charge compensators. The phosphors were synthesized via the solid-state reaction method. Phase analysis was performed using X-ray powder diffraction, and the crystallite size was determined through Williamson-Hall plots. UV-visible spectroscopy was used to study the absorption characteristics, which showed prominent peaks due to Sm^{3+} activator ions. The bandgap was determined by the Kubelka-Munk function, which also allowed analysis of its changes with varying co-dopant concentrations. Energy dispersive X-ray spectroscopy (EDS) and field emission scanning electron microscopy (FESEM) were used to analyze the samples' elemental composition and surface morphology. Photoluminescence (PL) measurement recorded enormous enhancement in the emission intensity in the presence of K^+ and Li^+ ions. For a 0.05 mol Sm^{3+}, maximum emission was achieved. Luminescence decay time has been recorded to lie in microseconds. The thermoluminescence study also provided some essential details regarding various trap states, densities, and their corresponding activation energy of charge carriers. The chromaticity coordinates of the Sm^{3+} ions' characteristic red emission were determined, highlighting the phosphor's capability to emit within the desired spectral range. These findings demonstrate that Sm^{3+}-doped $Ca_2Ga_2GeO_7$ phosphors co-doped with monovalent ions are promising materials for use in red light emitting diodes (LEDs) and advanced display technologies.

2. Results

Fig. 1 presents the PL spectra of Sm^{3+}-doped $Ca_2Ga_2GeO_7$, showing the influence of charge compensator ions such as K^+ and Li^+ on the emission intensity. The PL spectra, as shown in Fig. 1(a) for $Ca_{2-x}Ga_2GeO_7:xSm^{3+}$, with a variation in Sm^{3+} concentration (x = 0.01 to 0.07), exhibit the characteristic emission peak at ~600 nm due to the $^4G_{5/2} \rightarrow {}^6H_{7/2}$ transition and additional transitions at ~570 nm and ~650–720 nm. This can be ascribed to the increased emission intensity due to increases in concentration with Sm^{3+} ions until their optimum level around $0.05Sm^{3+}$ has been achieved, followed by a decrease in the intensity due to the concentration quenching effects. Fig. 1(b) shows examples of $Ca_{1.95-y}Ga_2GeO_7: 0.05Sm^{3+}, yK^+$, where an extra dosage of K (y= 0 to 0.12 mol) enhanced its related emission intensities against its reference $Ca_{1.95}Ga_2GeO_7:0.05Tb^{3+}$ shaded in green. This is due to the more efficient charge compensation, avoiding the non-radiative losses to equilibrate the charge mismatch developed due to Sm^{3+} doping. Fig. 1(c) shows spectra of $Ca_{1.95-z}Ga_2GeO_7:0.05Sm^{3+}, zLi^+$ with Li^+ ion as charge compensator (z = 0 to 0.12) [1]. Here, PL intensity is also increased, and the variation trend is similar to K^+ doping. However, specific differences in optimal doping level and peak enhancements might be due to the smaller ionic radius of Li^+ compared to that of K^+. Indeed, both charge compensators effectively reduce the quenching mechanism and enhance the luminescent efficiency, and peaks in Fig. 1(b) and Fig. 1(c) are more intense compared to Fig. 1(a). These results underline the important role of charge compensator ions in the optimization of Sm^{3+}-doped materials for their photoluminescence properties for applications in lighting and display technologies [2]. Charge compensator ions play a significant role in improving the photoluminescence properties of Sm^{3+}-doped materials, making them suitable for lighting and display applications [2].
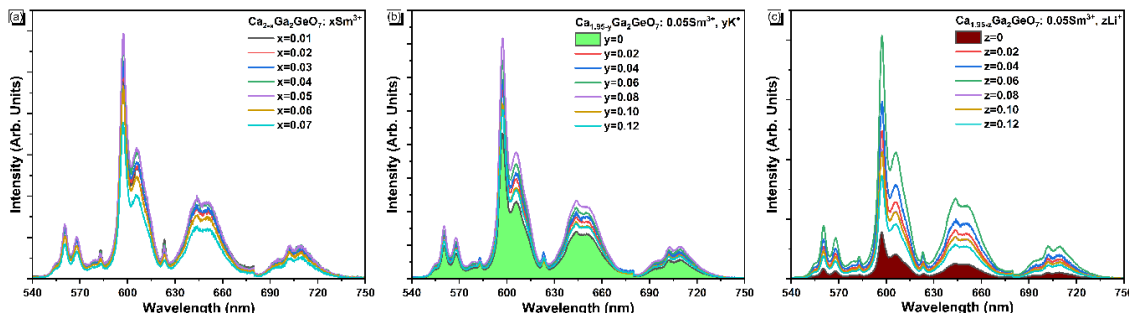
Fig. 17: Emission spectra for (a) $Ca_2Ga_2GeO_7$ phosphor material, doped with Sm^{3+} with its concentration varying from 0.01 mol to 0.07 mol, (b) $Ca_{1.95-y}Ga_2GeO_7: 0.05 Sm^{3+}$, y K^+ and (c) $Ca_{1.95-z}Ga_2GeO_7: 0.05 Sm^{3+}$, z Li^+.

3. References

[1]   J. Zhou, X. Yu, T. Wang, D. Zhou, J. Qiu, *J. Rare Earths* **2017**, *35*, 241.
[2]   U. Mushtaq, I. Ayoub, M. Y. A. Yagoub, N. J. Shivaram, E. Coetsee, H. C. Swart, V. Kumar, *Appl. Phys. A* **2024**, *130*, 494.

List of Posters

Poster No.	Presenter	Title
1	A. K. Bedyal	Upconversion luminescence properties of undoped and Er^{3+} doped $Ba_3Yb(BO_3)_3$ Phosphors
2	Onyekachi Kalu	Defect emissions of a self-textured growth radio frequency (RF) sputtered $Cd_{0.015}Mg_{0.10}Zn_{0.885}O$ thin film.
3	R. E. Kroon	Er^{3+}-Yb^{3+} Co-doped $La_2Zr_2O_7$ and $Y_2Zr_2O_7$ Phosphors for Optical Thermometry and Latent Fingerprint Detection
4	Anurag Pandey	Optimization of doping concentration for upconversion emission from Zn_2GeO_4:Er^{3+} phosphor
5	Tshepho Trevor Makgale	Novel Tin Dioxide-coated Gold and Silver Nanomaterials for Enhanced Solar Steam Generation
6	Delicacy Ntshalintshali	Structural and optical properties of Dy^{3+}-doped La_2ZnTiO_6 nanophosphors prepared via sol-gel method
7	C. Dlamini	Enhanced Green and Orange-Red Dual Luminescence Emissions of $Zn_{0.5}Ca_{0.5}Al_2O_4$: Tb^{3+}, Sm^{3+} Phosphors Stimulated by Crystallinity: Effects of Annealing Temperature
8	Mbali Marole	Sodium-Ion Energy Storage Devices Characterization Using a Novel Low-Cost Microcontroller-Based Instrument
9	Pule Nche	Influence of fuel ratio and dopant concentration on luminescent properties of Eu-doped SnO_2
10	Ezekiel Omotoso	Analysis of temperature-dependent characteristics of Cr/P-doped Si Schottky barrier diodes before and after 5.4 MeV 241Am irradiation
11	Lethabile Masiu	Characterization and synthesis of Eu^{2+} doped $SrAl_2O_4$ phosphor for green emission
12	Sandeep Eswaran Panchu	Innovative toxic-free exfoliation of bulk g-C_3N_4: morphological evolution of ultra-thin (1D/2D) g-C_3N_4 nano-sheet/tube to accelerate sunlight-driven photocatalytic activity
13	Jatani Ungula	Influence of Ga^{3+} on ZnO nanorods grown on GZO thin film seed layer by chemical bath deposition
14	Jatani Ungula	Effect of different sources of Cu-dopant on material properties of ZnO NRs grown on a GZO film by chemical bath deposition for photovoltaic applications
15	Chantel Mare	Ab initio investigation of the boron vacancy complex
16	K.B. Morebodi	Luminescence properties of Ce^{3+} and Eu^{2+} doped $Ca_4(PO_4)_2O$ phosphors
17	T.P. Mokoena	Synthesis and Characterization of Titanium Tellurium Oxide Nanostructured Materials
18	Sarojini Jeeva Panchu	Pressure Dependent integration of white light emission in SiQDs@EuZIF-8 metal organic frameworks
19	Sizwe Sibiya	Optimization of the ETL titanium dioxide layer for inorganic perovskite solar cells
20	C.R. Ratlhagane	The effect of varying annealing periods on the structure, morphology and photoluminescence properties of $CaAl_2O_4$/$BaAl_2O_4$:0.1% Eu^{3+} mixed phases via sol-gel method
21	G. J. Odendaal	Comparative study on absolute photoluminescence quantum yield measurements of $Y_3Al_5O_{12}$:Ce phosphor powder
22	Nkosikhona Thando Dlamini	Study on the optical characteristics of $SrTiO_3$/$Ti_3C_2T_x$ and their influence on the BTEX gas sensing performance
23	Kholofelo Seloane	Structure and Luminescence Correlation on CO Sensing Performance of p-n Cr_2O_3/SnO_2 Heterostructures
24	Quinton Mohlala	Structural, chemical, and luminescence properties of Bi doped ZnO
25	Lindokuhle Mabizela	Influence of Ag on the optical properties of MOF-derived Co_3O_4-In_2O_3 nanocomposites applied for xylene vapour detection

26	Lucas Erasmus	Influence of excitation power on down-shifting ZnO
27	Jodinio Lemena	W18O49 NPs for the trace detection of Acetone Vapour
28	Chulumanco Tyesi	Influence of noble metals loading on $In_2O_3/SnO_2/MoS_2$ ternary structure for improved optical, structural, and SO_2 gas sensing characteristics
29	Sharon Kiprotich	Synthesis and characterization of Ag-ZnO using citrus reticulata peel extract
30	Karabo Masilela	A comparative study of optical properties and Hydrogen Sulfide Gas Sensor Performance of CuO/CeO_2 Nanocomposite
31	Sharon Kiprotich	Synergetic Effects of Zn:Fe Co-Doped TiO_2 Nanoparticles on the Structural, Optical and Morphological Properties
32	Fokotsa Victor Molefe, Mmantsae Diale	Annealing effects on hydrothermally prepared SnO_2 thin films deposited by spray pyrolysis and their potential for ETL in PSCs
33	Mosima Kgomo-Masoga	Highly acetone responsive nanosensor layer based on nanostructured cube-like α-Fe_2O_3: Effects of Cr dopant ion
34	Mohammed Hamed	Improved light harvesting in polymer solar cells using copper-doped zinc bimetallic nanocomposite
35	Tshegofatso Moipolai	Structural and Optical Propeprties of V^+ Ion Implanted CZTS Thin Films
36	Fortunate Elegbeleye	Effect of Additional Polyene and Methoxy Functional moiety on the Spectral Properties of Polyene-Diphenylaniline Organic Molecules for Applications in Solar Energy

Upconversion luminescence properties of undoped and Er^{3+} doped Ba$_3$Yb(BO$_3$)$_3$ Phosphors

A. K. Bedyal[1], Durgaprasad D Ramteke[2], H. C. Swart[3] and Vinay Kumar[3, 4]

[1]*Department of Physics, School of Sciences, Cluster University of Jammu, Canal Road, J & K 180001, India*
[2]*Paebbl The re-stored carbon com, Scheepsbouwweg, 29, 3089 JW Rotterdam, The Netherlands*
[3]*Department of Physics, University of the Free State, P.O. Box 339, Bloemfontein, ZA9300, South Africa*
[4]*Department of Physics and Astronomical Sciences, Central University of Jammu, Raya-Suchani, Samba, J & K, India*

Corresponding author: ankushkumar@clujammu.ac.in, ankushbadiyal@gmail.com

1. Introduction

The near-infra-red (NIR) photons used in the excitation of up-conversion (UC) luminescence materials are transformed into a low wavelength emitted photon through multi-photon processes. Upconversion materials are efficiently useful for solar cell energy conversion of IR light. Solar cells with upconversion material generate electricity by IR light, which increases the conversion efficiency of solar cells. It is also useful for other applications such as color displays, optoelectronics, sensor technology, imaging, biological labeling, UC lasers, and so on [1-2]. With very high luminescence efficiency and excellent temperature sensing ability, the UC phosphors may be best for use in practical applications. A rare earth-containing borate matrix is advantageous because of its low cost and easily made singly made double fluorescent material. In this study, Ba$_3$Yb(BO$_3$)$_3$ has been chosen as the host as the selected material already has Yb^{3+} ions in it. Therefore, it is interesting to explore the effect of Er^{3+} ions on the luminescence properties of this phosphor.

2. Results:

Fig. 1 shows the PXRD patterns of the undoped and x mol % Er^{3+} (x=1, 2, 4 6 mol. %) doped Ba$_3$Yb(BO$_3$)$_3$ phosphors along with the simulated XRD data of Ba$_3$Yb(BO$_3$)$_3$. The diffraction peaks of the doped samples at different concentrations are very well matched with the diffraction patterns (simulated data) of the host which corresponds to the hexagonal system with the space group P63cm. Observation of no additional impurity peak corresponding to Er^{3+} confirms the incorporation of Er^{3+} ions in the host matrix successfully by replacing the Yb^{3+} ions.

The UC spectra of undoped Ba$_3$Yb(BO$_3$)$_3$ and x mol % Er^{3+} (x=1, 2, 4 6 mol. %) doped Ba$_3$Yb(BO$_3$)$_3$ phosphors under 980 nm excitation are shown in Fig. 2. The UC spectra of the phosphors consist of a green and a red region. The green region has a band centered at 525 nm and a number of sharp peaks from 515 nm to 580 nm, whereas the red region consists of a number of sharp peaks from 630 to 710 nm arising due to the transitions from the excited states ^{2}H$_{11/2}$, ^{4}S$_{3/2}$, ^{4}F$_{9/2}$ to the ground state ^{4}I$_{15/2}$ covering the whole visible region of the spectrum. The spectra also depict that with the increase in Er^{3+} ion concentration, the UC intensity increased continuously.
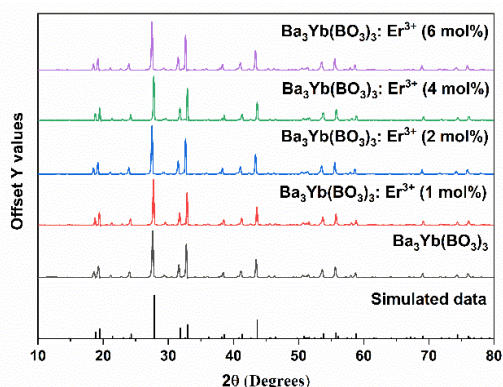
Fig. 1 PXRD patterns of the undoped and Er^{3+} doped Ba$_3$Yb(BO$_3$)$_3$ phosphor along with the simulated standard data.
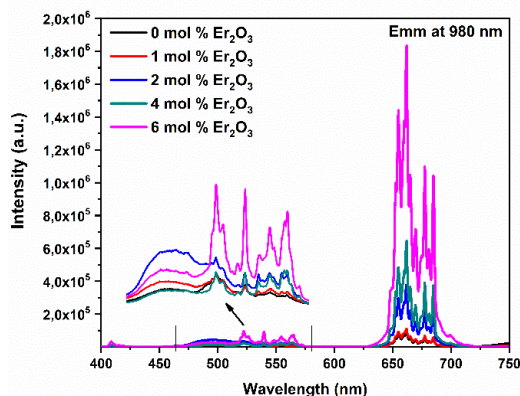
Fig. 2 Photoluminescence spectra of the undoped and Er^{3+} doped Ba$_3$Yb(BO$_3$)$_3$ phosphor.

4. References

1.   B. Dong, B. Cao, Y. He, Z. Liu, Z. Li, and Z. Feng, (2012). *Advanced Materials*, *24* (2012), 1987.
2.   P. D., Howes, R., Chandrawati, and M. M. Stevens. *Science*, 346 (2014) 6205.

Defect emissions of a self-textured growth radio frequency (RF) sputtered $Cd_{0.015}Mg_{0.10}Zn_{0.885}O$ thin film.

KALU, O. [a, b*], REYES-ROJAS, A. [b]

[a] Federal University of Lafia, Department of Physics, P.M.B. 146, Lafia, Nasarawa State. Nigeria

[b] Centro de Investigación en Materiales Avanzados, S.C., Departamento Física de Materiales, Miguel de Cervantes 120, Complejo Industrial Chihuahua, 31109 Chihuahua, CHIH, Mexico.

Corresponding author. E-mail address: kalu.onyekachi@science.fulafia.edu.ng

Introduction

ZnO remains a preferred candidate for luminescent-based materials. It is believed that doping ZnO NPs could generate suitable materials as light emitters and absorbers in the visible and infrared regions. The effect of co-doping with divalent elements/ions of MgO and CdO with narrower bandgap can lead to defect emission and enhance luminescence intensity as a compelling contender in optoelectronics devices [1].

Results and Discussion

$Cd_{0.015}Mg_{0.10}Zn_{0.885}O$ (CMZO) thin film with a self-textured growth and texture fraction (TF) of 95.8% for (002) peak orientation along the c-axis is deposited on Si substrate using radio frequency (RF) magnetron sputtering [2]. The crystal structure of the thin film and their crystallographic parameters from the Rietveld refinement established a hexagonal wurtzite structure with a grain size of 34.34(2) nm and a smooth surface roughness of 2.8 nm (square root of the mean square). The optical band gap estimated for the thin film is 3.52 eV. At the same time, the photoluminescence intensity was strong in the UV region with a broad yellow emission at 582 nm that is optically active as defect emission of oxygen interstitial (Oi). Defect emissions of blue, orange, red, and near-infrared intensities decreased compared to the yellow emission due to depletion of the recombination of photo-generated holes or charge carriers [**Error! Bookmark not defined.**]. CMZO thin films hold great potential for optoelectronic devices and applications in the UV and yellow regions.
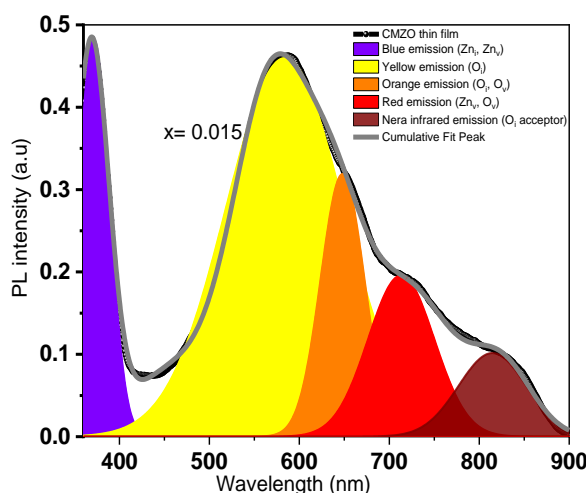
Fig.1: PL measurement of CMZO thin film

References

[1] O. Kalu, M. R. Correia, A. Cantarero, H. A. Martinez-Rodriguez, J. A. Duarte-Moller, A. Reyes-Rojas. *J. Phys. Chem. Solids* **146**, *(2020) 109611*

[2] O. Kalu, A. Nathan Abutu, H. Esparza Ponce, A. Ramirez-DelaCruz, R.E. Kroon, A. Reyes-Rojas. *Mater. Chem. Phys. 308, (2023)128314.*

Er³⁺-Yb³⁺ Co-doped La₂Zr₂O₇ and Y₂Zr₂O₇ Phosphors for Optical Thermometry and Latent Fingerprint Detection

B. V. Naveen Kumar[1], <u>R. E. Kroon</u>[1]

[1]*Department of Physics, University of the Free State, Bloemfontein, South Africa, 9300*
Corresponding author e-mail address: Basina.VNK@ufs.ac.za

1. Introduction

Upconversion (UC) luminescent materials doped with rare-earth (RE) ions have gained considerable attention for applications in colour displays, optoelectronics, sensor technology, imaging, biological labelling, and optical data storage. UC luminescence, involving the emission of high-energy photons through the absorption of low-energy photons (anti-stokes luminescence), is widely used in fluorescence intensity ratio (FIR) techniques for optical thermometry [1]. Conventional FIR methods rely on thermally-coupled energy levels (TCLs) within an energy gap (200–2000 cm⁻¹) obeying Boltzmann-distribution law [2], but this limits sensitivity due to the restricted energy difference. In contrast, thermometers based on non-thermally coupled energy levels (NTCLs) overcome these constraints, providing enhanced sensitivity without energy gap restrictions, thus offering greater flexibility and optimal thermometric performance [3]. Pyrochlore oxides ($A_2B_2O_7$) exhibit exceptional structural and chemical adaptability, making them suitable for diverse applications. Their unique structure, an ordered variant of disordered fluorite, is influenced by the size and charge of cations, particularly in lanthanide zirconates where the A-site cation size dictates the crystal structure [4]. The transition between pyrochlore and defect fluorite phases has been studied using X-ray diffraction (XRD), but a more detailed approach is required to fully understand the local disorder and structural complexity. This work compares the structural and optical properties of RE-activated $La_2Zr_2O_7$ (LZO) exhibiting ordered pyrochlore phase and $Y_2Zr_2O_7$ (YZO) with defective fluorite phase compounds synthesized via two methods namely, combustion (CMB) and microwave hydrothermal (MHT) methods.

2. Results

The structural characterization through XRD results confirmed the successful formation of LZO and YZO, both compounds with having the expected phases. The optical characterization studies, including photoluminescence (PL) under ultraviolet (UV) excitation and UC PL under 980 nm and 1550 nm laser excitation, revealed distinct luminescent properties. Under 378 nm excitation, both phosphor systems exhibited emissions spanning the visible (500–725 nm) and near-infrared (900–1600 nm) regions, with peak intensities at 545 nm, 980 nm, and 1530 nm. The UC PL results show enhanced green emission for Er³⁺-Yb³⁺ co-doped LZO and red emission for Er³⁺-Yb³⁺ co-doped YZO upon 980 nm laser excitation. Under 1550 nm laser excitation, the Er³⁺-doped samples exhibited superior luminescence compared to their Er³⁺-Yb³⁺ co-doped counterparts. Optical thermometry studies found that the Er³⁺-Yb³⁺ co-doped LZO prepared by the MHT method achieved a maximum absolute sensitivity of 54×10^{-4} K⁻¹ at 393 K (Fig. 1(a)) and 30.7×10^{-4} K⁻¹ at 313 K (Fig. 1(b)) for 980 nm and 1550 nm laser excitations, respectively. Similarly, the Er³⁺-Yb³⁺ co-doped YZO sample prepared by the CMB method achieved a maximum absolute sensitivity of 22×10^{-4} K⁻¹ at 433 K and 17.2×10^{-4} K⁻¹ at 353 K, respectively. Besides optical thermometry studies, the brightest among the samples, i.e., Er³⁺-Yb³⁺ co-doped LZO synthesized via the MHT method, demonstrated strong green luminescence under 980 nm laser excitation, offering potential for latent fingerprint (LFP) detection applications (Fig. 2).
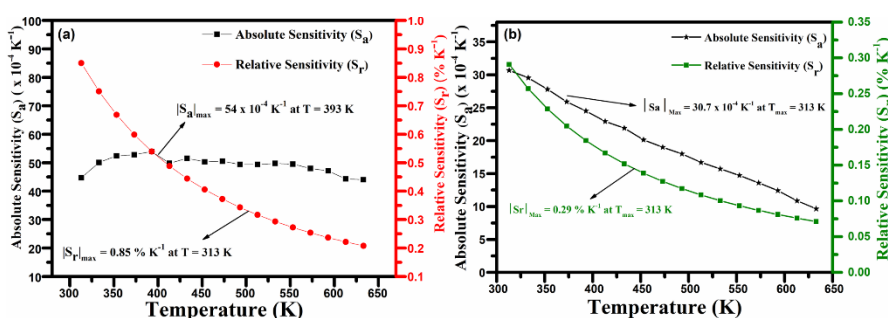
Fig.1: Sensitivity parameters of Er³⁺-Yb³⁺ co-doped LZO samples for (a) λ_{ex} = 980 nm and (b) λ_{ex} = 1550 nm.
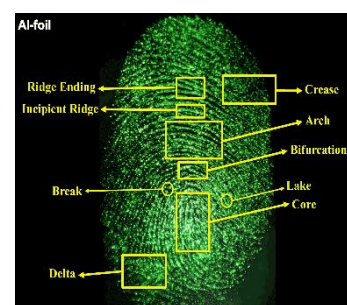
Fig. 2: LFP image using Er³⁺-Yb³⁺ co-doped LZO sample synthesized via MHT method under λ_{ex} = 980 nm.

3. References

[1] S. Jiang, P. Zeng, L.Q. Liao, S.F. Tian, H. Guo, Y.H. Chen, C.K. Duan, M. Yin, *J. Alloys Compd,* **617** (2014) 538.
[2] S.A. Wade, S.F. Collins, G.W. Baxter, *J. Appl. Phys,* **94** (2003) 4743.
[3] Q. Xiao, X. Dong, X. Yin, H. Wang, H. Zhong, B. Dong and X. Luo, *Mater. Res. Bull*, **141** (2021) 111326.
[4] E. Reynolds, et al., *Inorg. Chem,* **52** (2013) 8409.3

10th South African Conference on Photonic Materials – Amanzi 2025

Optimization of doping concentration for upconversion emission from Zn$_2$GeO$_4$:Er^{3+} phosphor

Anurag Pandey[1, 2], Vinod Kumar[3], Sumit Kumar[4], R. E. Kroon[1], H. C. Swart[1]

[1]*Department of Physics, University of the Free State, P. O. Box 339, Bloemfontein 9300, South Africa.*
[2]*J. H. S. Balbhadrapur, Ramnagar, Jaunpur-222137, Uttar Pradesh, India*
[3]*Department of Physics, The University of the West Indies, St. Augustine, Trinidad and Tobago.*
[4]*Department of Chemistry, Bharat Sevak Samaj College, Supaul, B. N. Mandal University, Bihar, India.*
Corresponding author e-mail addresses: vinod.phy@gmail.com, swarthc@ufs.ac.za

1. Introduction

The present research deals with the upconversion emission behaviour of Er^{3+}-activated Zn$_2$GeO$_4$ phosphors synthesized using a solid-state reaction technique. A series of phosphors have been prepared by changing the concentration of the dopant to optimize the concentration for optical emissions.

2. Results

The phase formation of the Zn$_2$GeO$_4$ was confirmed through X-ray powder diffraction analysis with a negligible effect due to the dopant [1]. The scanning electron microscopy analysis was performed to obtain the grain size and their formations. Micro-sized, well-arranged grains were obtained throughout the phosphor.

Using 980 nm excitation, the effect of the doping concentration on the upconversion emission spectra has been captured. The comparison of the upconversion emission showed that 3 mol% of Er^{3+} was the optimum concentration to be used in the present host to achieve maximum upconversion emission. To confirm the involved upconversion process, a power dependence upconversion emission study was done, and the involvement of a two-photon absorption process was responsible for the upconversion in the present investigation [2]. A schematic energy level structure is proposed to display the observed upconversion emission of the Zn$_2$GeO$_4$:Er^{3+} phosphor.
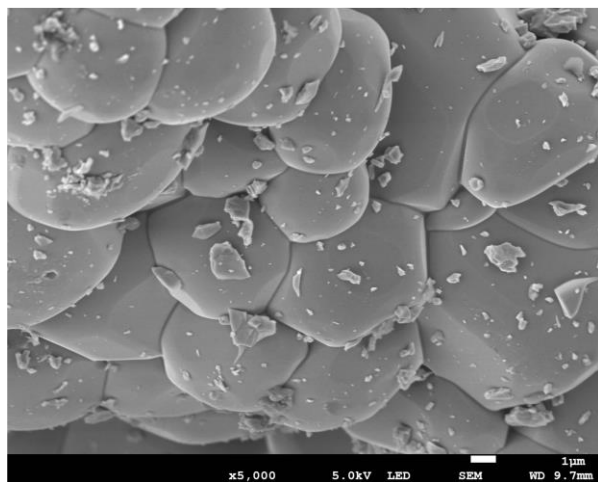
Fig. 18: SEM image for optimized Er^{3+} activated Zn$_2$GeO$_4$ phosphors.
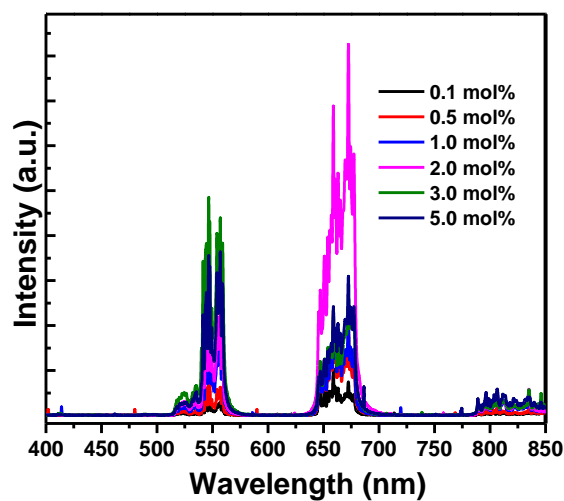
Fig. 2: UC emission for Er^{3+} activated Zn$_2$GeO$_4$ phosphors excited by 980 nm.

3. References.

[1] B. Li, S. Song, X.J. Sun, J. Peng, B. Wang and Y. Xing, C*hem. Res. Chinese Universities, 28(5)* (2012) 764-767.
[2] Chandni Kumari, Amalesh Kumar, S.K. Sharma, J. Manam, Vacuum, 207 (2023) 111599.

Novel Tin Dioxide-coated Gold and Silver Nanomaterials for Enhanced Solar Steam Generation

Tshepho Trevor Makgale[1] and **Mmantsae Diale**[1]

[1] University of Pretoria, Hatfield, Pretoria, South Africa
Corresponding author e-mail address: u14007739@tuks.co.za

1. Introduction

Solar steam generation (SSG), which harnesses the abundant and clean energy of sunlight, has emerged as one of the most promising technologies in addressing global freshwater scarcity [1]. One of the important applications of SSG is in water purification and desalination, which are processes critical to ensuring access to clean water. However, traditional SSG systems, which rely on sunlight to directly heat the entire bulk water, suffer from low solar energy conversion efficiency and result in insufficient bulk water temperatures [2, 3]. To overcome these limitations, researchers have explored a variety of solar absorbers including metallic nanomaterials [4], carbon-based materials [5] , semiconductors, and polymers to develop more efficient, modern solar-driven evaporation systems. A particularly promising approach involves nanofluid-based SSG systems, where plasmonic noble metals like gold (Au) and silver (Ag) serve as direct-absorption solar energy collectors. In this study, Au and Ag's nanostructures were coated with tin dioxide (SnO_2), and their blended mixtures were assessed to develop enhanced photothermal materials for solar steam generation.

2. Results

The ultraviolet-visible (UV-Vis) spectra in Fig. 1 revealed distinct surface plasmon resonance (SPR) peaks at 410 nm and 560 nm for the uncoated materials, indicating their characteristic plasmonic properties. In contrast, the SnO_2-coated materials displayed a broader absorption profile spanning from 350 — 850 nm, highlighting the impact of the SnO_2 coating on the optical behavior of the nanomaterial and the synergistic effects of material blending. Transmission electron microscopy (TEM) images in Fig. 2 showed that the SnO_2-coated Ag-Au nanomaterials in sample A were fully encapsulated within the SnO_2 layer, presenting a uniform and well-defined structure. Conversely, the uncoated Ag-Au nanomaterials in sample B exhibited a diverse range of sizes and shapes, as expected. The figure also demonstrates the color variations between the two samples: the coated nanomaterials exhibit a pale-gold hue, while the uncoated materials show a clear-gold color. These observations further highlight the influence of SnO_2 encapsulation on the optical and structural properties of the nanomaterials. Under 1.3511 Suns, solar steam generation efficiencies were 10.87, 10.71, and 10.32 for SnO_2-coated materials, uncoated materials, and pure water, respectively. Additionally, SnO_2-coated nanofluids showed a higher heat capacity (7734.12 J/°C·Kg) compared to CTAB-coated nanofluids (7709.25 J/°C·Kg) and pure water (4200 J/°C·Kg), demonstrating superior thermal performance.
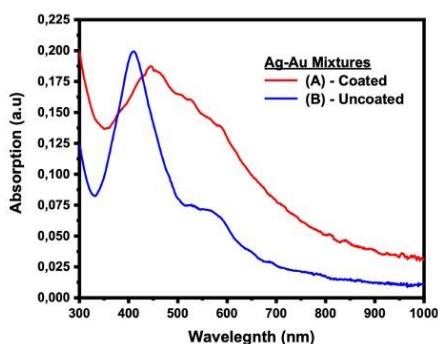
Fig. 19: The UV-Vis spectra of SnO_2-coated and uncoated silver-gold (Ag-Au) blended nanomaterials in colloidal solutions.
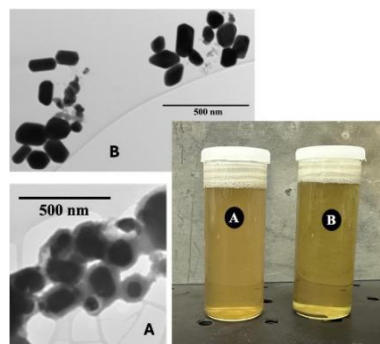
Fig. 2: TEM images of silver-gold (Ag-Au) nanomaterials: (A) SnO_2-coated sample and (B) uncoated sample.

3. References

[1]   J. Li, Y. Li, W. Song, X. Li, L. Yang, and L. Yan, "Boosting interfacial solar steam generation by three-dimensional bilayer cellulose aerogels," *J Colloid Interface Sci,* vol. 650, no. Pt A, pp. 339-349, Nov 15, 2023, doi: 10.1016/j.jcis.2023.06.205.

[2]   P. Zhang, Q. Liao, H. Yao, Y. Huang, H. Cheng, and L. Qu, "Direct solar steam generation system for clean water production," *Energy Storage Materials,* vol. 18, pp. 429-446, 2019, doi: 10.1016/j.ensm.2018.10.006.

[3]   S. N. Farabi *et al.*, "The future of solar-driven interfacial steam generation for sustainable water desalination: Drivers, challenges, and opportunities-review," *Results in Engineering,* vol. 23, 2024, doi: 10.1016/j.rineng.2024.102649.

[4]   Z. Deng *et al.*, "The emergence of solar thermal utilization: solar-driven steam generation," *Journal of Materials Chemistry A,* vol. 5, no. 17, pp. 7691-7709, 2017, doi: 10.1039/c7ta01361b.

[5]   H. Ghasemi *et al.*, "Solar steam generation by heat localization," *Nat Commun,* vol. 5, p. 4449, Jul 21, 2014, doi: 10.1038/ncomms5449.

Structural and optical properties of Dy^{3+}-doped La$_2$ZnTiO$_6$ nanophosphors prepared via sol-gel method

Delicacy Ntshalintshali[1], Moipone A. Malimabe[2], Hendrik C. Swart[3], Lehlohonolo F. Koao[1]

[1] *Department of Physics, University of the Free State (Qwaqwa campus), Private Bag X13, Phuthaditjhaba, 9866, South Africa*
[2] *Department of Chemistry, University of the Free State (Qwaqwa campus), Private Bag X13, Phuthaditjhaba, 9866, South Africa*
[2] *Department of Physics, University of the Free State (Bloemfontein campus), P.O. Box 339, Bloemfontein 9300, South Africa*
Corresponding author e-mail address: delicacy74@gmail.com

1. Introduction

Phosphor materials research has gained prominence due to the prospective applications of rare-earth (RE^{3+}) ions-activated phosphors in sensors, displays, and lighting. Low power consumption, high luminous efficacy, and environmentally friendly characteristics make phosphor-converted white light-emitting diodes (pc-wLEDs) attractive. The most accepted and commercially available pc-wLEDs are based on combining a blue-chip and yellow phosphor or a blue-chip, green, and red phosphor. However, the emitted white light from commercial LEDs suffers several disadvantages. Due to the lack of favourable components, they exhibit a highly correlated colour temperature (CCT 6000–8000 K) and a low colour rendering index (CRI < 80) [1]. The drawback of this technology has led researchers to focus their attention on synthesizing efficient red phosphors. Some hosts used as a part of RE^{3+}-doped red-emitting phosphors are titanates, molybdates, fluorides, tungstates, germinates, and silicates. The possibility of using RE^{3+}-doped phosphors in solid-state lighting and colour displays has greatly interested all RE^{3+} ions, particularly blue and yellow-emitting trivalent dysprosium (Dy^{3+}) ions. The Dy^{3+} ion is a vital activator whose emissions centres are based on the advantage of simultaneously emitting ($^4F_{9/2} \rightarrow {}^6H_{15/2}$), ($^4F_{9/2} \rightarrow {}^6H_{13/2}$), ($^4F_{9/2} \rightarrow {}^6H_{13/2}$), and ($^4F_{9/2} \rightarrow {}^6H_{9/2}$) electronic transition emissions in the ultra-violet (UV), blueish green, yellow, and red wavelengths [2]. This work reports a new example of a Dy^{3+}-activated Zn^{2+}-based lattice structure, namely La$_2$ZnTiO$_6$. The blue-emitting phosphors exhibit emission colour-tuneable behaviour. An in-depth investigation of the effect of Dy^{3+} ions on luminescence properties was conducted. The results indicated that it would be a suitable component for pc-LEDs that emit yellow light.

2. Results

X-ray diffraction results indicated that all La$_2$ZnTiO$_6$:x%Dy^{3+} ($0 \leq x \leq 7.0$) nanophosphors exhibited monoclinic crystal structures. The UV-Vis spectra revealed that the reflectance spectra were dominated by absorption edges around 300 to 400 nm and 740 to 960 nm. Fig. 1 illustrates the emission spectra of La$_2$ZnTiO$_6$:x%Dy^{3+} ($0 \leq x \leq 7.0$) nanophosphors after monitoring the excitation at 264 nm. Four emission bands were observed at 481, 575, 664, and 752 nm which are attributed to Dy^{3+} electronic transition [2]. The International Commission on Illumination (CIE) colour chromaticity diagram obtained from the emission spectra is shown in Fig. 2. The undoped La$_2$ZnTiO$_6$ displayed a white-yellow colour. At the same time, after doping with the x mol% of Dy^{3+}, there was a slight shift to yellow colour emission.
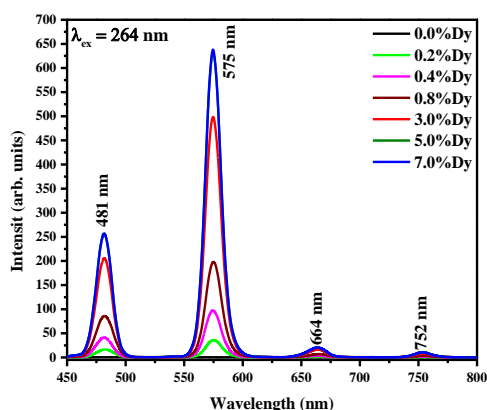
Fig. 20: Emission spectra of La$_2$ZnTiO$_6$:x%Dy^{3+} ($0 \leq x \leq$ 7.0) nanophosphors.
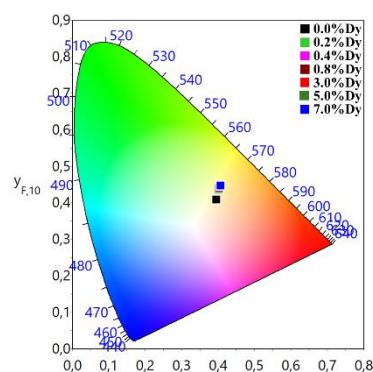
Fig. 2: The CIE colour chromaticity diagram of La$_2$ZnTiO$_6$:x%Dy^{3+} ($0 \leq x \leq 7.0$) nanophosphors.

3. References

[1] N. Sonali, V. Chauhan, P.C. Pandey, C. Shivakumara. *ACS Appl. Opt. Mater.* **2** (2024) 41-56.
[2] R. Shrivastava, J. Kaur, V. Dubey. *J. Fluoresc.* **26** (2016) 105-111.

Enhanced Green and Orange-Red Dual Luminescence Emissions of $Zn_{0.5}Ca_{0.5}Al_2O_4$: Tb^{3+}, Sm^{3+} Phosphors Stimulated by Crystallinity: Effects of Annealing Temperature

C. Dlamini[1,3], T.P. Mokoena[2], V.M. Maphiri[3], M.R. Mhlongo[3]

[1]*Department of Physics, Sefako Makgatho Health Sciences University, P.O. Box 94, Medunsa, 0204, South Africa*
[2]*Department of Physics, University of Free State (QwaQwa Campus), Private bag X13, Phuthaditjhaba, 9866, South Africa*

[3]*Department of Physics, Sefako Makgatho Health Sciences University, P. O. Box 94, Medunsa, 0204, South Africa*

Corresponding author e-mail address: Rebecca.mhlongo@smu.ac.za

1. Introduction

Luminescent rare earth activated phosphor materials have transformed the perspective of photonics with applications in the fields such as light-emitting diodes, illumination, display technologies, optoelectronic devices, and biomedical [1]. Samarium (Sm^{3+}) and Terbium (Tb^{3+}) are excellent activators for red and green-emitting phosphors, respectively. They show emissions at 552 and 610 nm assigned to $^5D_4 \rightarrow {}^7F_3$ and $^4G_{5/2} \rightarrow {}^6H_{7/2}$ transitions of Tb^{3+} and Sm^3, respectively [2]. $Zn_{0.5}Ca_{0.5}Al_2O_4$ doped with 0.1%Tb^{3+} and co-doped with Sm^{3+} were prepared by sol-gel method and the effect of annealing temperature was investigated. The crystal structure was confirmed by x-ray diffraction (XRD) and the functional groups were identified by Fourier transform infrared spectroscopy (FTIR). The particle morphology and elemental composition were analysed by scanning electron microscopy (SEM) and energy dispersive x-ray spectroscopy (EDS), respectively. The luminescence characteristics of nanophosphors were analysed by photoluminescence (PL).

2. Results

Fig.1 presents the PL excitation and emission spectra of nanophosphors monitored at the emission wavelength of 552 nm, and the excitation peak located at 238 nm, corresponds to the $^7F_6 \rightarrow {}^5D_4$ transition of Tb^{3+}. The sample annealed at 1200 ºC has a relatively high intensity at around 428 nm ($^5D_4 \rightarrow {}^7F_6$) transition of Tb^{3+}. In Fig. 2 under the emission wavelength of 610 nm, two excitation peaks located at 369 and 408 nm ascribed to $^6H_{5/2} \rightarrow 4G_{9/2}$, $^6P_{7/2}$ transitions of Sm^{3+} ions were acquired [3]. The 408 nm excitation wavelength produced several peaks at around 573, 610, 660, and 705 nm assigned to $^4G_{5/2} \rightarrow {}^6H_{5/2}$, $^6H_{7/2}$, $^6H_{9/2}$, and $^6H_{11/2}$ transitions of Sm^{3+}, respectively.
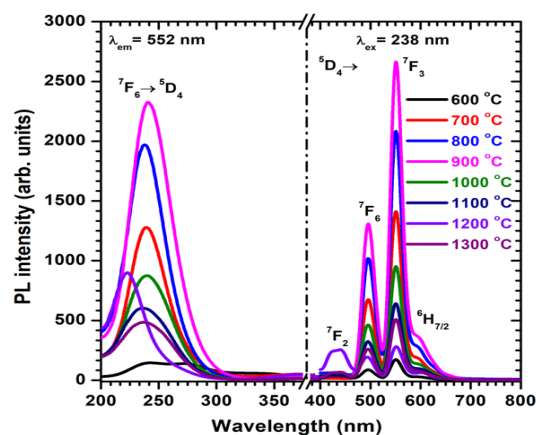
Fig.1: PL excitation and emission spectra of $Zn_{0.5}Ca_{0.5}Al_2O_4$: Tb^{3+}, $Sm3^+$ excited under the 238 nm wavelength.
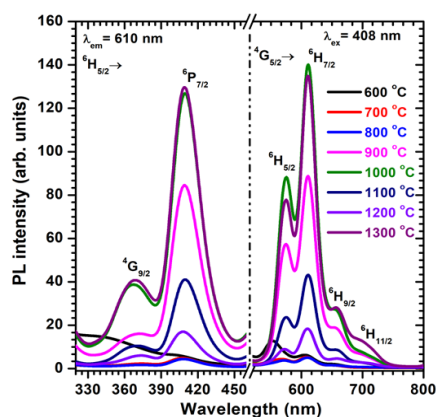
Fig.2: PL excitation and emission spectra of $Zn_{0.5}Ca_{0.5}Al_2O_4$: Tb^{3+}, $Sm3^+$ excited under the 408 nm wavelength.

3. References

[1] G. Kumar K, P. Balaji, K. Aravinth, N. Ahmed, C. Balaji, Cera. Int. 48 (2022) 36045.
[2] D. Gao, S. Liu, Y. Li, L. Cheng, X. Zhang, J. Zhang, S. Xu, X. Li, Y. Cao, Y. Wang, H. Yu, Y. Zhang, X. Sha, L. Wang, B. Chen, Mater. Chem. Phy. 297 (2023) 127388.
[3] R. Paikaray, T. Badapanda, H. Mohapatra, T. Richhariya, N. S. Tripathy, Mater. Tod. Commu. 40 (2024) 109296.

Sodium-Ion Energy Storage Devices Characterization Using a Novel Low-Cost Microcontroller-Based Instrument

Mbali Marole, Kamohelo Tshabalala, Richard Ocaya.

[1] *University of the Free State, Phuthaditjhaba.*
Corresponding author e-mail address: 2017107414@ufs4life.ac.za

1. Introduction

This work addresses the challenge of characterizing the chemistry and electrical performance of sodium-ion supercapacitors (SCs) and batteries, driven by growing interest in alternatives to lithium-ion technology. The primary objective is to design and implement a cost-effective, microcontroller-based instrument for accurate, real-time voltage and current characterization of these devices. The developed system connects to a computer via a USB interface for data transmission, processing, and storage, enabling rapid electrochemical analysis through cyclic voltammetry. The design prioritizes affordability while achieving performance comparable to commercial instruments. The instrument automates the charging and discharging of electrochemical devices using switchable constant currents, controlled by an Arduino Uno microcontroller and electromechanical relays. Key parameters, including capacitance, equivalent series resistance (ESR), energy density, and power density, are evaluated. Circuit designs were developed and simulated in LTSpice before construction, with a commercial 20F/2.5V SC serving as a test standard. Measurements on the standard SC yielded capacitance values between 18-22 F, stored energy between 43.56-53.24 J, and an ESR of 5.59 Ω, aligning well with commercial specifications. Oscillatory behavior observed during high-current discharges highlighted SC degradation. After calibration, the instrument was used to characterize fabricated SCs in practical applications, such as powering light-emitting diodes (LEDs) and resistive loads. The SCs demonstrated energy capacities up to 4750 mAh and powered LEDs for several hours. Comparative measurements using a commercial digital multimeter validated the accuracy of the instrument. The results confirm the developed reliability and utility of the instrument for SC evaluation while identifying challenges such as self-discharge, temperature sensitivity, and scalability for practical use. This work establishes a foundation for future research and development in affordable characterization tools and energy storage technologies.

2. Results

Testing with a commercial 20F/2.5V SC yielded results aligning with specifications, confirming accuracy. The instrument was further used to characterize fabricated SCs, demonstrating energy capacities up to 4750 mAh and successfully powering LEDs for hours. Comparative measurements with a commercial multimeter validated the instrument's performance.
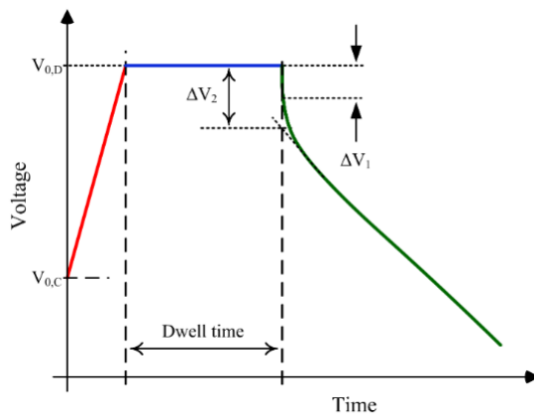
Fig. 21: Charging/discharging profile of the SC
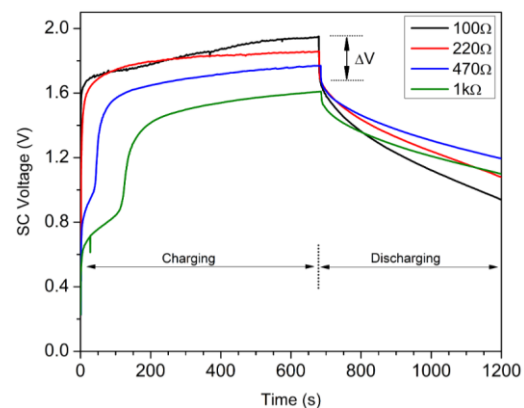
Fig. 2: Charging and discharging voltage profiles of the fabricated SC. Constant charging current 2.8V.

3. References

[1] C. Cohen-Tannoudji, B. Diu and F. Laloë. *Quantum Mechanics* (Wiley-VCH, 2005), Chap. 3.
[2] A. Bauknecht, S. Siebentritt, J. Albert and M. C. Lux-Steiner. *J. Appl. Phys.* **89** (2001) 4391.

Influence of fuel ratio and dopant concentration on luminescent properties of Eu-doped SnO$_2$

Pule Nche, R.E. Kroon

Department of Physics, University of the Free State, Bloemfontein ZA-9300, South Africa
Corresponding author e-mail address: pule.nche22@gmail.com

1. Introduction

Although SnO$_2$ is documented as a prominent transparent conducting oxide (TCO) due to its high electron mobility, chemical stability, and very high transparency in the visible region, it is not applied for luminescent applications. This restricts its use in multifunctional devices that need both conductivity and luminescence properties. Doping SnO$_2$ with rare-earth (RE) ions such as Eu^{3+} may add luminescent properties, resulting in dual-functional luminescent TCO material, thus leading to new possibilities for applications in transparent displays, sensors, as well as advanced optoelectronic devices. One of the important components required for the solution combustion synthesis (SCS) of oxide materials, besides an oxidizer (e.g. metal nitrates) and the correct temperature, is fuel. Urea is regarded as an ideal fuel [1]. The stoichiometric compositions of fuels and oxidizers are important since they affect the oxide material's properties, and therefore studying this effect could yield vital information on producing optimized alternative TCOs for practical applications. In this study, the SnO$_2$ powders were synthesized using the SCS method where tin nitrate was the oxidizer and the fuel used was urea.

2. Results

Optical studies were performed using photoluminescence (PL) spectroscopy to investigate the role of fuel composition as well as Eu^{3+} dopant concentration on the luminescence properties of the synthesized SnO$_2$:Eu^{3+} phosphor powder samples. Emission spectra were recorded at excitation wavelengths of 300 nm (Fig. 1) and 394 nm (Fig. 2) for the samples prepared using urea (U) at different fuel amounts (L = low, S = stoichiometric, H = high) and with different Eu^{3+} concentrations of 0.2 mol% and 2 mol%. In Fig. 1, the most intense spectrum was observed for the sample prepared with a low (L) fuel amount and a dopant concentration of 0.2 mol%, whereas the sample with 2 mol% Eu^{3+} concentration and low fuel amount resulted in the most intense spectrum in Fig. 2. The symmetry of the SnO$_2$ lattice sites occupied by Eu^{3+} ions is represented by the presence and relative intensities of the Eu^{3+} peaks [2]. The luminescent intensity of a Eu^{3+} peak depends on the host crystal, and this dependence alludes to the transfer of energy from the SnO$_2$ crystal to the Eu^{3+} ion. The predominant transition in Fig. 1 is the magnetic dipole (MD) transition $^5D_0 \rightarrow {}^7F_1$, indicating that the Eu^{3+} ions are located at a site with inversion symmetry/centrosymmetric site [3]. In Fig. 2, however, the electric dipole (ED) transition $^5D_0 \rightarrow {}^7F_2$ is the dominant transition, meaning that the Eu^{3+} ions are occupying non-centrosymmetric sites, possibly located at interstitial and/or distorted sites of the SnO$_2$ host lattice.
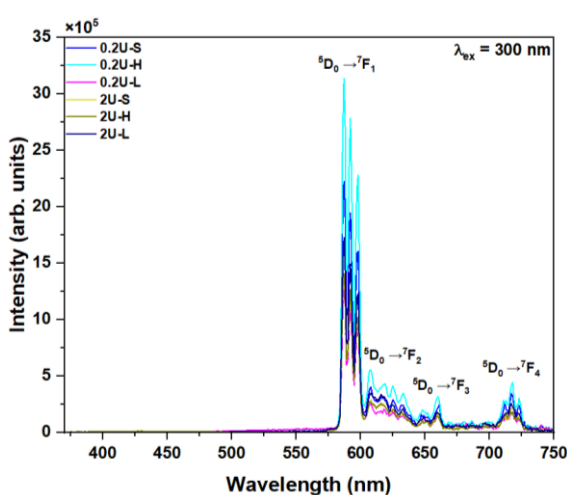
Fig. 22: Emission spectra of Eu-doped SnO$_2$ acquired at λ_{ex} = 300 nm
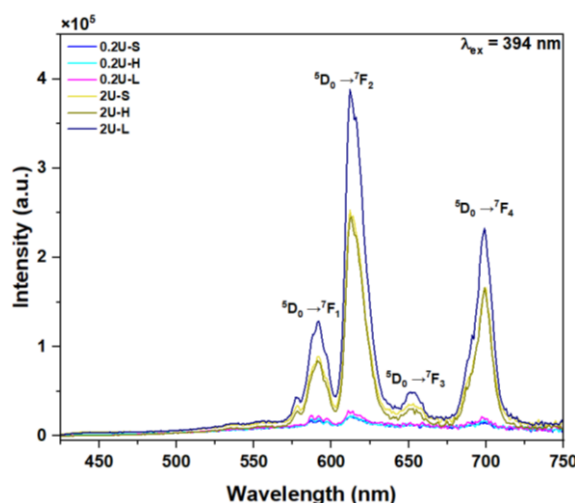
Fig. 2: Emission spectra of Eu-doped SnO$_2$ acquired at λ_{ex} = 394 nm

3. References

[1] M.S. Hedge, S.T. Aruna, T. Rattan, and K.C. Patil. *Chemistry of nanocrystalline oxide materials: combustion synthesis, properties and applications* (World Scientific, 2008).
[2] S. Bazargan and K.T. Leung. *Journal of Chemical Physics* **137** (2012) 184703.
[3] D.F. Crabtree. *Journal of Physics D: Applied Physics* **11** (1978) 1545.

Analysis of temperature-dependent characteristics of Cr/P-doped Si Schottky barrier diodes before and after 5.4 MeV ^{241}Am irradiation

Ezekiel Omotoso[1,2,3], Walter E. Meyer[1], Aletta R.E. Prinsloo[2], F. Danie Auret[1], Emmanuel Igumbor[1] and Charles J. Sheppard[2]

[1] *Department of Physics, University of Pretoria, Pretoria, Private Bag X20, Hatfield 0028, South Africa*
[2] *Cr Research Group, Department of Physics, University of Johannesburg, Johannesburg, PO Box 524, Auckland Park 2006, South Africa*
[3] *Department of Physics and Engineering Physics, Obafemi Awolowo University, Ile-Ife, 220005, Nigeria*
Corresponding author's e-mail address: omotoeze@gmail.com

1. Introduction

The study of transition metals has gained significant attention in the last decade due to their unique properties including durability, magnetic characteristics, and conductivity. Among these metals, titanium has been extensively researched for Schottky barrier diodes (SBDs) due to its thermal stability and low contact resistance, while chromium, despite its high work function (4.50 eV) and valuable surface magnetic and adhesive properties, has been less commonly used as a Schottky contact [1]. Metal-semiconductor (M-S) SBDs are crucial components in electronic devices, with applications ranging from rectification to signal conditioning [2]. The performance of these devices depends not only on the metallic contacts but also on the substrate materials and deposition techniques used in their fabrication. Research on Cr SBDs evaporated on n-Si by electron beam deposition, and their behaviour under cryogenic as well as room temperature irradiation remains limited and needs to be investigated. Temperature-dependent current-voltage (*IV*) and capacitance-voltage (*CV*) characteristics of Cr/n-Si SBDs were measured in the temperature range of 60 – 300 K, before and after irradiation with alpha particles from an 5.4 MeV ^{241}Am source at a fluence of 1.3×10^{10} cm^{-2}.

Chromium SBDs of thickness 1000 Å were evaporated via electron beam deposition on n-Si. The SDBs fabricated were initially characterized by *IV*, *CV* and DLTS to confirm the diodes' suitability. Post-irradiation characterization by *IV*, *CV*, and DLTS measurements was also employed to understand the effect of measuring temperatures as well as irradiation on current transport, barrier inhomogeneity, and defects in diodes. A morphological study was also carried out.

2. Results

The reverse leakage current decreased with decreasing temperature as shown in Fig. 1, indicating the inactivity of deep-level defects at lower temperatures. Alpha-particle irradiation led to slightly more noticeable lateral inhomogeneity in the Schottky barrier height at the interface of Cr and n-Si, causing a deviation in the modified Richardson constant from the theoretical value (112 A.cm^{-2}K^{-2}). Despite the presence of deep-level defects obtained by deep level transient spectroscopy as shown in Fig. 2, the Cr/n-Si SBDs exhibited resistance to alpha-particle irradiation, which suggests their potential for use in temperature-varying environments.
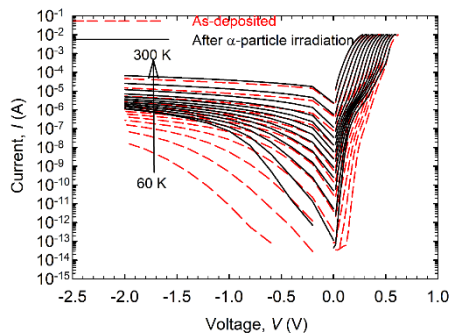
Fig. 23: The semi-logarithmic IV characteristics of the Cr/n-Si SBDs.
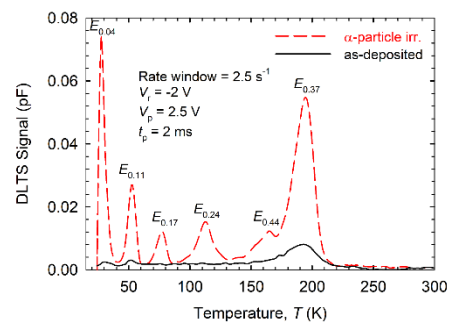
Fig. 2: The DLTS spectra of defects induced in n-Si after irradiation.

3. References

[1] A. Kulkarni and L. Chang. *Thin Solid Films* **301**(1-2) (1997) 17-22.
[2] B. Sharma. *Metal-semiconductor Schottky barrier junctions and their applications*, Springer Science & Business Media 2013.

Characterization and synthesis of Eu^{2+} doped $SrAl_2O_4$ phosphor for green emission

Lethabile Masiu, Mart-Mari Duvenhage, MYA Yagoub

Physics Department, University of the Free State, P.O. Box 339, Bloemfontein 9300, South Africa
lethabilemasiu@gmail.com

1. Introduction

This study presents a comprehensive analysis of $SrAl_2O_4$ phosphors synthesized and characterized through X-ray diffraction (XRD), photoluminescence (PL), and UV-Vis spectroscopy. The XRD analysis revealed the successful formation of monoclinic $SrAl_2O_4$ with prominent peaks (CIF file-2002284) at 2θ angles of 28.38°, 29.28°, 29.91°, 34.80°, and 35.11° at an annealing temperature of 1600°C. This indicates the successful crystallization of the desired phase, while unreacted $SrCO_3$ was observed at lower temperatures, suggesting incomplete reaction and the necessity for high-temperature annealing to achieve phase purity [1].

The structural effects of Eu^{2+} doping were thoroughly examined, demonstrating interesting trends. At low Eu^{2+} concentrations, lattice contraction was observed, likely due to the substitution of Sr^{2+} with the smaller Eu^{2+} ions [2]. As the doping concentration increased to intermediate levels, lattice expansion occurred, which could be attributed to the stress relief and redistribution of Eu^{2+} within the lattice [3]. However, further doping, saturation, and clustering effects were noted, suggesting that excessive Eu^{2+} leads to aggregation rather than further incorporation into the lattice, potentially impeding luminescent efficiency. Photoluminescence (PL) analysis highlighted the optimal luminescent properties of $SrAl_2O_4$: Eu^{2+} synthesized through a two-step calcination and annealing process. This method ensured the complete reduction of Eu^{3+} to Eu^{2+} in Ar-5%H_2 using a Chengyi-1700 ceramic furnace with a gas mixture, which was critical for achieving strong luminescence. The PL results showed enhanced emission intensity, indicating the effective role of the synthesis process in optimizing the luminescent properties. The 1.0 mol% Eu^{2+} doped sample (Fig. 1) was identified as the optimal candidate for enhanced luminescent applications, as it exhibited superior luminescent intensity and stability.

UV-Vis spectroscopy results in Fig. 2 supported the PL findings by showcasing distinct absorption features attributed to Eu^{2+} doping. The absorption spectra exhibited characteristic bands corresponding to Eu^{2+} (4f-5d), reinforcing the successful doping and its impact on the optical properties of the phosphor.

Complementary analyses, including Scanning Electron Microscopy (SEM) and Time-of-Flight Secondary Ion Mass Spectrometry (TOF-SIMS), further corroborated these findings. SEM provided insights into the morphology and uniformity of the phosphor particles, while TOF-SIMS offered detailed compositional analysis, confirming the homogeneous distribution of Eu^{2+} within the $SrAl_2O_4$ matrix. Additionally, X-ray Photoelectron Spectroscopy (XPS) analysis was employed to further validate the oxidation state of europium in the sample. The XPS results confirmed the presence of Eu^{2+}, which is crucial for the phosphor's luminescent properties. This comprehensive study underscores the importance of precise synthesis and doping strategies in optimizing the optical properties of $SrAl_2O_4$ phosphors, paving the way for their application in advanced luminescent technologies.

2. Results
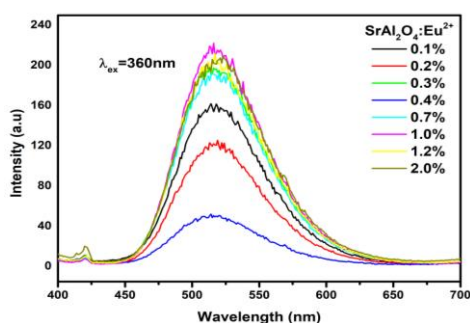
Fig 1: PL of Eu^{2+} doped $SrAl_2O_4$ excited at 360 nm
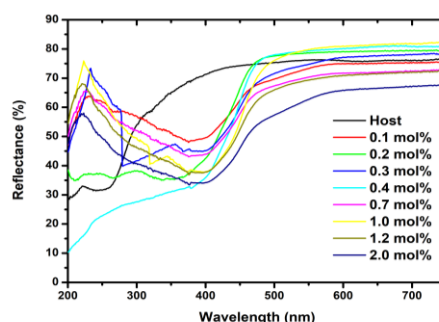
Fig 2: The reflectance and absorption of the $SrAl_2O_4$: Eu^{2+}

3. References

[1] Liu, Y., et al. (2018). High-temperature synthesis and phase purity of $SrAl_2O_4$ phosphors. *Ceramics International*, 44(8), 9919-9926.
[2] Chen, H., et al. (2020). Structural and luminescent properties of Eu^{2+} doped $SrAl_2O_4$ phosphors. *Journal of Luminescence*, 219, 116945.
[3] Wang, X., et al. (2021). Redistribution of Eu^{2+} in $SrAl_2O_4$ lattice and its impact on optical properties. *Journal of Alloys and Compounds*, 866, 158855.

Innovative toxic-free exfoliation of bulk g-C3N4: morphological evolution of ultra-thin (1D/2D) g-C3N4 nano-sheet/tube to accelerate sunlight-driven photocatalytic activity

Sandeep Eswaran Panchu[1], Hendrik C. Swart[1]

[1] *Department of Physics, University of the Free State, P.O. Box
, Bloemfontein 9300, South Africa*

Corresponding author e-mail address: sandeepeswaran37@email.ac.za

1. Introduction

This study explores a green, in-situ solvothermal exfoliation of bulk g-C3N4 into nanosheets, enhancing photocatalytic degradation of CR and TC under sunlight without secondary pollution [1-3]. This study presents a novel approach to exfoliate and dope bulk g-C3N4 (CN) with heteroatoms, generating free oxygen ions (O^{2-}) and significantly enhancing its optoelectronic and physicochemical properties. The bulk CN transformed from thick multilayers into 2D ultrathin nanosheets and 1D nanotubes, improving band structure, pore network, surface area, and charge carrier separation.

2. Results

The exfoliated CN (CN-48) achieved 220% and 180% higher degradation rates for CR and TC, respectively, compared to bulk CN. The total organic carbon and chemical oxygen demand is 70% and 74%, respectively. CN-48 maintained sustainable CR (98%) and TC (93%) degradation over five cycles. This eco-friendly method offers a superior, scalable pathway for enhanced photocatalytic performance under sunlight.
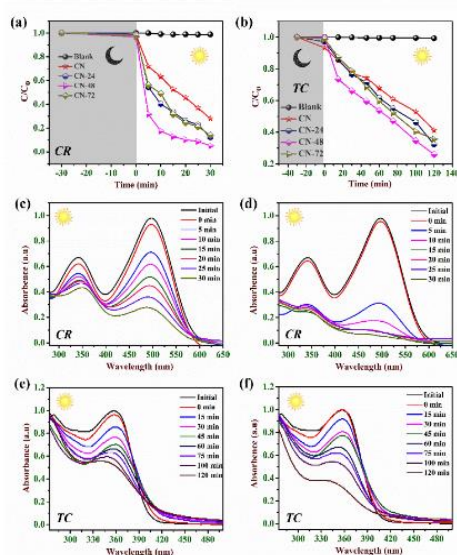
Fig. 1: Photocatalytic activity: (a) CR degradation and (b) TC degradation. Evolution of CR degradation: (c) CN and (d) CN-48. Evolution of TC degradation: (e) CN and (f) CN-48.
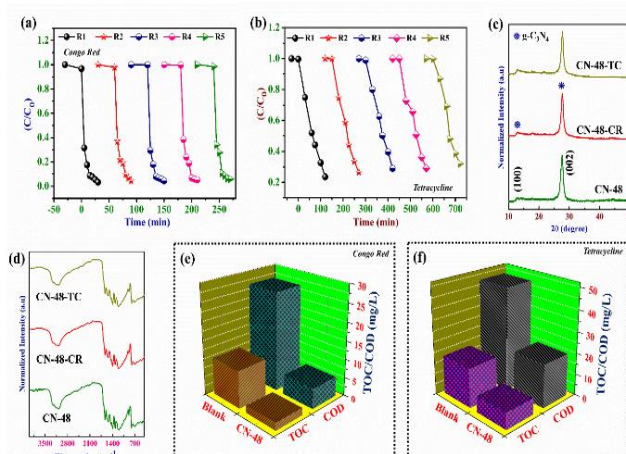
Fig. 2: Reusability of CN-48: (a) CR and (b) TC degradation. Stability analysis of CN-48 after 5 consecutive degradations of CR and TC: (c) XRD pattern and (d) FTIR spectra. TOC and COD quantification of before and after degradation: (e) CR degradation and (f) TC degradation

3. References

1. Shekardasht, M. B.; Givianrad, M. H.; Gharbani, P.; Mirjafary, Z.; Mehrizad, A. *Diam Relat Mater* **2020**, 109, 108008.
2. Aditya, M. N.; Chellapandi, T.; Prasad, G. K.; Venkatesh, M. J. P.; Khan, M. M. R.; Madhumitha, G.; Roopan, S. M. *Diam Relat Mater* **2022**, 121, 108790.
3. Guo, F.; Huang, X.; Chen, Z.; Sun, H.; Shi, W. *Sep Purif Technol* **2020**, 253, 117518.

Influence of Ga^{3+} on ZnO nanorods grown on GZO thin film seed layer by chemical bath deposition

Jatani Ungula[1], Sharon Kiprotich[2], Hendrik Swart[3]

[1] *Department of Pure and Applied Sciences, Kenya Methodist University, P.O Box 267, Meru 60200, Kenya*

[2]*Department of Physical and Biological Sciences, Murang'a University of Technology, Murang'a, Kenya*
[3]*Department of Physics, University of the Free State, PO Box 339, Bloemfontein 9300, Republic of South Africa*

Corresponding author e-mail: jatani.ungula@kemu.ac.ke;

1. Introduction

Among the many applications, ZnO has potential for use in dye-sensitized solar cells (DSSCs), light-emitting diodes, and chemical sensors. Well-aligned ZnO nanorods (ZNRs) are suitable for use in DSSCs because they provide larger surface areas than bulk ZnO and ZnO films required to provide anchoring sites for the dye. Additionally, ZNRs provide a direct conduction pathway for charge transfer from the position of electron-hole pair generation to the collecting electrode [1]. To understand better the properties of the ZNRs grown on the Gallium-doped ZnO (GZO) transparent conductive film by chemical bath deposition, herein, we showed that doping of ZNRs with various amounts of 0.5, 1, 1.5, 2, 3, 5 mol% Ga, modifies the structural, optical and morphological properties of ZNRs. The SEM images showed that all undoped and variously doped ZNRs were well-aligned and effectively established on the GZO seed layer. The average length and diameter of the nanorods were approximately 1 μm and 90 nm, respectively. X-ray diffraction patterns showed that the estimated crystallite size increased with the concentration up to 3 mol% Ga and it decreased again at the higher concentration of 5 mol% and was in the order of 100 nm. It was found that the peaks of all the samples related to the wurtzite structure ZnO (100), (002), and (101) diffraction peaks. The well-pronounced (002) peak indicates that the nanorods were preferentially oriented in the c-axis direction. Under UV (325 nm He-Cd Laser) excitation all samples yielded good luminesce and revealed excitonic emission as well as deep-level emission of ZnO. The PL intensity increased with the Ga 3+ ions concentration up to 3 mol% and then decreased with a further increase of the doping concentration. The DLE peak shifted significantly to higher excitation wavelength with concentrations of added Ga as shown in Fig 1. The band gap was found to decrease from 3.29 eV to 3.25 eV, Fig 2, with an increase in Ga amount added pointing to an inverse relation between the optical band gaps and Ga-doping concentration. The so-grown optimized Ga-doped ZNRs semiconductor achieved at 2 mol% Ga, along with the underlying GZO seed layer, offers a promising combination for the manufacture of the photoelectric component of DSSCs.

2. Results
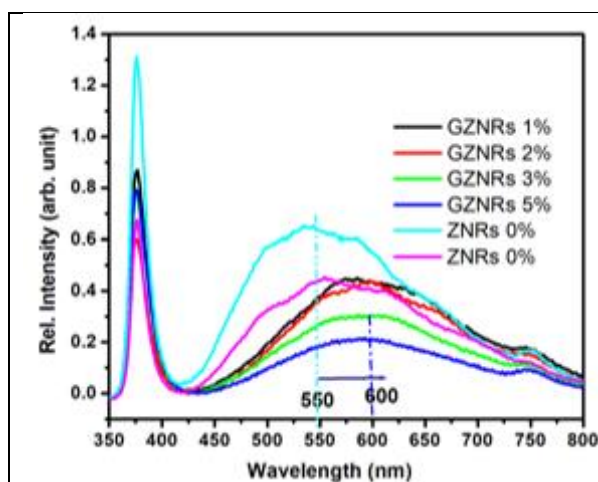
Fig. 24: PL emission spectra for ZNRs, GZNRs 1, 2, 3, and 5 mol. % Ga doping
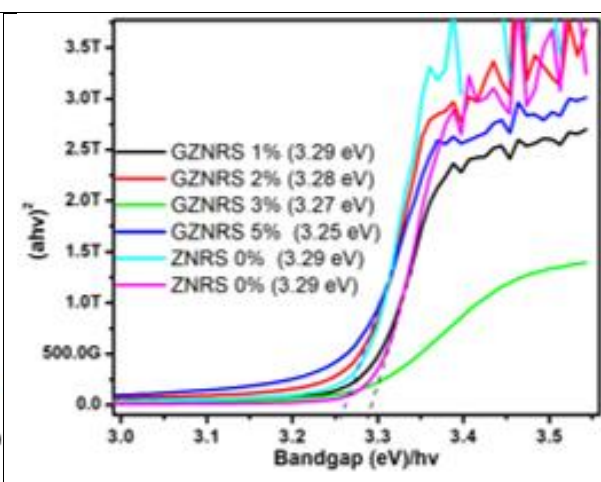
Fig. 2: The Band gap plot for ZNRs, GZNRs 1, 2, 3, and 5 mol. % Ga doping

3. References

[1] O. Lupan, V.M. Guérin, I M. Tiginyanu, V.V. Ursaki, L. Chow, H. Heinrich, T. Pauporté, Well-aligned arrays of vertically oriented ZnO nanowires electrodeposited on ITO-coated glass and their integration in dye-sensitized solar cells, Journal of Photochemistry and Photobiology A: Chemistry 211 (2010) 65-73.

Effect of different sources of Cu –dopant on material properties of ZnO NRs grown on a GZO film by chemical bath deposition for photovoltaic applications

Jatani Ungula[1], Sharon Kiprotich[2], Hendrik Swart[3]

[1] *Department of Pure and Applied Sciences, Kenya Methodist University, P.O Box 267, Meru 60200, Kenya*

[2]*Department of Physical and Biological Sciences, Murang'a University of Technology, Murang'a, Kenya*
[3]*Department of Physics, University of the Free State, PO Box 339, Bloemfontein 9300, Republic of South Africa*

Corresponding author e-mail address: jatani.ungula@kemu.ac.ke;

1. Introduction

The controlled incorporation of dopants like copper into ZnO nanorods (ZNRs) grown by chemical bath deposition (CBD) is still challenging despite its critical importance for the development of optoelectronic devices such as dye-sensitized solar cells (DSSCs), and piezoelectric devices (1). In this context, the effects of different sources of copper precursor on material properties of the ZNRs during the CBD of ZNRs grown on Ga-doped ZnO (GZO) seed layers is investigated in detail. The present findings provide a deep insight into the physicochemical processes at work during the CBD of ZNRs following the addition of different sources of copper precursor. The study also explores how the varied copper sources affect the incorporation of Cu into ZNRs, which is considered beyond the electrostatic forces usually driving the incorporation of dopants such as Al and Ga. X-ray diffraction, scanning electron microscopy, UV-Vis, and photoluminescence (PL) are used to characterize the properties of pure-ZNRs (ZNRs), copper (II) nitrate-doped ZNRs (CNZNRs), copper (II) sulphate-doped ZNRs (CSZNRs) and copper (II) chloride-dope ZNRS (CCZNRs). The structural investigations confirmed that all samples grown had wurtzite hexagonal structures and that the c-axis was the sole orientation of growth. The CNZNRs presented the sample with the highest crystallinity and lowest strain. SEM images showed miniaturized morphology for the CCZNRs sample but well-formed and aligned CCZNRs and CNZNRs counterparts, Fig. 1(a) and (b). Similarly, good luminescence and a low density of deep-level defects as marked by high PL emission intensity ratios were observed for ZNRs, CNZNRs, and CSZNRs in that order, but diminished luminescence in the case of copper chloride doping. The optical analysis displayed the highest percentage transmittance for CNZNRs and a red shift in the absorption edges and peaks with changes in Cu-dopant precursor. The bandgap values were observed to increase from 3.27-3.29 eV corresponding to ZNRs and CCZNRs. CNZNR samples exhibited enhanced crystallinity, good alignment, density, and good emission characteristics compared to the ZNRs and those doped with other Cu sources. Thus, the CNZNR semiconductor, along with the underlying GZO transparent conducting seed layer offers a promising combination for the manufacture of the photoelectric component of DSSCs.

2. Results
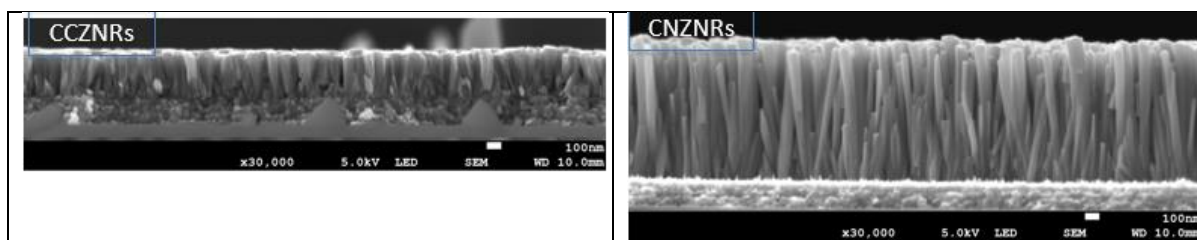
Fig. 1(a) cross-sectional view SEM image for CCZNRs grown on GZO seed layer

Fig. 25(b) cross-sectional view SEM image for CNZNRs grown on GZO seed layer

3. References

[1] C. Lausecker, B. Salem, X. Baillin, O. Chaix-Pluchery, H. Roussel, et al..Chemical Bath Deposition of ZnO Nanowires Using Copper Nitrate as an Additive for Compensating Doping. Inorganic Chemistry, 2021, 60 (3), pp.1612-1623.

Ab initio investigation of the boron vacancy complex

Chantel Mare

Department of Physics, University of Pretoria, South Africa

Corresponding author e-mail address: chantel.mare@up.ac.za

1. Introduction

The substitutional boron-vacancy complex ($B_s V$) is investigated using density functional theory. The results of these theoretical calculations are compared to previously done experimental as well as computational studies. All calculations were performed using spin-polarized density functional theory (DFT) using optimized norm-conserving Vanderbilt Pseudopotential and Quantum Espresso. All calculations were performed using a 216-atom supercell and sampled at gamma point. The electronic structure of the second nearest neighbour configuration of the defect is investigated and compared with the previously done EPR study by Watkins [1]. The metastability of the defect is also investigated and compared to previous calculations performed by Jones *et. al* [2]. It is shown that in both the neutral and negative charge states, the lowest energy configuration is the second nearest neighbour configuration with C_1 symmetry. In the positive charge state, the second nearest neighbour configuration with C_{1h} symmetry is found to be the lowest energy state.

2. Results

It was found that the second nearest neighbour configuration had lower energy than the first nearest neighbour configuration for each charge state. In the case of the negative and neutral charge state, the configuration with C_1 symmetry was found to have the lowest energy, while in the case of the positive charge state, the configuration with C_{1h} symmetry was found to have the lowest energy. This can be explained by the removal of the dangling bond when in the positive charge state and is in accordance with the model first proposed by Watkins [1]. In [2] it was shown that in the positive charge state the second nearest neighbour configuration with C_1 symmetry is almost degenerate with the C_{1h} configuration, however in our work, we have shown that these configurations have a 0.1 eV difference between these two configurations. This discrepancy can be explained using different pseudopotentials to perform DFT calculations.
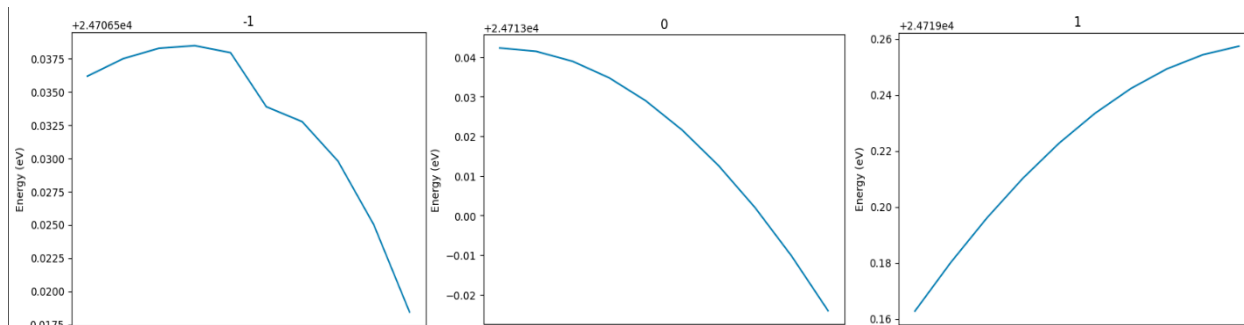
Fig. 26: Energy of the second nearest neighbour configuration (C_{1h} to C_1) in different charge states.

3. References

[1] Watkins, G.D., 1976. EPR of a trapped vacancy in boron-doped silicon. *Physical Review B*, *13*(6), p.2511.
[2] Adey, J., Jones, R., Palmer, D.W., Briddon, P.R. and Öberg, S., 2005. Theory of boron-vacancy complexes in silicon. *Physical Review B—Condensed Matter and Materials Physics*, *71*(16), p.165211.

Luminescence properties of Ce^{3+} and Eu^{2+} doped $Ca_4(PO_4)_2O$ phosphors

K.B. Morebodi, S.N. Ogugua, R.E. Kroon, H.C. Swart

Department of Physics, University of the Free State, Bloemfontein, ZA-9300, South Africa
Corresponding author: SwartHC@ufs.ac.za

1. Introduction

Phosphor materials have been widely studied in both science and industries for applications in solar cells, fingerprint detection, white light-emitting diodes, and temperature sensing[1]. In the field of luminescence, phosphor thermometry makes use of temperature-sensitive powders known as thermographic phosphors. These powders consist of a host material doped with a known percentage of rare earth, transition, or post-transition metal ions that act as the activators[2]. Traditional contact temperature monitoring devices, such as thermocouples and liquid-filled thermometers, have slow response times and low-temperature resolution[3]. The incorporation of thermographic dual emitting centers such as Ce^{3+} and Eu^{2+} in certain host materials is being studied across the globe[4]. However, there have been limited studies on phosphate-based phosphors that investigate morphology and use the luminescent intensity ratio (LIR) technique, which has the capability to improve the response time, temperature resolution, and stability of the optical thermometer.

2. Results

A series of colour-tunable $Ca_4(PO_4)_2O:3\%Ce^{3+}/y\%Eu^{2+}$ (y = 0.1, 0.3, 0.5, and 0.7 mol %) phosphors were synthesized using the solid-state reaction method at a fixed temperature of 1350 °C for 12 h. The excitation spectra (λ_{emi} = 427 nm) showed broad bands with a maximum at 322 nm assigned to the 4f-5d transitions, as shown in Fig.1. Under 322 nm excitation, the luminescence emission spectra of the phosphors exhibited two broad bands in the blue and red wavelength regions (Fig. 2), assigned to the 5d – 4f transitions of Ce^{3+} and Eu^{2+}, respectively. Through energy transfer from Ce^{3+} to Eu^{2+}, a wide range of tuneable emission colours spanning from blue via white to pale orange were achieved. X-ray photoelectron spectroscopy confirmed the presence of Ce^{3+} and Eu^{2+}, which supports the dual (blue and red) emission observed from photoluminescence spectra. The temperature-dependent photoluminescence (TDPL) of $Ca_4(PO_4)_2O:3\%Ce^{3+}$, $0.7\%Eu^{2+}$, measured in a temperature range of 303 to 423 K, using the LIR method, showed absolute and relative temperature sensitivities of 0.55×10^{-2} K^{-1} at 370 K, and 1.05 %K^{-1} at 423 K, respectively. The quantum yield and lifetime of the materials decreased from 43 % to 24 % with an increasing Eu^{2+} concentration.
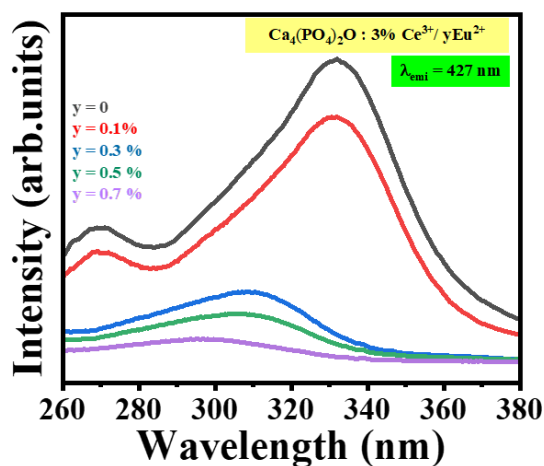
Fig. 1: PL excitation of $Ca_4(PO_4)_2O$: 3 % $Ce^{3+}/$ yEu^{2+}monitored at an emission wavelength of 427 nm.
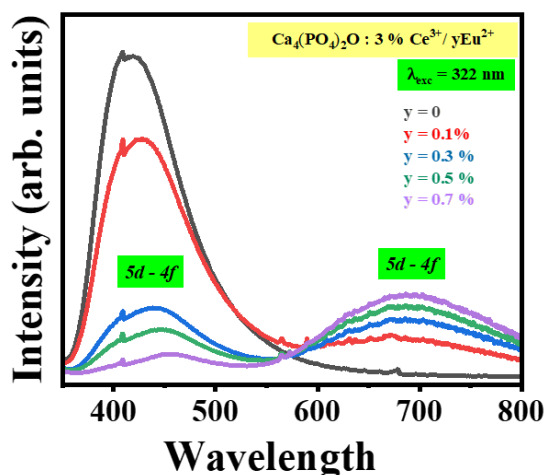
Fig. 2: PL emission of $Ca_4(PO_4)_2O$: 3 % $Ce^{3+}/$ yEu^{2+} monitored at an excitation wavelength of 322 nm.

3. References

[1] G.B. Nair, H.C. Swart and S.J. Dhoble. *Progress in Material Science* **109** (2020) 100622.
[2] S.N. Ogugua, *et al. Dalton Trans.* **53** (2024) 4551.
[3] C. Li, *et al. J. Alloys and Compd.* **838** (2020) 155675.
[4] J. Zhao, X. Sun, and Z. Wang. *Chem. Phys. Lett.* **691** (2018) 68.

Synthesis and Characterization of Titanium Tellurium Oxide Nanostructured Materials

T.P. Mokoena[1], V.N. Adoons[1], T.A. Nhlapo[2], T.C. Mokhena[3], L. Kotsedi[4]

[1]*Department of Physics, University of the Free State (QwaQwa Campus), P. Bag x13, Phuthaditjhaba, 9866, South Africa*
[2]*Department of Medical Physics, Sefako Makgatho Health Sciences University, P.O Box 146, Medunsa 0204, South Africa*
[3]*DSI/Mintek Nanotechnology Innovation Center, Advanced Materials, Mintek, Randburg, 2125, South Africa*
[4]*iThemba Labs-National Research Foundation, Old Faure Road, Somerset West, 7129, South Africa*
Corresponding author email: MokoenaTP@ufs.ac.za

1. Introduction

Titanium tellurium oxide ($TiTe_3O_8$) is a versatile semiconductor metal oxide that has been explored and revealed numerous applications in optical storage, deflectors, laser devices, dosimeters, and gas sensors. A relatively high purity $TiTe_3O_8$ was prepared by solid-state reaction method sintered at 700 ºC for 2 hours (h). The structural properties were examined by X-ray powder diffraction (XRPD). Scanning electron microscopy (SEM) and transmission electron microscopy (TEM) were used to investigate particle morphology. Furthermore, the elemental composition of this prepared material was explored by energy-dispersive X-ray spectroscopy (EDS). The strongest ultraviolet (UV) absorption was witnessed from the diffuse reflectance spectroscopy (DRS) measurements. The luminescence characteristics showing broad blue emission upon the UV excitation were analysed by photoluminescence (PL).

2. Results

Fig. 1 presents the XRPD patterns of $TiTe_3O_8$ nanostructures prepared by various molar ratios of TiO_2 and TeO_2. The structure confirmed a cubic phase of $TiTe_3O_8$ (see Fig. 2) with a space group Ia3, and the XRPD patterns were indexed by JCPDS card: 70 – 2439. Most peaks belonging to $TiTe_3O_8$ were marked with (♣), while other peaks were induced by (♦) TeO_2 and (♥) TiO_2-anatase, as these were used as reagents during the reaction.
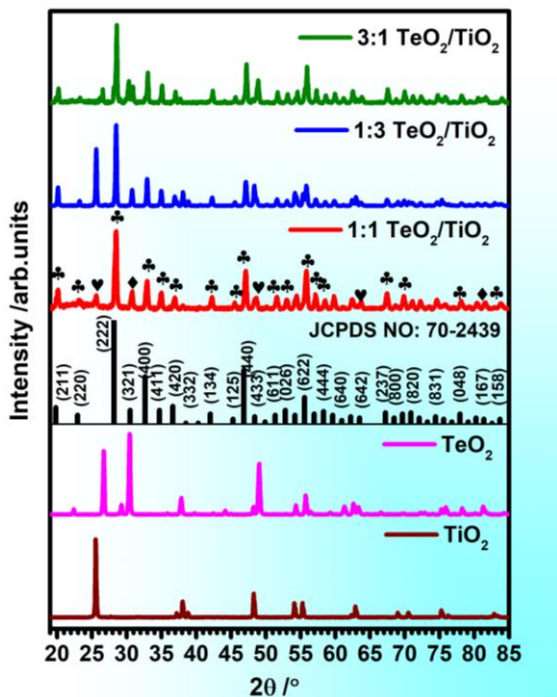
Fig. 1: XRPD of $TiTe_3O_8$ nanostructures.
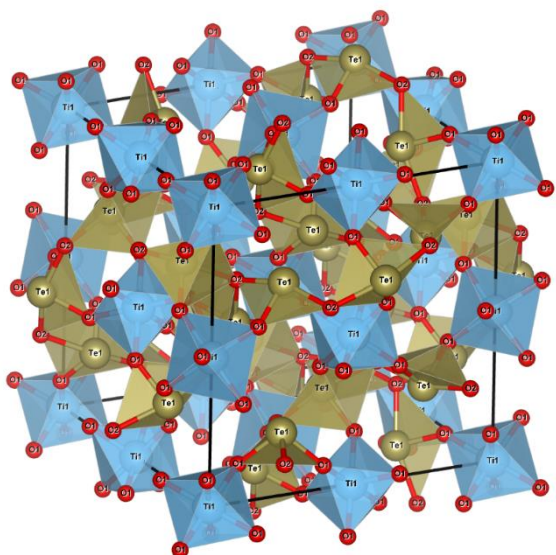
Fig. 2: Cubic crystal structure of $TiTe_3O_8$ drawn by VESTA.

Pressure dependent integration of white light emission in SiQDs@EuZIF-8 metal-organic frameworks

Sarojini Jeeva Panchu*, Sandeep Eswaran Panchu, Mart-Mari Duvenhage, Hendrik C Swart**

Department of Physics, University of the Free State, Bloemfontein-9301, South Africa.
Corresponding author e-mail address: SwartHC@ufs.ac.za, sarojinijeeva@gmail.com

1. Introduction

Luminescent metal−organic frameworks (MOFs) exhibit great potential as materials for nanophotonic applications because of their programmable properties and tunable structures. In particular, luminescent guests (LG) can be hosted by MOFs due to their porosity and guest confinement capacity, forming the LG@MOFs composite system.

We have developed silicon quantum dots (Si QDs) encapsulated with various concentrations of europium (Eu) in the ZIF-8 (Si QDs@EZIF-8) network resulting in higher PLQY (7%). By encapsulating Si QDs and Eu ions using ZIF-8, we can tune their emission wavelengths from blue to visible light, thus covering a broad range of visible spectrums in solid-state conditions. This encapsulation technique could effectively prevent the aggregation-caused quenching (ACQ) effect.

2. Results

By applying various pressures ranging from 1-7 tons, the Luminescence effect was enhanced. The applied pressure of 3 Ton reduced fluorescence intensity in all composites, and an increased pressure of 7 Ton gradually increased fluorescence. The study opens new avenues for tailoring LG@MOF applications under varied pressure conditions, which can guide future research.
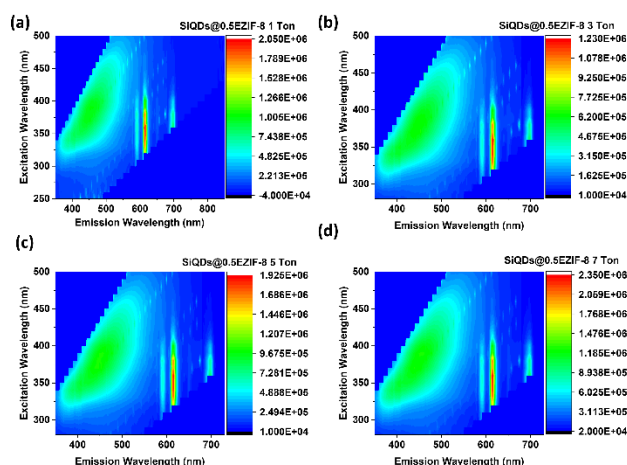
Fig. 27: Excitation and Emission mapping of SiQDs@0.5EZIF-8 under various applied pressures.

3. References

[1]   Z. Li, C. Xiao, Y. Yang, S. P. Harvey, D. H. Kim, J. A. Christians, M. Yang, P. Schulz, S. U. Nanayakkara, C.-S. Jiang, J. M. Luther, J. J. Berry, M. C. Beard, M. M. AlJassim and K. Zhu, Extrinsic ion migration in perovskite solar cells, Energy Environ. Sci., 2017, 10, 1234–1242.

[2] Wu, L. Y.; Mu, Y. F.; Guo, X. X.; Zhang, W.; Zhang, Z. M.; Zhang, M.; Lu, T. B. Encapsulating Perovskite Quantum Dots in Iron-Based Metal–Organic Frameworks (MOFs) for Efficient Photocatalytic CO2 Reduction. *Angew. Chem., Int. Ed.* **2019**, *58*, 9491– 9495.

[3] Konstantatos, G.; Huang, C. J.; Levina, L.; Lu, Z. H.; Sargent, E. H. Efficient infrared electroluminescent devices using solution-processed colloidal quantum dots. *Adv. Funct. Mater.* **2005**, *15*, 1865– 1869.

Optimization of the ETL titanium dioxide layer for inorganic perovskite solar cells

Sizwe Sibiya[1], Mmantsae Diale[1*]

[1] Department of Physics, University of Pretoria, Private Bag X20, Pretoria, 0028, South Africa [2]Institution2, Address
Corresponding author e-mail address: mmantsae.diale@up.ca.za

1. Introduction

In this study, compact-TiO_2 capped with meso-TiO_2 electron transport layers (ETLs) were grown via spray pyrolysis, with deposition time controlling layer thickness and morphology. Deposition times of 15–60 s optimized FTO/c-TiO_2 and FTO/c-TiO_2/m-TiO_2 ETLs. X-ray diffraction confirmed a crystalline rutile c-TiO_2 structure with structural crystallinity increasing with thickness. Crystallite size improved from 22 to 24 nm, while defect and dislocation densities decreased. SEM showed full surface coverage with compact grains, grain sizes ranging from 195.57–242.34 nm for c-TiO_2 and decreasing to 15.74 nm for m-TiO_2 at higher deposition times. UV-Vis spectra showed limited visible-light absorption, with no photoluminescence peaks. Electrical measurements revealed improved conductivity (3×10^6–1.18×10^7 S/m) and reduced resistivity. The 7 s m-TiO_2 film exhibited the best conductivity, enhancing charge carrier mobility (1.059×10^3–2.523×10^3 $cm^2V^{-1}s^{-1}$). These improvements suggest meso-epitaxial TiO_2 films enhance TiO_2 ETL-based inorganic perovskite solar cell performance.

2. Results

The optical characteristics of c-TiO_2 thin films are shown in Fig. 1 (a-d). Fig. 9(a) depicts the UV-Vis absorption spectra of c-TiO_2 thin films with varying deposition for controlled thickness. All films exhibited characteristic c-TiO_2 absorption peaks at 430 and 432 nm, consistent with the literature report [1]. Notably, the absorption of the films confirmed improved transparency, with a significant absorption reduction between 380 and 450 nm. This reduction was attributed to the wide bandgap of TiO_2 polymorphs [26], leading to high-quality ETL films in PSCs.
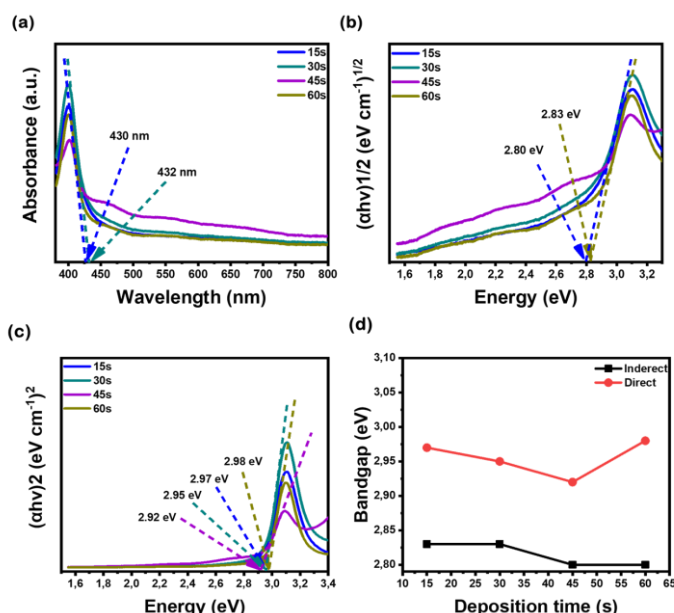
Fig. 28: UV-Vis's measurement showing (a) absorption spectra, (b) Tauc's plot for direct, (c) indirect bandgap, and (d) a comparison of bandgap optical properties of FTO/c-TiO_2 rutile thin films deposited using spray pyrolysis.

3. References

[1] Sadeghzadeh-Attar, A. and M.R. Bafandeh, *Effect of annealing on UV-visible absorption and photoluminescence behavior of liquid phase deposited TiO2 nanorods.* International Journal of Applied Ceramic Technology, 2019. **16**(6): p. 2429-2440.

The effect of varying annealing period on the structure, morphology, and photoluminescence properties of $CaAl_2O_4/BaAl_2O_4$:0.1% Eu^{3+} mixed phases via sol-gel method

C.R. Ratlhagane[1], A. Bele[1*], G.G. Matlou[2]

[1]*Department of Physics, Sefako Makgatho Health Sciences University, P. O. Box 94, Medunsa, 0204, South Africa*
[2]*Scanning Electron Microscopy Unit, Sefako Makgatho Health Sciences University, P. O. Box, Medunsa, 0204, South Africa*

Corresponding authors: abongile.bele@gmail.com

1. Introduction

Rare earth ions (RE^{3+}) doped nanophosphors have emerged as materials with great potential in light-emitting diode (LED) manufacturing [1]. Although investigations have been done on single-phase host materials, little has been explored on the mixed phases [2-5]. Mixed phases might result in new and advanced phosphor materials with the combined properties of their bulk counterparts. For example, Yuan et al. [3] showed that the mixed oxide $ZnO/ZnAl_2O_4$ has excellent stability and much higher photocatalytic activity than their bulk oxide counterparts. This study investigates the effect of varying annealing period on the structure, morphology, and optical properties of $CaAl_2O_4/BaAl_2O_4$:0.1% Eu^{3+}.

2. Results

$CaAl_2O_4/BaAl_2O_4$:0.1% Eu^{3+} mixed phases nanophosphors were successfully synthesized via the citrate sol-gel method. The effect of varying annealing period on the structure, morphology and photoluminescence properties of the prepared nanophosphors was investigated. X-ray diffraction (XRD) suggested that the prepared nanophosphor consists of hexagonal ($CaAl_2O_4$ and $BaAl_2O_4$). Scanning electron microscopy (SEM) revealed that the morphology of the prepared nanophosphors depends on the annealing period. Energy dispersive spectroscopy (EDS) confirmed the expected elements being Ca, Ba, Al, O and Eu. Transmission electron microscopy (TEM) confirmed that the prepared phosphor particles are in the nanoscale range. Photoluminescence (PL) results in Fig. 1 shows the emission spectra of $MgAl_2O_4$. The results showed emission peaks, which are ascribed to the intrinsic defects within the $CaAl_2O_4$, $BaAl_2O_4$, and Eu^{3+} transitions.
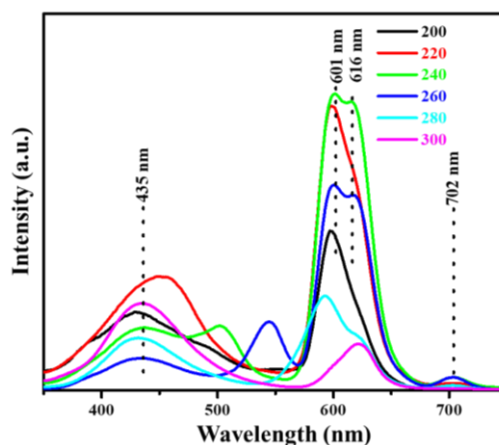
Fig. 29: the emission spectra of $CaAl_2O_4/BaAl_2O_4$:0.1% Eu^{3+}

3. References

[1] E.N. Alvar, M. Rezaei, H.N. Alvar. *Powder Tech*. **198** (2010) 275.
[2] Y. H. Li, X.L. Zhang, C.X. Fan, M. Liu, B. Zhai, H. Lin. *Adv. Mat. Res.* **399-401** (2012) 904
[3] X. Yuan, X. Cherng, Q. Jing, J. Niu, D. Peng, Z. Feng, X. Wu. *Mat*. **11** (2018) 1624.
[4] Y. Takebuchi, H. Fukushima, T. Kato, D. Nakauchi, N. Kawaguchi, T. Yanagida. *Jap. J. of App. Phys.* **59** (2020) 052007.
[5] W. Nantharak, W. Wattanathana, W. Klysubun, T. Rimpongpisarn, C. Veranitisagul, N. Koonsaeng, A. Laobuthee,. *J. of All and Comps*. **701** (2017) 1019.

Comparative study on absolute photoluminescence quantum yield measurements of $Y_3Al_5O_{12}$:Ce phosphor powder

<u>G.J. Odendaal</u>[1,2] L.J.B. Erasmus[1], R.E. Kroon[1], B.S. Richards[2], H.C. Swart[1], A. Turshatov[2]

[1]Department of Physics, University of the Free State, Bloemfontein, South Africa
[2] Institute of Microstructure Technology, Karlsruhe Institute of Technology, Karlsruhe, Germany
Corresponding author e-mail address: OdendaalGJ@ufs.ac.za

1. Introduction

The internal photoluminescence quantum yield (PLQY) of a luminescent material is defined as the ratio of the number of photons emitted to the number of photons absorbed by a material. This is a crucial parameter in various fields of physics, chemistry, and engineering, including photocatalysis, photovoltaics, and luminescence studies. Accurate PLQY measurements are essential for material characterisation and device optimisation. However, discrepancies can arise due to variations in instrumentation, calibration procedures, and sample preparation techniques between different laboratories and setups [1,2]. Additionally, variations in PLQY measurements can also arise due to systematic errors related to sample-specific properties. To address these challenges in improving the accuracy of PLQY measurements, commercial $Y_3Al_5O_{12}$:Ce phosphor (with manufacturer PLQY specification of 97 %) was measured using two different integrating sphere setups at the institutions of the authors (University of the Free State (UFS) and Karlsruhe Institute of Technology (KIT)) to evaluate the measurement variability. Additionally, the influence of different sample holders, sample concentration, and possible correction analysis was investigated.

2. Results

The PLQY was measured at UFS using an Edinburgh Instruments FLS980 system with excitation at 455 nm. As shown in Fig. 1a this system is equipped with a Xe lamp as an excitation source and utilises a powder tray to load powder samples. The result obtained agreed with the manufacturer's specification of 97%. The measurements carried out at KIT using a custom-built system, as shown in Fig. 1b with LED excitation at 450 nm, gave a close value PLQY of 95.2% for the same material. However, this configuration requires an additional powder sample holder such as a borosilicate tube, cuvette, or capillary. Analysis of the deviation between these two geometries highlights the importance of minimising the specular reflection of the LED excitation from the sample and sample holder and reducing the re-absorption of the luminescence within the integrating sphere. Error propagation analysis [2] and the effect of sample concentration when diluted with non-luminescent $BaSO_4$ were investigated and discussed.
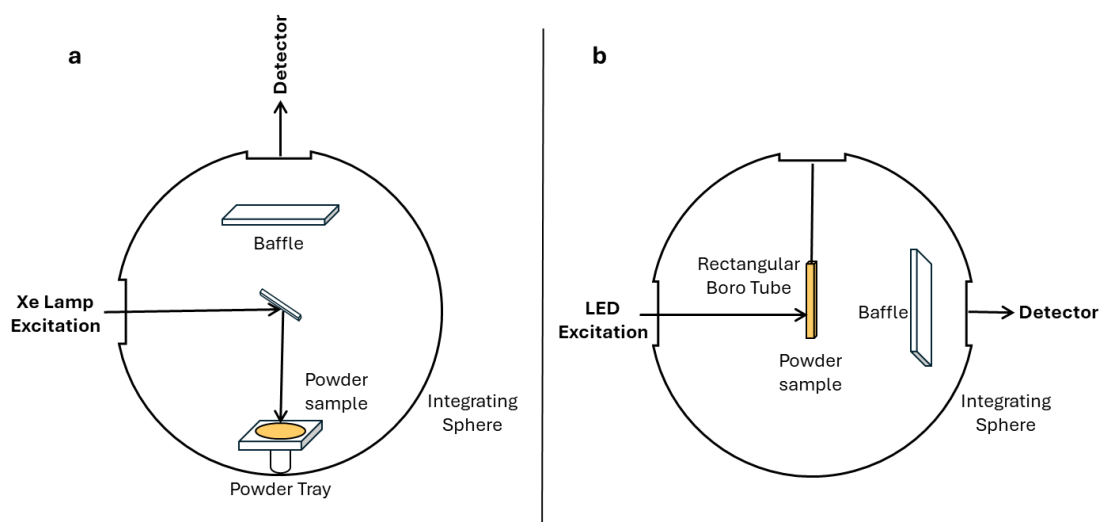
Fig. 30: Schematic illustration of the PLQY measurement system configurations: a) UFS, utilising the Edinburgh Instruments FLS980 system, and b) KIT, utilising a custom-built system.

3. References

[1] S. Fiedler, F. Frenzel, C. Würth, I. Tavernaro, M. Grüne, S. Schweizer, A. Engel, U. Resch-Genger. *Anal. Chem.* **96** (2024) 6730.
[2] E. Madirov, D. Busko, F.A. Cardona, D. Hudry, S. V. Kuznetsov, V.A. Konyushkin, A.N. Nakladov, A.A. Alexandrov, I.A. Howard, B.S. Richards, A. Turshatov. Adv Photonics Res **4** (2023) 2200187.

Study on the optical characteristics of SrTiO$_3$/Ti$_3$C$_2$T$_x$ and their influence on the BTEX gas sensing performance.

Nkosikhona Dlamini, Zamaswazi P. Tshabalala, Hendrik C. Swart, David E. Motaung.

Physics Department, University of the Free State, P.O. Box 339, Bloemfontein 9300, South Africa
Corresponding author e-mail address: nkosikhonatdlamini003@gmail.com

1. Introduction.

Benzene, toluene, ethylbenzene, and xylene (BTEX) are lethal volatile organic compounds derived from the refining of crude oil and burning of coal. We interact with these gases in our living spaces as they are emitted by paints, adhesives, and pesticides. Long-term exposure to BTEX results in serious health problems, and even death [1]. Monitoring and early detection of low concentrations of these gases are of great importance. Thus, over the years efforts have been made to fabricate materials with high selectivity, great stability, sensitivity, low energy consumption, and fast response/recovery time. Often, problems associated with most materials are the poor sensitivity and selectivity towards the BTEX gases and high operating temperature. The study aims to address these issues by utilizing the properties of strontium titanate perovskites (SrTiO$_3$) and MXenes (Ti$_3$C$_2$T$_x$, T$_x$ = -O, -OH, -F), by creating a SrTiO$_3$/MXene heterostructure with improved electronic and optical properties for superior BTEX gas sensing characteristics.

2. Results

Strontium titanate (SrTiO$_3$) perovskite nanostructures were synthesized via the hydrothermal method, while Ti$_3$C$_2$T$_x$ was synthesized through the in-situ LiF/HCl method. Subsequently, composite SrTiO$_3$/MXene was synthesized by varying the precursor's concentration and physically mixing SrTiO$_3$ with Ti$_3$C$_2$T$_x$, respectively. X-ray powder diffraction confirmed the cubic (Pm$\overline{3}$m) structure and the layered hexagonal structure for SrTiO$_3$ and Ti$_3$C$_2$Tx respectively (see Fig. 1). The observed peaks of the composite also confirmed the presence of each constituting material indicating a correctly formed heterostructure. Scanning electron microscope images showed that the SrTiO$_3$ favored nanospheres, and the MXene favored a sheet-like morphology. The SrTiO$_3$/MXene composite had a homogenous dispersion of the nanospheres on the nanosheets. UV-Vis diffuse reflectance of the SrTiO$_3$ samples showed to be highly reflective with an absorption edge around 385-390 nm. while the Ti$_3$C$_2$T$_x$ has an absorption in the infrared region. Moreover, using the Kubelka-Munk function the indirect band gap of 3.21 eV was estimated for pure SrTiO$_3$. The MXene showed a very narrow direct band gap of 0.89 eV while, the SrTiO$_3$/MXene composite showed a band gap of 2.59 eV, which confirmed the incorporation of the SrTiO$_3$ into MXene. The SrTiO$_3$/MXene composite is proposed to perform prominent gas sensing with enhanced sensitivity attributed to the narrow band gap allowing easy flow of the electrons to the conduction band.
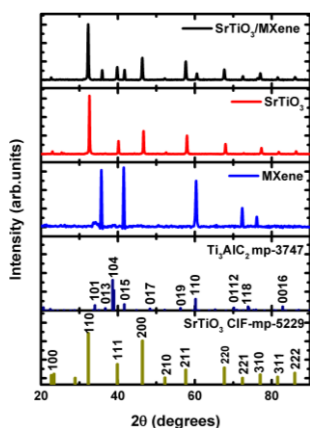
Fig. 31: XRPD reflections for, SrTiO$_3$, Ti$_3$C$_2$T$_x$, and SrTiO$_3$/MXene .
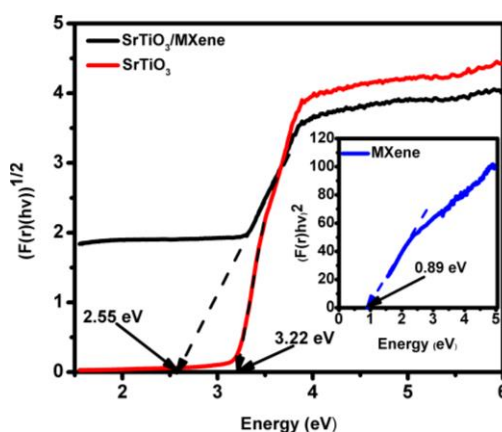
Fig. 2: Band gap values extracted using Kubelka-Munk Function vs photon energy

3. References.

[1] Dutta, K., Chattopadhyay, P.P., Lu, C.W., Ho, M.S. and Bhattacharyya, P. A highly sensitive BTX sensor based on electrochemically derived wall connected TiO$_2$ nanotubes. *Applied Surface Science*, **354** (2015).353-361.

Structure and Luminescence Correlation on CO Sensing Performance of p-n Cr_2O_3/SnO_2 Heterostructures

Kholofelo M. Seloane, Rapelang G. Motsoeneng, Rethabile Makole, Shaun Cronje, Hendrik C. Swart, David E. Motaung

University of the Free State, Bloemfontein 9300
Corresponding author e-mail address: SeloaneKM@ufs.ac.za

1. Introduction

Carbon monoxide (CO) is a flammable and explosive gas generated by the spontaneous combustion of coal at low temperatures in coal mines. Naturally, CO is considered an indicator gas for monitoring natural coal combustion [1]. It is also hypertoxic to human health. As a result, a maximum permissible level of 35-50 ppm is permitted for 8 h, or else it will result in nausea, dizziness, shock, and even death if not regulated [2]. The ability to reliably monitor CO gas levels is thus imperative. Various studies have reported the formation of heterostructures where both p-type and n-type are combined at the interface to achieve overlapping or closer Fermi energy levels, resulting in increased charge transfer and a broader depletion layer and thus leading to improved sensing performance [1]. Thus, the current study focuses on the fabrication of n-p SnO_2/Cr_2O_3 and p-n Cr_2O_3/SnO_2 heterostructures for the detection of CO utilizing the hydrothermal synthesis method, followed by calcination at 450 °C for 3 h.

2. Results

The structural studies confirmed the formation of n-p and p-n heterostructures of SnO_2/Cr_2O_3 and Cr_2O_3/SnO_2 nanostructured materials. Scanning electron microscopy analysis showed spherical nanoparticles with minimal agglomerations and Brunauer-Emmett-Teller (BET) confirmed mesoporous nanomaterials with large surface areas of 105.44 m²/g for the Cr_2O_3/SnO_2. The optical analysis indicated a shift towards higher wavelengths, corresponding with an energy band gap reduction, which can be explained by lattice distortion and surface defects [2]. The spectra exhibited shoulder peaks indicating heterojunction formation, with a band gap at 2.3 eV corresponding to the reduced band gap of SnO_2 (3.6 eV) and at 3.03 eV relating to that of Cr_2O_3 (3.0–3.4 eV). The nanoparticles showed weak emission at 600 nm (2.01 eV), correlating with interactions between interfacial tin vacancies and oxygen vacancies. The spectra also showed a peak at 2.3 eV, associated with a single oxygen vacancy. It can be deduced from the results that Cr_2O_3/SnO_2 displayed a superior response towards CO gas due to a higher surface area and surface defects, allowing better gas adsorption.
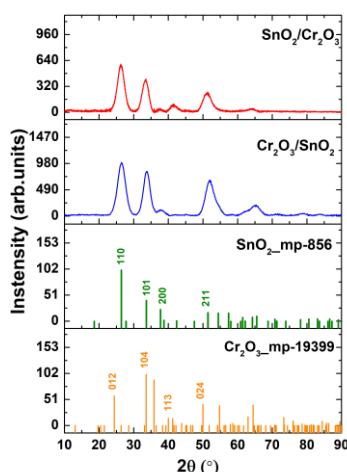
Fig. 32: XRPD patterns of the heterostructures.
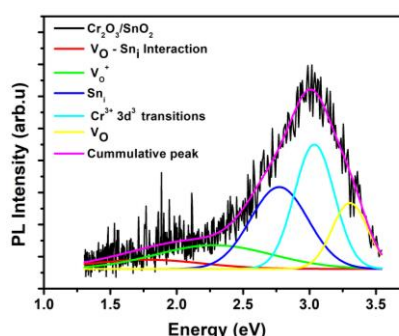
Fig. 2: Deconvoluted PL spectrum of the Cr_2O_3/SnO_2 heterostructure showing surface defects.

3. References

[1] U.T. Nakate, R. Ahmad, P. Patil, Y. Wang, K.S. Bhat, T. Mahmoudi, Y.T. Yu, E-K. Suh, Y-B. Hahn, Journal of Alloys and Compounds, **797** (2019) 456-464.
[2] M.M. Abdullah, F.M. Rajab, S.M. Al-Abbas, AIP Advances, **4**(2) (2014) 027121.

Structural, chemical and luminescence properties of Bi doped ZnO

B.T.Q. Mohlala[1], S. Cronje[1], M.M. Duvenhage, E. Coetsee, R.E. Kroon

[1] *University of the Free State, Department of Physics, P.O. Box 339, Bloemfontein, 9300, South Africa*

Corresponding author e-mail address: mohlalabtq@ufs.ac.za

1. Introduction

The structural, chemical, and luminescence properties of Bi-doped ZnO phosphors were investigated. Bi-doped ZnO phosphors are unique due to the ability of Bi to alter the electrical and optical properties of ZnO, allowing for improved performance in applications like photocatalysis and optoelectronics [1]. The samples were prepared using the combustion and pulsed laser deposition (PLD) methods. The X-ray powder diffraction (XRPD) patterns of both the powder and thin films showed a polycrystalline hexagonal structure (Fig. 1). The crystallite size for the powders was 31, 39, and 34 nm for the undoped, 0.1 mol% Bi, and 0.3 mol% Bi respectively. The crystallite size of thin films was found to be 16, 19, and 20 nm for the undoped, 0.1 mol% Bi and 0.3 mol% Bi respectively with (002) plane as a preferred orientation. Scanning electron microscopy (SEM) images showed that the morphology of the thin films changed with Bi doping concentration. X-ray photoelectron spectroscopy (XPS) was used to analyse the chemical state of both powders and thin films and the results confirmed that there were Bi^0 and Bi^{3+} charge states present but the Bi^{3+} were most abundant. The photoluminescence (PL) emission spectra of the powders excited at 325 nm at room temperature (Fig. 2) showed a peak in the blue region (434 nm) and a broad peak in the red region (635 nm). The excitation spectra showed the typical UV absorption below 350 nm associated with the bandgap, a blue band at 420 nm associated with Bi doping, and emission at 730 nm which has not been reported before [2,3]. The luminescence of doped and undoped thin film samples was measured at room temperature. They showed a broad blue emission (400 – 500 nm) and a broad visible emission (642 nm) which blue shifted for doped samples. Under low temperatures (at 5 K in vacuum) the undoped thin films showed two sharp UV emissions at 369 and 381 nm which were associated with near band edge emissions and a broad visible emission around 617 nm and the intensity enhanced at low temperatures compared to when done at room temperature. There were emissions at 723 and 736 nm, which were associated with the second order of the near band edge (NBE) emissions and were not related to Bi doping.

2. Results
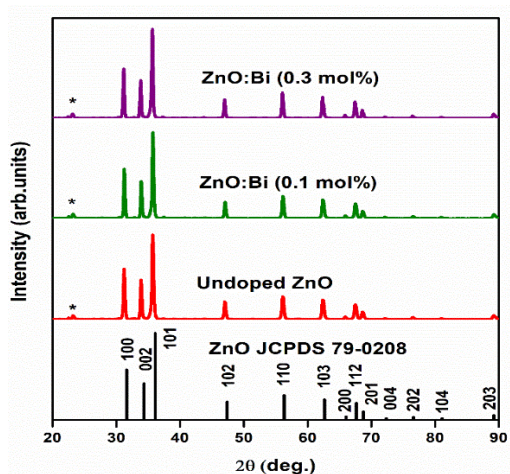
Fig. 33: XRPD patterns for undoped and Bi-doped ZnO powders.
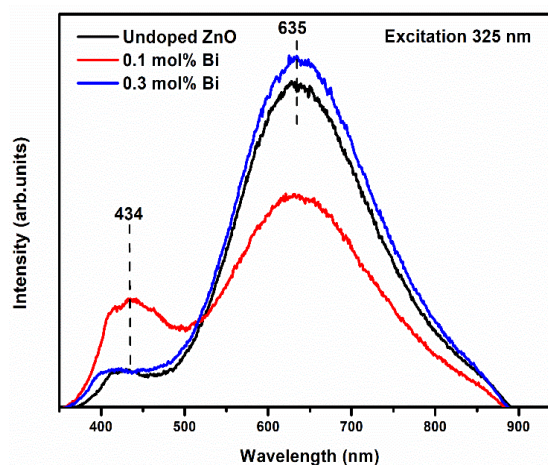
Fig. 2: PL emission spectra of Bi doped ZnO phosphor powders at 325 nm excitation.

3. References

[1] Jinsong Sun, Jinxing Cao, Xiaohong Jiang, *J. Alloys and Compounds,* **896** (2022) 162801.
[2] Pathak T K, Swart H C and Kroon R E, *Spectrochim. Acta A. Mol Biomol Spectrosc,* **190** (2017) 164.
[3] Ravichandran A T, Karthick R, Ravichandran K, Ravinder D and Chandramohan R, *J. Mater. Sci.* **29** (2018) 2784.

Influence of Ag on the optical properties of MOF-derived Co_3O_4-In_2O_3 nanocomposites applied for xylene vapour detection

Lindokuhle Mabizela, Rethabile Makole, Hendrik C. Swart and David E. Motaung

Department of Physics, University of the Free State, Bloemfontein, Park West, 9301

Corresponding author e-mail address: mabizelalp@ufs.ac.za

1. Introduction

Anthropogenic air pollution is one of the leading factors in environmental disasters and human health issues [1]. Volatile organic compounds (VOCs) such as benzene and toluene are some of the most common compounds that contribute to air pollution. They are emitted from automobile exhaust, combustion of coal, petrochemical and printing industries, and rubber manufacture. When people are exposed to these compounds over a different period, they become at risk of developing ailments such as s aplastic anemia, headache and dizziness, respiratory irritation, and deterioration of the central nervous system [2]. This has therefore inclined researchers to develop sensors to monitor and detect these hazardous gases.

Semiconductor metal oxide (SMO)--based sensors have been widely used to detect benzene and xylene due to their low cost, portability, and facile development. However, they have some drawbacks, which include poor selectivity and high consumption of energy, thus limiting their practical application. Therefore, there is an urgent need for sensors that can address issues associated with SMO-based sensors. Loading noble metals on the surface of SMO has been studied and reported to be ideal for improving the sensor selectivity and lowering the sensor operating temperature [3]. The effect of the noble metals on the gas-sensing properties of SMOs can further be elucidated by loading on highly porous materials such as metal-organic frameworks (MOFs). MOF-derived SMOs are exemplary options for smart sensing due to their large surface area, high porosity, abundant active site for gas adsorption, and improved selectivity [4]. In this work, the effect of Ag on the optical properties of MOF-derived Co_3O_4-In_2O_3 nanocomposites and subsequent changes in gas in sensing abilities to xylene-isomers is investigated.

2. Results

The photoluminescence spectrum of MOF-derived Co_3O_4-In_2O_3 depicted in Fig. 1, showed a low-intensity broadband emission at 3.05 eV, which is believed to be due to the near-band edge emission. The relatively low intensity is indicative of the likeness of the MOF-derived Co_3O_4-In_2O_3 emission process to be non-radiative. The non-radiative process tends to induce crystal defects which influence the gas sensing abilities. As shown in Fig. 2, a high response of 41 to 100 ppm of xylene is exhibited by the MOF-derived Co_3O_4-In_2O_3 nanocomposites. The observed results show that the MOF-derived Co_3O_4-In_2O_3 has a photoluminescence emission that can be improved and sensor sensitivity towards xylene.
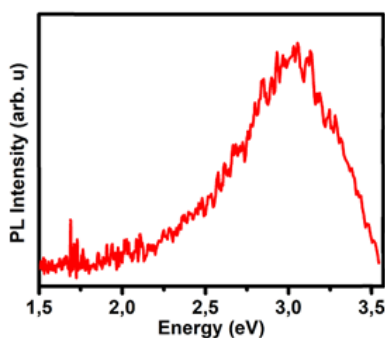
Fig. 34: PL emission spectrum of MOF-derived Co_3O_4-In_2O_3.
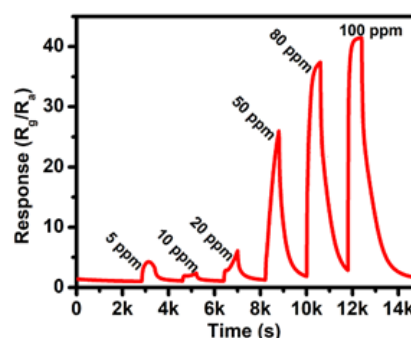
Fig. 2: Response of MOF-derived Co_3O_4-In_2O_3.to xylene vapour as a function of time at 150 °C.

3. Reference

1. Manisalidis, I., et al., *Environmental and health impacts of air pollution: a review.* Frontiers in public health, 2020 **8** (2020) 14.
2. Muda, I., et al., *Associated health risk assessment due to exposure to BTEX compounds in fuel station workers.* Reviews on Environmental Health, **39(3)** (2024) 435-446.
3. Choi, Y.M., et al., *Ultrasensitive detection of VOCs using a high-resolution CuO/Cu2O/Ag nanopattern sensor.* Advanced Functional Materials, **29(9)** (2019) 1808319.
4. Theka, T.J., H.C. Swart, and D.E. Motaung, *Recent trends, advances, and challenges in MOFs-derived metal oxide semiconductor-based sensors for BTEX detection: A review.* Inorganic Chemistry Communications, (2024) 112884.

Influence of excitation power on down-shifting ZnO

L.J.B. Erasmus[1], **R.E. Kroon**[1]

[1] *University of the Free State, 205 Nelson Mandela Drive, Park West, Bloemfontein*
Corresponding author e-mail address: erasmuslb@ufs.ac.za

1. Introduction

It is well known that the excitation power density has a non-linear effect on the resulting emission from photoluminescent upconverting phosphor materials [1]. Therefore, it has become standard practice to report the power density of the excitation source when publishing upconversion measurements, although this is usually not the case when reporting on down-shifting and converting materials since it is assumed that the photoluminescent intensity response is linear. Also, little regard is given to the effect of excitation power density on the different mechanisms responsible for the emission in some materials. To demonstrate that excitation power density is an important parameter, this study will investigate the power density dependence of the exciton and defect-associated emission peaks of prepared zinc oxide (ZnO). This semiconductor material was chosen due to its wide application in displays, solar cells, and light-emitting diode technologies [2].

2. Results

For this study, commercial ZnO with intentionally induced oxygen vacancies was acquired from Phosphor Technologies [3]. To reduce the defect emission and enhance the exciton peak, the material was annealed in the atmosphere for 8 h at 900 °C. The prepared material was studied using a custom-constructed 320 nm laser photoluminescence system. The excitation intensity was varied by three orders of magnitude by introducing a series of neutral density filters between the excitation source and the sample. The resulting down-shifting emission was measured and is shown in Fig. 1. As illustrated in Fig. 2, the exciton peak shows a different relationship as a function of excitation power density when compared to the defect emission. The mechanisms behind these results will be discussed. This study demonstrates that the ratio of excitation peak to defect peak depends strongly on the excitation power density, which explains why the same sample measured in different measurement systems can show different emission data using the same excitation wavelength.
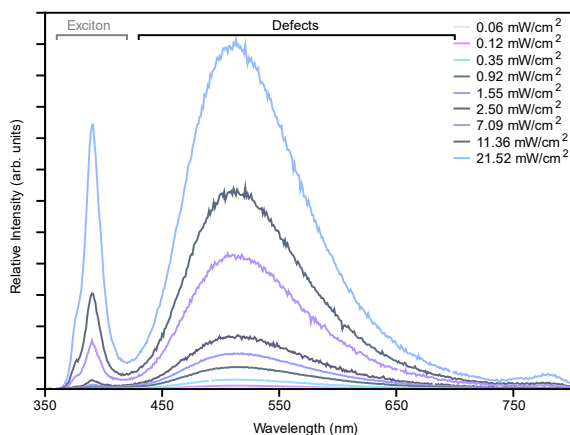
Fig 1: Emission spectra of prepared ZnO at various excitation power densities showing the exciton (left) and defects (right) related emissions.
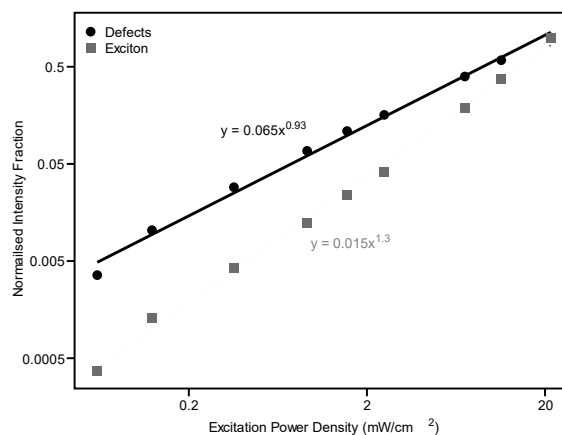
Fig 2: The relationship between the emission intensity associated with the exciton and defects emissions as a function of the excitation power density.

3. References

[1] M. Pollnau, D. R. Gamelin, S. R. Lüthi, H. U. Güdel, and M. P. Hehlen, "Power dependence of upconversion luminescence in lanthanide and transition-metal-ion systems," *Phys Rev B*, vol. 61, no. 5, pp. 3337–3346, Feb. 2000, doi: 10.1103/PhysRevB.61.3337.

[2] P. Kaur, S. Rani, and B. Lal, "Excitation dependent photoluminescence properties of ZnO nanophosphor," *Optik (Stuttg)*, vol. 192, p. 162929, 2019, doi: https://doi.org/10.1016/j.ijleo.2019.162929.

[3] H. Rai, Prashant, and N. Kondal, "A review on defect-related emissions in undoped ZnO nanostructures," *Mater Today Proc*, vol. 48, pp. 1320–1324, 2022, doi: https://doi.org/10.1016/j.matpr.2021.08.343.

$W_{18}O_{49}$ NPs for the trace detection of Acetone Vapour

Jodinio Lemena, Richard A. Harris, Jacob J. Terblans, Hendrik C. Swart, David E. Motaung

Department of Physics, University of the Free State, P.O. Box 339, Bloemfontein ZA9300, South Africa
Corresponding author e-mail address: jodiniod@gmail.com

1. Introduction

The detection of acetone has become a rich vein of research due to its applications for health monitoring and self-diagnosis. Acetone serves as a distinctive biomarker for diabetes, making its concentration in human breath an essential factor for diagnosing diabetic patients. Generally, healthy individuals exhale acetone levels below 1 ppm (ranging from 0.3 to 0.9 ppm). However, in individuals with diabetes, these levels rise to approximately 2.2 ppm for type 1 diabetics and around 1.7 ppm for those with type 2 diabetes [1]. Tungsten oxides ($WOx \leq 3$) are highly valued for their chemical stability, affordability, ease of synthesis, and structural versatility. Notably, they exhibit various non-stoichiometric phases ($WO_x < 3$), including WO_2, $W_{18}O_{49}$, W_5O_{14}, and $W_{20}O_{58}$. These phases contain abundant oxygen vacancies, which enhance their ability to adsorb gas molecules, making them effective as sensing materials [1]. Despite advancements in $WOx \leq 3$-based acetone sensors, achieving both ppb-level detection and high response at low concentrations while operating at room temperature (RT) remains a significant challenge. This paper focuses on addressing these limitations by creating a $W_{18}O_{49}$ nanoparticle sensor that can detect trace amounts of acetone at RT.

2. Results

Powder X-ray diffraction (XRD) patterns confirmed the successful formation of $W_{18}O_{49}$. TEM elemental mapping further validated these claims as a uniform distribution of Tungsten and oxygen was seen. The atomic wt% of oxygen compared to tungsten was considerably less indicating the presence of oxygen vacancies. Diffuse UV-Vis spectroscopy was employed to characterize the optical properties where it was noted that $W_{18}O_{49}$ displayed a wide absorption range spanning the UV to NIR regions, which was attributed to the high abundance of oxygen vacancies in the lattice, inducing localized surface plasmon resonance (LSPR). Fig. 2 shows the estimated bandgap of 2.39 eV from the indirect allowed transition of the Kubelka-Munk function. The estimated bandgap is well in line with reported estimates of 2.89 eV [2], and 2.54 eV [3]. The presence of these oxygen vacancies was then further corroborated by PL analysis, which showcased blue emission under 325 nm excitation credited to oxygen vacancies. PCA analysis of gas sensing results revealed that acetone displayed unique characteristics allowing it to be distinguishable among gasses, such as m-xylene, p-xylene, o-xylene, ethanol, and methanol.
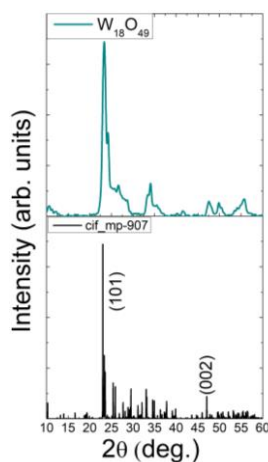
Fig. 35: XRD spectrum of $W_{18}O_{49}$ nanoparticles
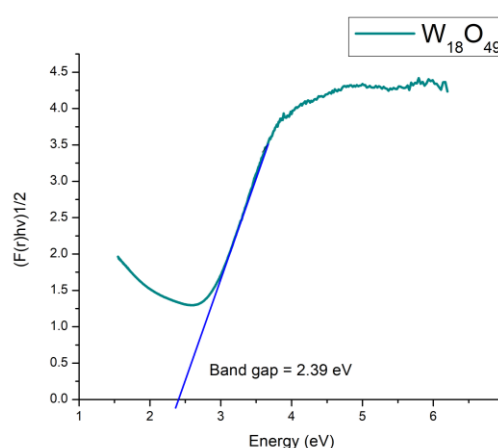
Fig. 2: Tauc plot of $W_{18}O_{49}$ nanoparticles and consequent

3. References

[1] Sun, S., Wang, M., Chang, X., Jiang, Y., Zhang, D., Wang, D., Zhang, Y. and Lei, Y., 2020. $W_{18}O_{49}/Ti_3C_2T_x$ Mxene nanocomposites for highly sensitive acetone gas sensor with low detection limit. *Sensors and Actuators B: Chemical*, *304*, p.127274.

[2] Liu Y, Li X, Su H et al. Plasmonic $W_{18}O_{49}$/attapulgite nanocomposite with enhanced photofixation of nitrogen under full-spectrum light. Journal of Materials Science: Materials in Electronics 2019; 30: 20019–20028.

[3] Xiong, Y., Wu, B., Lin, Y., Zhang, M. and Chen, J., 2024. Facile synthesis of hierarchical $W_{18}O_{49}$ microspheres by solvothermal method and their optical absorption properties. *Discover Nano*, *19*(1), p.89.

Influence of noble metals loading on In_2O_3/SnO_2/MoS_2 ternary structure for improved optical, structural, and SO_2 gas sensing characteristics.

Chulumanco Tyesi, , Elizabeth Coetsee, Rapelang G. Motsoeneng, Hendrik C. Swart, David E. Motaung

Physics Department, University of the Free State, P.O. Box 339, Bloemfontein 9300, South Africa
Corresponding author e-mail address: 222059717@ufs4life.ac.za

1. Introduction

Sulfur dioxide (SO_2) is a hazardous air pollutant with damaging environmental and health impacts, making it necessary to develop highly sensitive and selective gas sensors [1]. Sulfur dioxide (SO_2) is prevalent in South Africa primarily due to the anthropogenic processes the country is reliant on, such as coal combustion for electricity generation, industrial activities, and metal smelting. Exposure to SO_2 irritates the respiratory system, leading to lung inflammation, asthma attacks, and chronic diseases [2]. Gas sensors are crucial for monitoring SO_2 levels for public health. In this study, In_2O_3/MoS_2, In_2O_3/SnO_2/MoS_2, SnO_2/In_2O_3/MoS_2, and SnO_2/MoS_2 nanostructures were synthesized via the hydrothermal method for SO_2 gas detection. Gas sensing experiments were performed to evaluate the sensitivity of each composition toward SO_2. The sensors were further loaded via wet impregnation with Au and Ag nanoparticles to enhance their performance. This study highlights the potential of In_2O_3/SnO_2/MoS_2-based sensors for effective SO_2 detection, paving the way for improved environmental monitoring applications.

2. Results

The structural properties of the samples were confirmed using X-ray Powder Diffraction (XRPD), showing the successful formation of the metal oxide hybrid structures. Fig. 1 shows distinct peaks corresponding to SnO_2, In_2O_3, and MoS_2. The well-defined and high-intensity peaks indicate good crystallinity, and the variations in intensity suggest differences in phase composition. The confirmed presence of MoS_2 in the composites introduces the desired layered structure that enhances charge transport. The mixed metal oxides, particularly In_2O_3/SnO_2/MoS_2, exhibit synergistic effects, improving sensor performance through enhanced electron mobility and catalytic activity. Optical properties were investigated through UV-Vis spectroscopy. Fig. 2 shows the manipulation of the reflectance spectra using the Kubelka-Munk function that results in band gap values ranging from 2.9 to 3.4 eV, which influence the electronic transitions and charge carrier mobility crucial for gas sensing performance. Gas sensing experiments were performed to evaluate the sensitivity and selectivity of each composition toward SO_2 gas. The sensors were further loaded via wet impregnation with Au and Ag nanoparticles to enhance their performance. The noble metal loading significantly improved response and selectivity due to enhanced catalytic activity and electronic modulation. The study shows that In_2O_3/SnO_2/MoS_2-based sensors can be used to detect SO_2 effectively, which opens the door to better environmental monitoring applications.
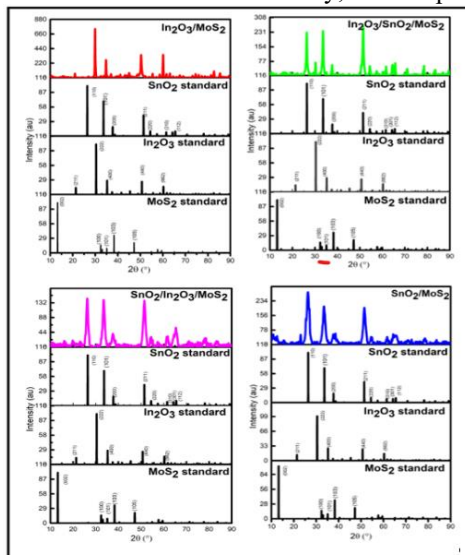
Fig. 1. XRD spectra for In_2O_3/MoS_2, In_2O_3/SnO_2/MoS_2, SnO_2/In_2O_3/MoS_2, and SnO_2/MoS_2.
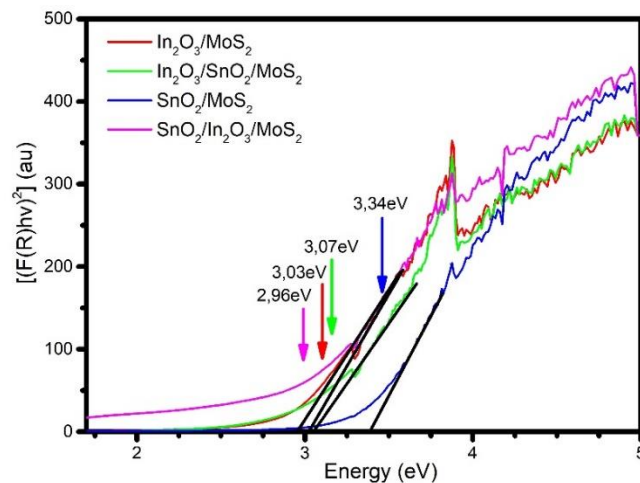
Fig. 2. Band gap values were extracted using the Kubelka-Munk Function.

3. References

[1] Bikis, A. (2023). Urban air pollution and greenness in relation to public health. Journal of Environmental and Public Health, 2023, 1–18.
[2] Steyn, M., & Kornelius, G. (2018). An economic assessment of SO_2 reduction from industrial sources on the highveld of South Africa. *Clean Air Journal*.

10th South African Conference on Photonic Materials – Amanzi 2025

Synthesis and characterization of Ag-ZnO using citrus reticulata peel extract

Joan Jepngetich, Peter W Njoroge, Sylvia Opiyo, <u>Sharon Kiprotich</u>[*]

Department of Physical and Biological Sciences, Murang'a University of Technology,
P.O Box 75, Murang'a 10200, Kenya
Corresponding author e-mail address: Skiprotich@mut.ac.ke

1. Introduction

Solar cells have the ability to convert sunlight into electrical energy, therefore they are considered as the best source of energy since they do not emit toxic gases into the atmosphere. In 2020 fossil fuel accounted for 83.1% of energy consumed globally thus a major contributor of greenhouse gases [1]. To minimize the use of fossil fuels, solar cells have been considered to be effective despite facing major setbacks such as their cost and effectiveness. In this research Ag-ZnO nanoparticles (NPs) were synthesized using *Citrus reticulata* as a capping agent to be used as a photoanode in the solar cell so that it can improve its effectiveness. Pure and Ag-ZnO NPs were synthesized using the chemical precipitation method with *Citrus reticulata* peel extract as a capping agent. The synthesis method involved the use of plant extracts such as leaves [2], fruits [3], and stems [4]. The plant extracts act as a capping and reducing agent for the development of nanoparticles, with phytochemicals playing a key role in shaping the properties of the nanoparticles. The effects of the capping agent on the material properties of ZnO and Ag-ZnO were reported. All nanoparticles formed were in the range of 8-14 nm in size. When doped with silver, an increase in the bandgap energies was observed for pure and capped Ag-ZnO nanoparticles. Fig. 1 shows the XRD pattern of annealed pure and Ag-ZnO nanoparticles. The results obtained showed that both capped and uncapped ZnO and Ag-ZnO NPs maintained the hexagonal wurzite structure. The Ag patterns disappeared when the samples were annealed. The pure ZnO pattern observed indicated that effective doping took place, and all the Ag^+ ions occupied the interstitial sites or were segregated into the non-crystalline region causing the ZnO lattice structure to be conserved [5]. Photoluminescence spectroscopy (PL) and Ultraviolet-visible spectroscopy were used to study the optical properties of nanoparticles. PL showed a significant shift towards the near band edge region when nanoparticles were doped with Ag. When Ag was added to ZnO the bandgap energy increased from 3.34 to 3.85 for uncapped nanoparticles and from 3.52 to 3.68 for *Citrus reticulata* capped Ag-ZnO nanoparticles as shown in Fig. 2. When a capping agent was added to doped ZnO nanoparticles the bandgap energy tended to decrease as compared to uncapped doped ZnO NPs.

2. Results
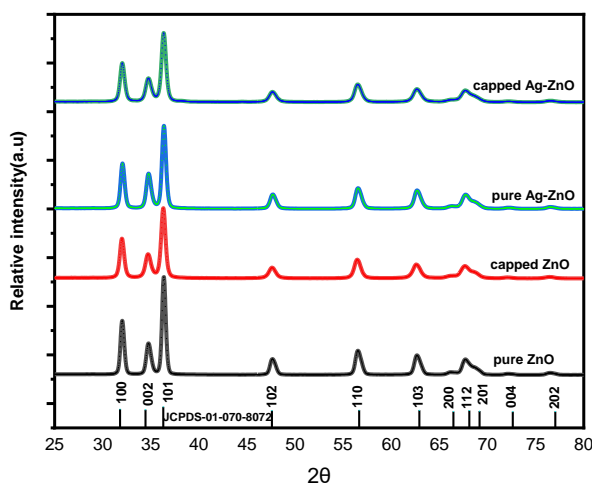
Fig.36: The XRD pattern for Ag-ZnO NPs annealed at 450 ºC.
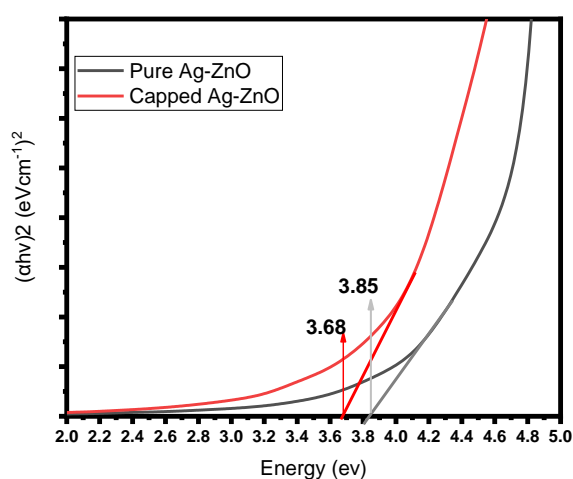
Fig. 2: Tauc's plot of pure and capped Ag-ZnO NPs.

3. References

[1] J.L. Holechek, H.M. Geli, M.N. Sawalhah, R. Valdez, R. (2022). *Sustainability*, *14*(8), 4792.
[2] A.M.E Shafey, (2020). *Green Processing and Synthesis*, *9*(1), 304-339.
[3] S. Ahmed, G. Kaur, P. Sharma, S. Singh, S. Ikram, (2018). *Journal of Applied Biomedicine*, *16*(3), 221-231.
[4] P. Karthiga, (2018). *Biotechnology Research and Innovation*, *2*(1), 30-36.
[5] M. Kim, K. Yim, J. Leem, S. Kim, G. Nam, D. Lee, J. Kim, J. Kim, (2011). *Journal of the Korean Physical Society*, *59*.

A comparative study of optical properties and hydrogen sulfide gas sensor performance of CuO/CeO₂ nanocomposite.

Karabo L.B. Masilela, Hendrik C. Swart, David E. Motaung

Physics Department, University of the Free State, P.O. Box 339, Bloemfontein 9300, South Africa
Corresponding author e-mail address: lulumasilelakb@gmail.com

1. Introduction

The toxicity of hydrogen sulphide can be life-threatening even at low concentrations, irritating the eyes, respiratory system, and skin. At high concentrations, the gas can result in death or paralysis [1,2]. Thus, the demand for reliable, highly selective, and sensitive hydrogen sulfide detection has fuelled an interest in novel materials. This study focuses on the application and creation of CuO/CeO₂ composite as the novel sensing material for the detection of hydrogen sulfide gas. With CuO being a p-type semiconductor and CeO₂ an n-type semiconductor, the p-n heterojunction between these materials enhances the capability of gas sensing. Chemical, optical, and structural properties were confirmed using X-ray photoelectron spectroscopy (XPS), X-ray powder diffraction (XRPD), and Ultraviolet-visible spectroscopy (UV-Vis). At low temperatures, the sensor demonstrated great selectivity, fast response and recovery duration, and high sensitivity for H₂S gas.

2. Results

Fig. 1(a) displays the XRD spectrums of CuO, CeO₂, and CuO/CeO₂ nanocomposite, confirming a clear formation of heterostructure. The UV-Vis energy spectrums displayed a band gap of 1.49 eV for CuO, while that of the CeO₂, and CuO/CeO₂ heterostructures were about 3.08 and 1.54 eV, respectively. The CuO/CeO₂ disclosed better SO₂ in comparison to its counterpart, which could be justified by a sufficient amount of heterojunctions allowing better SO₂ adsorption on the sensor surface.
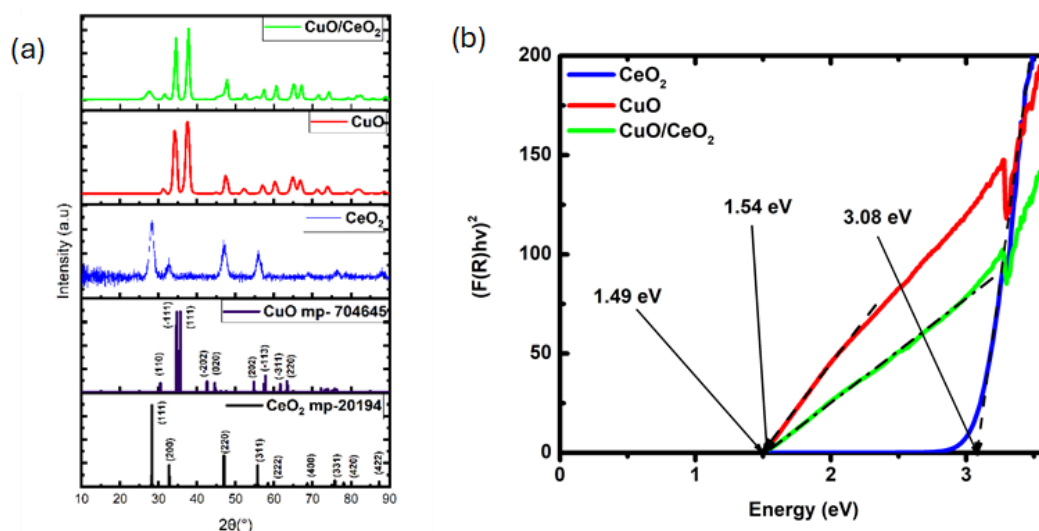
Fig. 1: (a) XRPD spectra and (b) UV Vis reflectance spectra of copper oxide (CuO), cerium oxide (CeO₂), and CuO/CeO₂ composite.

3. References

1. Zhu, M.L.; Zhang, L.J., A Novel H₂S Gas Sensor Applied to the Construction Workers During the Construction Process. Science of Advanced Materials. **11** (2019) 143–146.
2. Meng, F.N.; Di, X.P.; Dong, H.W.; Zhang, Y.; Zhu, C.L.; Li, C.Y.; Chen, Y.J. 2013. Ppb H₂S gas sensing characteristics of Cu₂O/CuO sub-microspheres at low-temperature. Sensors and Actuators B: Chemical. 182 (2013)197–204.

Synergetic Effects of Zn:Fe Co-Doped TiO$_2$ Nanoparticles on the Structural, Optical and Morphological Properties

Simon Waweru Gakuru[1], Sharon Kiprotich*[1], Peter Waithaka[1]Francis Birhanu Dejene[2]

[1]Department of Physical and Biological Sciences, Murang'a University of Technology, P.O Box 75, Murang'a 10200, Kenya
[2]Department of Physics, Walter Sisulu University, Mthatha Private Bag X1 UNITRA 5117
Corresponding author e-mail address: Skiprotich@mut.ac.ke

1. Introduction

Greenhouse gas emissions have led to adverse climatic effects and the mitigation measures put are not sufficient in combating the adversities, highlighting the urgent need for transducers to harness the abundant renewable solar energy to electrical energy [1]. Among the dye-synthesized solar cell (DSSC) components, the photoanode is a semiconductor comprising a transition metal oxide such as ZnO, CdO, SnO$_2$, and TiO$_2$, that plays a crucial role in light harvesting and charge transfer. TiO$_2$ is the preferred semiconductor due to its exceptional non-toxic nature and excellent thermal, optical, and chemical properties [2]. The efficiency of DSSC relies on the capacity of the photoactive nano-crystal electrode to harness visible light and transport the photo-excited electrons to the dye at the conduction band [3]. Co-doping using cations, anions, or both has been reported to have higher photocatalytic activity than mono-doped samples under visible light irradiation [4-6]. Co-doping Zn and Fe would improve the photo-response of TiO$_2$ as Zn has excellent charge mobility, and the fewer valence electrons create an acceptor band near that of TiO$_2$ used to trap photo-excited electrons reducing e-/h+ recombination rate [5, 6]. A facile sol-gel process was used to synthesize Zn:Fe co-doped TiO$_2$ nanoparticles (NPs) and study the synergistic effects on the structural, optical, and morphological effects of different co-doping ratios of Zn:Fe TiO$_2$ (Z:F-T) anatase and rutile phases as a potential photoanode in DSSC. Co-doping ratios of 1:1, 0.5:1, 1:0.5,1.5:1, and 1:1.5 Z:F were added to a constant amount of TTIP, ethanol and diethanolamine. Various techniques such as XRD, UV-Vis, EDX, SEM, and FTIR were used to determine the material properties of the as-prepared Zn:Fe co-doped TiO$_2$ NPs. It is worthwhile to note that, the metastable anatase phase of TiO$_2$ can be influenced by dopants to improve its structural, optical, and morphological properties while, the thermodynamic stable phase, rutile, is resistant to dopant modification and only accommodates the dopants in the crystal lattice.

2. Results

X-ray diffraction (XRD) patterns used to identify the phases and crystal structure of Z:F-T NPs are depicted in Fig. 1. The diffraction pattern for the anatase phase corresponded to the reported JCPDS card no 84-1286. The diffraction pattern showed the dopants caused surface modification that consequently led to the growth of new peaks while other peaks diminished in their intensity. The growth of new peaks results from interstitial doping of Fe, while the convolving of peaks is due to Zn substitution doping. Crystallite size computed using the Debye Scherer's equation showed that 1:0.5 Z:F-T NPs grew by 10.7 nm, forming the largest crystallite size with 24.45 nm. In the rutile phase, peaks grew and convolved like in the anatase phase, however, the phase stability did not allow significant growth of the NPs. The XRD spectra showed sharp peaks that indicate improved crystallinity.
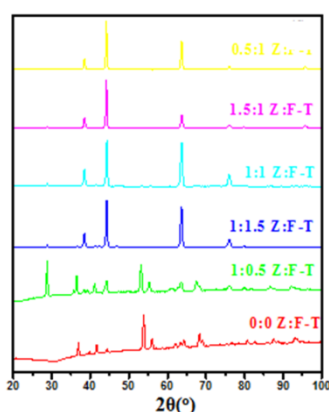
Fig.37: The XRD pattern for Zn:Fe co-dopedTiO$_2$ NPs.
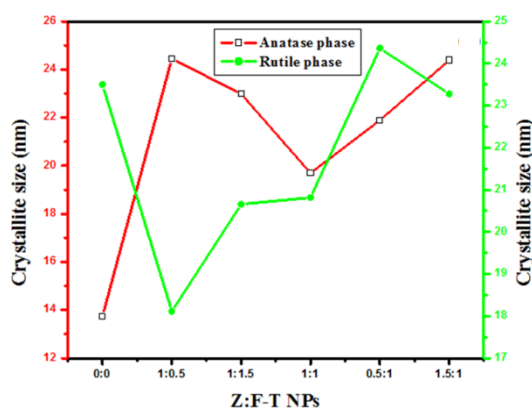
Fig. 2: Crystallite size of TiO$_2$ NPs with changes in the co-doping ratio.

3. References

[6] M.J. Grätzel J. photochem & photobi. C **4** (2003) 145.
[7] D. Kumar Eng. Res. Express. **3** (2021) 042004.
[8] R.K. Chava, Y.T. Yu YT,M. Kang. Nanomat. **14** (2024) 1782.
[9] G. Waweru, S. Kiprotich, P. Waithaka. Nanosci. &Nanotech. **13** (2024) 1.
[10] A. El Mragui, O. Zegaoui, Env.Sci.&P. Res. **28** (2021) 25130.
[11] G.K. Sukhadeve & R.S. Gedam. Chem. **341**(2023) 139990.

Annealing effects on hydrothermally prepared SnO$_2$ thin films deposited by spray pyrolysis and their potential for ETL in PSCs

Fokotsa Victor Molefe[1], Mmantsae Diale[1]

[1] *Department of Physics, University of Pretoria, Private Bag X20, Pretoria 0002, South Africa*
Corresponding author e-mail address: Mmantsae.diale@up.ac.za

1. Introduction

In the present time of accelerated industrialisation, the planet Earth faces environmental effects such as global warming and the depletion of the ozone layer associated with the combustion of fossil fuels during electricity generation. Such challenges fuelled the interest towards alternative means of generating clean, efficient and sustainable energy. Therefore, developing renewable energy materials for harnessing energy is important to remediate health issues associated with fossil fuels. At present, different photovoltaic (PV) technologies i.e. dye-sensitized solar cells (DSSC), organic solar cells (OSCs), and perovskite solar cells (PSCs), are being explored to serve as renewable energy sources. Among them, the PSCs have seen a momentous growth in efficiency with 26.1% achieved by using facile methods at low fabrication costs [1].

A compact, transparent, smooth, and uniform electron transport layer (ETL) is desirable in PSCs. The ETL is deemed an integral part of the PSCs responsible for collecting, transporting, and separating charges within the device. Among semiconductor metal oxides (SMOs), SnO$_2$ has been favoured due to its high transparency (>85%) for visible light and a broad optical energy band gap (E$_g$) (3.6-4.1 eV) at 300 K [2]. Inadequate knowledge of material properties while monitoring the T$_a$ still exists. To determine the annealing temperature (T$_a$) dependence on preferred orientation, texture coefficient (TC) analysis was performed using equation (1) [3].

$$TC_{(hkl)} = \frac{I_{(hkl)}\big/I_{0(hkl)}}{\dfrac{1}{N}\sum_1^N I_{(hkl)}\big/I_{0(hkl)}} \tag{1}$$

where *I(hkl)* refers to the measured relative intensity of SnO$_2$ thin films, *I$_{0(hkl)}$* denotes the intensity of the standard SnO$_2$ cassiterite phase and *N* represents the number of *hkl* diffraction peaks considered.

2. Results

The X-ray diffraction (XRD) patterns confirmed the formation of cassiterite SnO$_2$ phase consistent with JCPDS card no. 41-1445. The crystal growth of as-deposited thin film is preferentially oriented along the (110) crystallographic plane whereas the increase in T$_a$ favours the (211) crystallographic plane. Fig. 1 illustrates densely packed grain-like nanoparticles (NPs) with an average size of 73.3 nm formed through the segregation of irregular NPs at T$_a$ = 550°C. The absorption characteristics showed a redshift when increasing the T$_a$ which caused the narrowing of the E$_g$ as presented in Fig. 2.
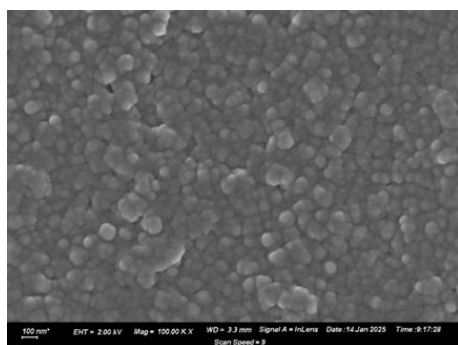
Fig. 38: SEM image of SnO$_2$ thin film annealed at 550°C.
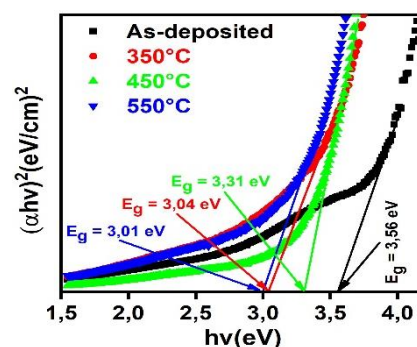
Fig. 2: Tauc's plots of as-deposited and annealed SnO$_2$ thin films.

3. References

[1] S. Mehmood, N. Shahzad, S. Nadeem and M. I. Shahzad. *Quantum J. Mol. Struct.* 1321 (2025) 139864.
[2] D. Xing, W. Pan, Z, Xie, Q-S. Jiang, Y. Wu, W. Xun, Y. Lin, X. Yang, Y. Zhang and B. Lin *Mater. Lett.* 327 (2022) 133079.
[3] G. Maharana, Y. Jayavelu, D. P. Joseph Albert and K. Manavalan. *Surfaces and Interfaces* **56** (2025) 105489.

Highly acetone responsive nanosensor layer based on nanostructured cube-like α-Fe$_2$O$_3$: Effects of Cr dopant ion.

M.B. Kgomo-Masoga [1,3], M.I. Nemufulwi[1,3] , M.S. Dhlamini[3] , G.H. Mhlongo[1,2*]

[1]Centre for Nanostructures and Advanced Materials (CeNAM), DSI-CSIR Nanotechnology Innovation Centre, Council for Scientific and Industrial Research, Pretoria 0001, South Africa

[2] Department of Physics, University of the Free State, Bloemfontein ZA9300, South Africa

[3] Department of Physics, University of South Africa, Johannesburg 1710, South Africa

dhlamms@unisa.ac.za: GMhlongo@csir.co.za:
kgomom@unisa.ac.za: murenn@unisa.ac.za

1. Introduction

In this work, the pure and Cr-doped α-Fe$_2$O$_3$ nanocubes at different doping levels of 0.5, 1, and 1.5 mol% were successfully synthesized via the hydrothermal approach, followed by annealing at 600 ℃. The influence of Cr metal ion-doping on the acetone gas sensing behavior of the cube-like α-Fe$_2$O$_3$ structures was investigated. Structural, morphological, textural, as well as surface defects analysis were conducted using XRD, SEM, BET, and PL respectively to comprehend the obtained improved acetone gas sensing trend emerging from the incorporation of Cr dopant ions.

2. Results

PL emission spectra of the pure and all Cr-doped α-Fe$_2$O$_3$ structures after excitation at 350 nm using a Xenon lamp were recorded and the results are presented in Fig. 1, to study the intrinsic defects present in the produced structures. Fig. 2 presents the responses of the pure and all Cr-doped α-Fe$_2$O$_3$-based sensors exposed to 90 ppm Acetone vapour from 120 to 360 ℃. All sensors displayed an increase in response values until reaching a maximum response value at 280 ℃, followed by a decline in response with a further increase in the working temperature. The observed increase in response values for all sensors can be ascribed to acetone target gas molecules attaining sufficient thermal energy to react with adsorbed oxygen ions [1]. The decrease in response values beyond 280 ℃ can be attributed to the desorption rate of the acetone molecules exceeding the adsorption rate [2]. Therefore, all sensing measurements were conducted at 280 ℃ for all sensors.
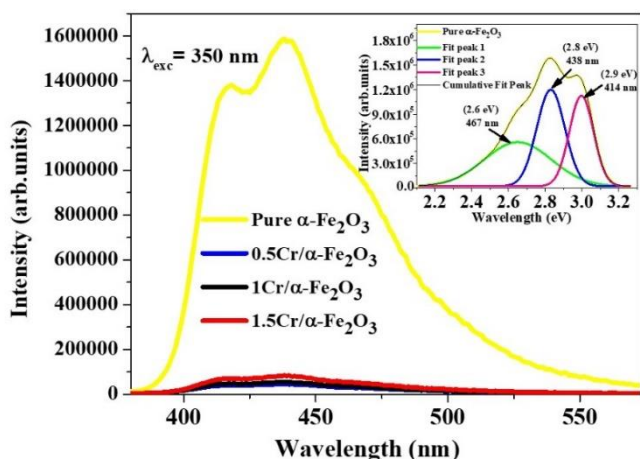
Fig. 1: PL spectra of the produced pure, 0.5Cr/Fe$_2$O$_3$, 1Cr /Fe$_2$O$_3$, and 1.5Cr/ Fe$_2$O$_3$ structures and the inset Gaussian fitting of the pure Fe$_2$O$_3$ product emission spectra.
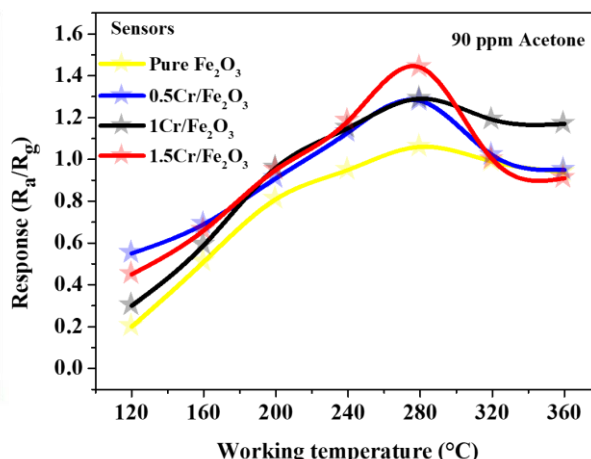
Fig. 2: Responses as a function of the working temperature from 120 to 360 ℃ for the pure, 0.5Cr/Fe$_2$O$_3$, 1Cr /Fe$_2$O$_3$, and 1.5Cr/Fe$_2$O$_3$ sensors towards 90 ppm of Acetone vapour.

3. References

[1]   X. Wu et al., "Hydrothermal synthesis of flower-like Cr$_2$O$_3$-doped In$_2$O$_3$ nanorods clusters for ultra-low isoprene detection," Colloids Surfaces A Physicochem. Eng. Asp., vol. 620, p. 126606, 2021.

[2]   D. Zhang, D. Wu, Y. Cao, X. Zong, and Z. Yang, "Construction of Co$_3$O$_4$ nanorods/In$_2$O$_3$ nanocubes heterojunctions for efficient sensing of NO$_2$ gas at low temperature," J. Mater. Sci. Mater. Electron., vol. 29, pp. 19558–19566, 2018.

Improved light harvesting in polymer solar cells using copper-doped zinc bimetallic nanocomposite

Mohammed S.G. Hamed[1], Thapelo Seimela[1], Mmantsae Diale*[1]

[1]Department of Physics, University of Pretoria, Private Bag X20, Hatfield 0028, South Africa
Corresponding author e-mail address: mmantsae.diale@up.ac.za

1. Introduction

Polymer solar cells (PSCs) are gaining attention as a favorable option in thin-film solar cell technologies due to their unique material properties and processing advantages. The ability to combine performance, cost-effectiveness, and compatibility with roll-to-roll printing methods ranks them as one of the fastest-developing areas of investigation in thin-film solar cell technologies[1]. However, the polymer absorber layer has several inherent problems, including low charge carrier mobility because of the disordered molecular structures and a narrow absorption spectrum that restricts its ability to efficiently harvest sunlight across the entire solar spectrum, particularly in the near-infrared (NIR) region[2]. In this study, the authors successfully synthesized copper-doped zinc bimetallic nanocomposites using a wet chemistry technique and looked into their application as a solar absorber medium in thin-film organic solar cells made with P3HT:PCBM blends.

2. Results

New thin film solar cells were produced using a conventional device architecture ITO/ PEDOT:PSS /P3HT:PCBM/ LiF/AL. Fig 2 shows the J-V curves of the PSCs with the addition of 0, 1, 2, and 3 wt% of Cu:Zn nanocomposite concentration in the active layer. The pristine device utilizing a P3HT: PCBM mixture has demonstrated a PCE of 3.28%. The performance of the device is significantly improved when Cu:Zn bimetallic nanocomposites are incorporated into the active layer of polymer solar cells. The best-performing device achieved a power conversion efficiency of 5.59% at a 1 wt% concentration of Cu:Zn nanocomposites in the active layer. This represents an enhancement of more than 70% compared to the pristine photoactive medium. The noted improvement in PCE is primarily because of the excitation of the localized surface plasmon resonance exhibited by the presence of Cu:Zn nanocomposite in the photoactive layer. Fig 1 shows the optical absorbance spectra for the polymer film that includes the 1\%, 2\%, and 3\% Cu:Zn bimetallic nanocomposite.
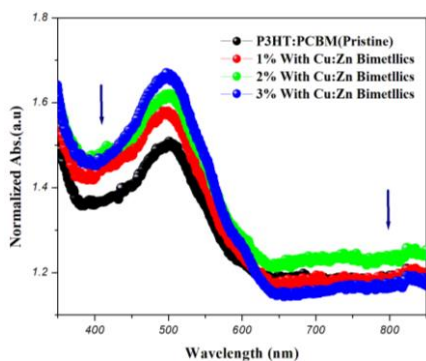
Fig. 39: Optical absorbance spectra of the polymer film containing Cu:Zn BMNCs
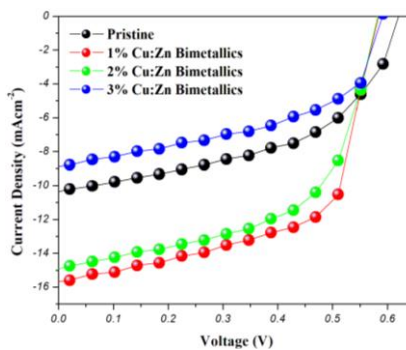
Fig. 2: J–V Curves for the devices fabricated using the pristine and with Cu:Zn BMNCs at different concentrations by weight.

3. References

[1] P.W.Blom, V.D.Mihailetchi, L.J.A.Koster and, D.E.Markov, Device physics of polymer: fullerene bulk heterojunction solar cells. Advanced Materials, 19(2007)1551-1566.
[2] F.Laquai, D. Andrienko, R.Mauer, P.WBlom, Charge carrier transport and photogeneration in P3HT: PCBM photovoltaic blends. Macromolecular rapid communications,36(2015)1001-25.

Structural and Optical Properties of V+ Ion Implanted CZTS Thin Films

T.B. Moipolai [1,2] **, M Madhuku**[1] **, S.J.Moloi**[2] **, M.A Masenya**[1]**, C.B Mtshali**[3]

1 iThemba LABS, TAMS Laboratory, P/ Bag 11, Wits, 2050, Johannesburg, South Africa
2 Department of Physics, University of South Africa, 28 Pioneer Avenue, Florida, Johannesburg,1710
3 iThemba LABS, Materials Research Department, P.O Box 722, Somerset West, 7129, Cape Town, South Africa
Corresponding author: tshegofatsomoipolai0083@gmail.com

1.   Introduction

The study presents the findings of the effect of ion implantation on pristine Copper Zinc Tin Sulphide (CZTS) thin films. The CZTS films were prepared utilizing a two stage process, i.e. e- beam deposition of metal precursors Cu, Zn and Sn followed by annealing in sulphur environment at 500°C for 30 min. These samples were further implanted with 150 keV V + ions utilizing fluences, 1×10^{16} , 3×10^{16} and 1×10^{17} ions/cm^2. Fundamental properties that governs the photovoltaic applications, i.e., structural and optical were investigated on pristine and ion implanted CZTS thin films using XRD, Raman and UV-VIS techniques. The Raman results highlighted the presence of defects in the CZTS samples. UV-VIS revealed energy band gap in the range 1.5 - 1.4 eV, and absorption within the UV range.

2. Results

Figure 1 presents the XRD diffraction peaks of the samples under investigation. All the CZTS samples indicated the presence of tetragonal kesterite CZTS phase with PDF 00-026-0575 [1]. Figure 2 presents the XRD diffraction patter of the most intense diffraction Peak (112) enlarged to show peak shifts and broadness upon implantation. An increament and lattice constants relaxation was noted as the fluence was increased to 1×10^{17} ions/cm ^{2}.
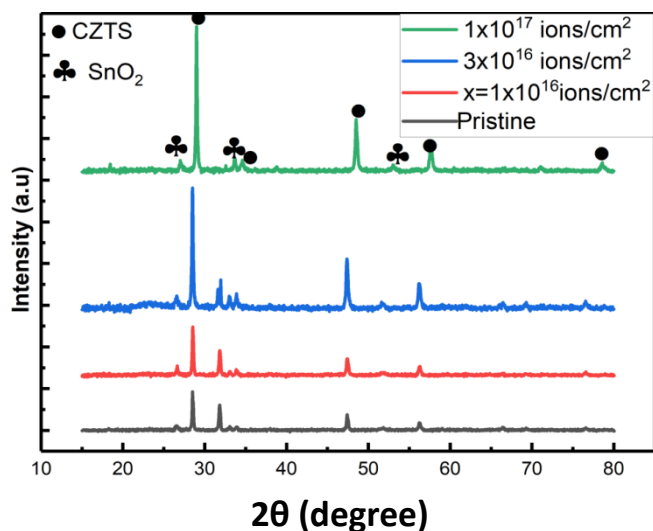
Figure. 40: Overlaid XRD pattern of pristine with the ion implanted CZTS samples.
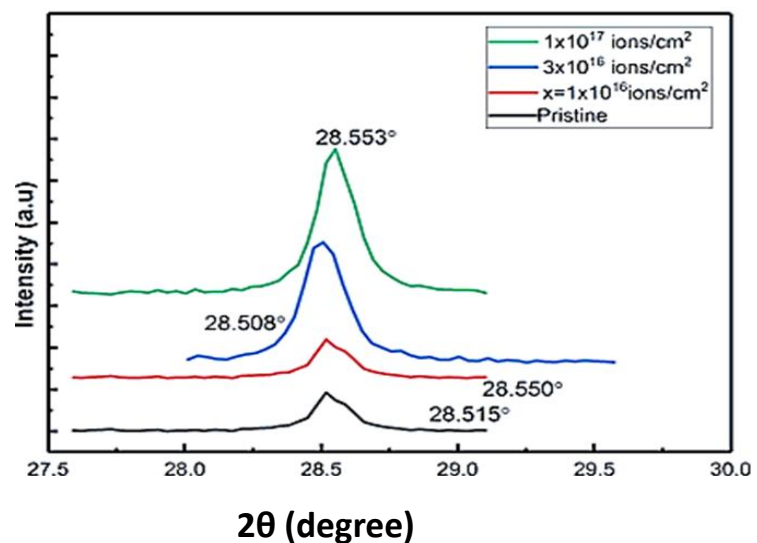
Figure 2: Most intense diffraction Peak (112) enlarged to show peak shifts and broadness upon implantation.

3. References

[1] T.P. Dhakal , C Peng, R Tobias, R Dasharathy , C.R. Westgate, Solar Energy 100, p23-30, (2014), https://doi.org/10.1016/j.solener.2013.11.035

Effect of Additional Polyene and Methoxy Functional moiety on the Spectral Properties of Polyene-Diphenylaniline Organic Molecules for Applications in Solar Energy

Ife Elegbeleye[1], Edwin Mapasha[1] Eric Maluta[2], Regina Mapanga[3]

[1] University of Pretoria, Hatfield 0028, South Africa.
[2] Department of Physics, University of Venda, Thohoyandou, South Africa.
[3] Council for Science and Industrial Research, P.O. Box 395, Pretoria, South Africa.
Corresponding author e-mail address: ifelove778@gmail.com

1. Introduction

The most clean and abundant renewable energy resource for humankind is solar energy. Dye-sensitized solar cells and silicon solar cells are photovoltaic devices for harvesting solar energy. Polyene-diphenylaniline organic dyes are a significant set of dyes that has stirred the interest of researchers as sensitizers in dye-sensitized solar cells based on TiO_2 semiconductors. The benefits of organic complexes over metal complexes are minimal cost, higher extinction coefficients, better compatibility with the environment, and good electrochemical properties. For instance, polyene-diphenylaniline with the simple donor-acceptor structure can be easily fabricated, they are cheaper and comprise of chemical structures that can be easily altered to improve their optical and catalytic properties. Their photocatalytic properties which include visible light to near-infrared light absorption have led to enormous interest in polyene-diphenylaniline dyes as photosensitizers. The influence of an additional methoxy functionalized group on the photocatalytic properties of polyene-diphenylaniline through the solar spectrum was studied using the density functional theory approach through GPAW, Avogadro, and ASE software.

The results showed that the maximum absorption wavelength was exhibited by the two phenyls-based complexes D5 and D7 with their maximum absorption peaks situated at wavelengths of 750 nm and 850 nm while the methoxy group-based complexes D9 and D11 exhibited absorption peaks at wavelengths of 800 nm and 900 nm as depicted in Fig 1. It was observed that D9 and D11, which comprise of additional methoxy, and polyene moiety show the highest absorption wavelength. In addition, the HOMO was delocalized on the dye molecule while the LUMO was delocalized on the TiO_2 semiconductor as shown in Fig 2, the HOMO-LUMO energy gap of 0.98 and 0.85 was associated with D9 and D11 dyes with the methoxy group when compared to HOMO LUMO energy gap of 1.32 and 1.08 obtained for D5 and D7 complexes. Their electron injection kinetics ΔG_{inject} analysis into the band gap of TiO_2 semiconductor depicts higher electron injection kinetics of -2.070 and -2.030 for D7 and D11 respectively compared to the similar organic complexes D5 and D9 without the additional polyene moiety with ΔG_{inject} of - 2.820 and -2.130 respectively. Our findings designate that adding a functional group to the conjugation length of an organic chromophore results in an increase in their light harvesting efficiency and a spectral shift of the absorption maxima towards a higher absorption wavelength connoting higher open circuit voltage and current density in DSSC. The study concluded that the spectral characteristics of organic complexes with donor-π-acceptor structures can be improved by adding functionalized groups.

2. Results
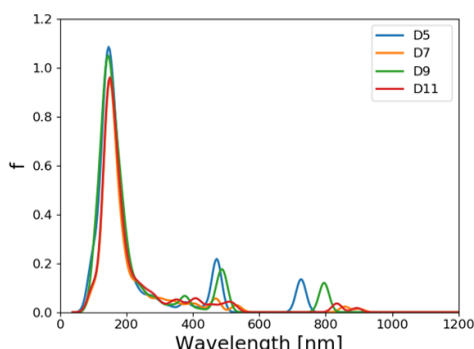
Fig. 41: simulated absorption spectra of D5, D7, D9 and D11 dye molecules.
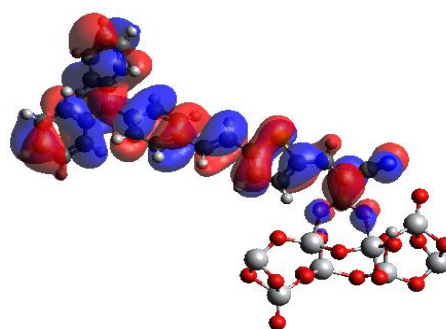
Fig. 2: Isodensity surfaces of the HOMO of D5 Dye molecule.

3. References

[1] W. Vallejo, M. Lerma, C. Díaz-Uribe. *Heli*.**11** (2025) 41092.
[2] E. Marcano. *De Gruyt.* **2** (2017) 1.
[3] D. kuang, P. Comte, S. M. Zakeeruddin, D. P. Hagberg, K. M. Karlsoon, L. Sun, M. K. Nazeeruddin, M. Gratzel. *Sol Energ.* **85** (2011)

1189.

Notes

Notes
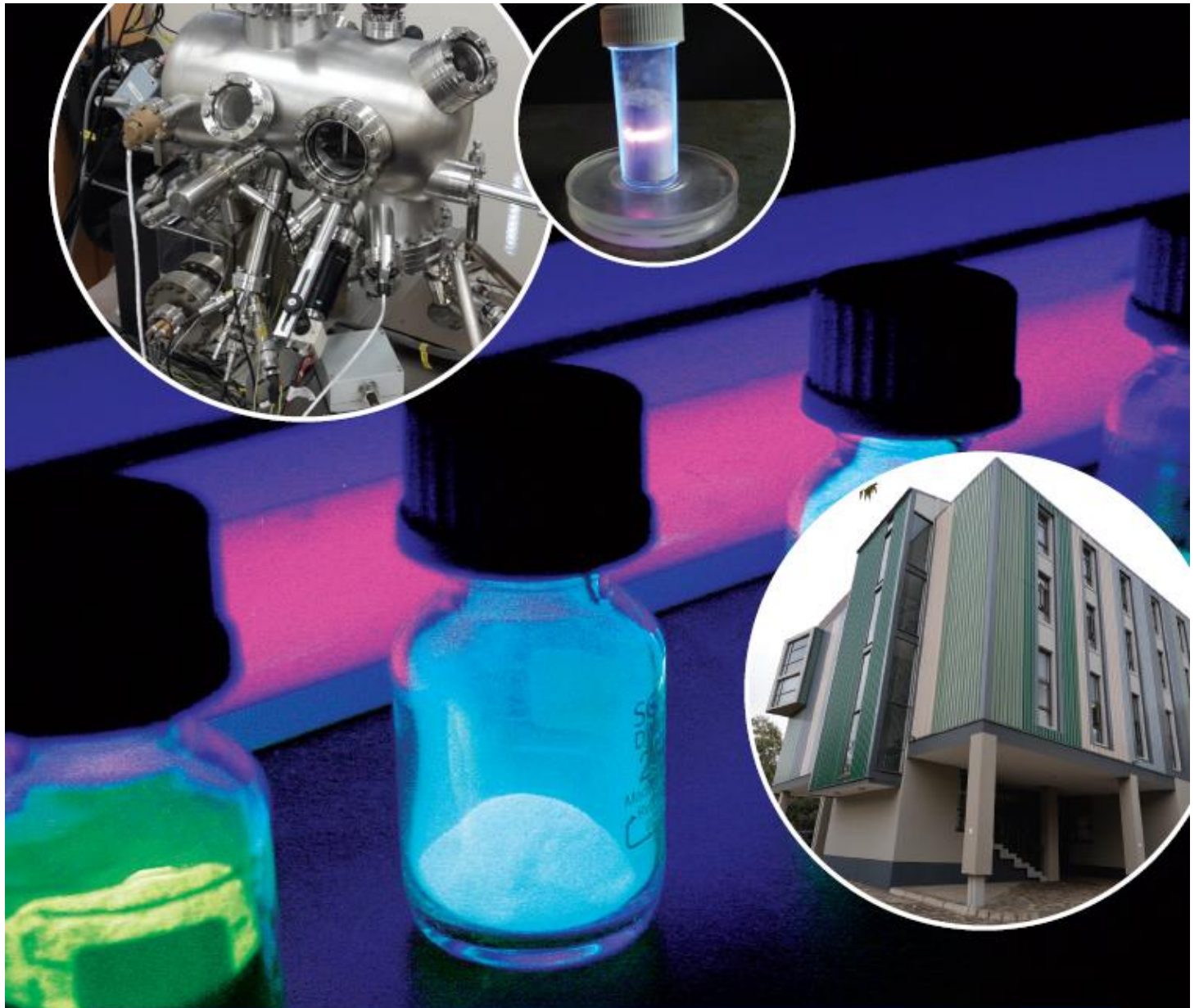
Don't stop dreaming.
Department of Physics

Inspiring excellence.
Transforming lives.

UNIVERSITY OF THE
FREE STATE
UNIVERSITEIT VAN DIE
VRYSTAAT
YUNIVESITHI YA
FREISTATA

UFS·UV
NATURAL AND
AGRICULTURAL SCIENCES
NATUUR– EN
LANDBOUWETENSKAPPE